Experimental Modal Analysis using Blind Source Separation Techniques

A thesis submitted to the University of Liège for the degree of "Docteur en Sciences de l'Ingénieur"

by

Fabien Poncelet

May 2010

Author's Coordinates

Fabien PONCELET, Ir.
Dynamic Research Group
Aerospace and Mechanical Engineering Department
University of Liège

Chemin des chevreuils, 1
4000 Liège
Belgium

Office phone: +32 4 366 4853
Email: fponcelet@ulg.ac.be

Members of the jury

Grigorios DIMITRIADIS (President of the jury)
Professor - University of Liège

Jean-Claude GOLINVAL (Co-supervisor)
Professor - University of Liège
Email: JC.Golinval@ulg.ac.be

Gaëtan KERSCHEN (Co-supervisor)
Professor - University of Liège
Email: G.Kerschen@ulg.ac.be

Vincent DENOEL
Professor - University of Liège

Luigi GARIBALDI
Professor - Politecnico di Torino (Italy)

Fabrice THOUVEREZ,
Professor - Ecole Centrale de Lyon (France)

Damien VERHELST
Stress Analysis Manager - Techspace Aero (Belgium)

Keith WORDEN
Professor - University of Sheffield (UK)

Abstract

This dissertation deals with dynamics of engineering structures and principally discusses the identification of the modal parameters (i.e., natural frequencies, damping ratios and vibration modes) using output-only information, the excitation sources being considered as unknown and unmeasurable.

To solve these kind of problems, a quite large selection of techniques is available in the scientific literature, each of them possessing its own features, advantages and limitations. One common limitation of most of the methods concerns the post-processing procedures that have proved to be delicate and time consuming in some cases, and usually require good user's expertise. The constant concern of this work is thus the simplification of the result interpretation in order to minimize the influence of this ungovernable parameter.

A new modal parameter estimation approach is developed in this work. The proposed methodology is based on the so-called Blind Source Separation techniques, that aim at reducing large data set to reveal its essential structure. The theoretical developments demonstrate a one-to-one relationship between the so-called mixing matrix and the vibration modes.

Two separation algorithms, namely the Independent Component Analysis and the Second-Order Blind Identification, are considered. Their performances are compared, and, due to intrinsic features, one of them is finally identified as more suitable for modal identification problems.

For the purpose of comparison, numerous academic case studies are considered to evaluate the influence of parameters such as damping, noise and non-deterministic excitations. Finally, realistic examples dealing with a large number of active modes, typical impact hammer modal testing and operational testing conditions, are studied to demonstrate the applicability of the proposed methodology for practical applications.

Acknowledgment

A doctoral thesis completion is, above all else, a personal and lonely work. But it would be unachievable without the involvement of many people.

First of all, I would like to express my gratitude to my wife, Barbara, for her constant encouragement provided during the course of my research. I probably could not succeed in achieving the present work without her presence and support.

Sincere acknowledgement to the current and former colleagues I had the pleasure to meet at the Dynamic Research Group *and more generally in the* Aerospace and Mechanical Engineering Department*. Thank you to all cheerful and smiling people passed in the corridors. All of you are contributors of this work and inalienably part of these few years of my life.*

I have also enjoyed my stay at the University of Sheffield where I found very close friends. Thank you to Professor Keith Worden for having made me feel welcome.

Particular acknowledgment must go to Professor Gaëtan Kerschen for his assistance during the course of my research. He gave me the opportunity of doing this thesis and provided me guidance and support. Thank you also for his meticulous reading of the thesis draft.

I also express my gratitude to my advisor Professor Jean-Claude Golinval for his help, advices and support, as well as for the confidence he placed on me.

Thank you to Damien Verhelst who provided me with one of the experimental structures tested in the work.

I would like to thank Professors Vincent Denoël, Grigorios Dimitriadis, Luigi Garibaldi, Fabrice Thouverez, Keith Worden, and the Techspace Aero representative Damien Verhelst for accepting to be members of my dissertation examination committee.

Finally, I wish to acknowledge the Walloon Government and Techspace Aero Company for their financial support to this research (Contract No 516108 - VAMOSNL).

Contents

List of Symbols and Abbreviations

$..^{\star}$	Conjugate transpose operator
$..^{H}$	Complex conjugate transpose operator for a matrix
α_i	Phase parameter
$\boldsymbol{\eta}(t)$	Normal coordinates
$\boldsymbol{\omega}$	Natural pulsation vector
$\boldsymbol{\sigma}_{noise}$	Noise signal
$\boldsymbol{\xi}$	Damping ratio vector
$\delta(t)$	Dirac's delta or unit impulse function
$\widetilde{\mathbf{f}}(t)$	Noisy excitation signal
$\mathbf{A}$	Mixing matrix of the BSS problem
$\mathbf{A}$, $\mathbf{B}$	State-space model matrices
$\mathbf{C}$	Viscous damping matrix
$\mathbf{C}_{\tau}^{\mathrm{x}}$	Time-lagged covariance matrix applied to the signals $\mathbf{x}$ for a delay τ
$\mathbf{D}$	EVD matrix containing eigenvalues
$\mathbf{D}$	Hysteretic damping matrix
$\mathbf{f}$	Natural frequency vector
$\mathbf{F}(\omega)$	Fourier transform of $\mathbf{f}(t)$
$\mathbf{f}(t)$	Time-varying excitation signal

$\mathbf{H}(\omega)$ Frequency response function

$\mathbf{h}(t)$ Impulse response function

$\mathbf{I}$ Identity matrix

$\mathbf{K}$ Stiffness matrix

$\mathbf{M}$ Mass matrix

$\mathbf{N}$ Vibration mode shape matrix

$\mathbf{n}$ Vibration mode shape vector

$\mathbf{r}$ State vector

$\mathbf{R}_{xy}(\tau)$ Cross-correlation function between the two signals x and y for the delay τ

$\mathbf{s}$ Sources or independent components of the BSS problem

$\mathbf{U}$ Unitary matrix

$\mathbf{V}$ EVD matrix containing eigenvectors

$\mathbf{W}$ Whitening matrix

$\mathbf{x}(t)$ Noisy time displacement response

$\mathbf{x}_w(t)$ Whitened noisy time displacement response

$\mathbf{Y}(\omega)$ Fourier transform of $\mathbf{y}(t)$

$\mathbf{y}(t)$ Time displacement response

$\mathbf{y}_w(t)$ Whitened time displacement response

$\otimes$ Convolution product

τ Delay

kurt(..) Kurtosis function

$cov(..)$ Covariance function

$E\{\mathbf{x}\}$ Mathematical expectation or expected value of $\mathbf{x}$

e_η NMSE between the identified and theoretical normal coordinates

$e_i(t)$ Slowly-varying envelope

n_s Number of sources

n_x or n_y Number of observed signals

n_{DOF} Number of degrees of freedom

PF_i Participation factor corresponding to the source s_i

r_ω Identified to theoretical frequencies ratio

r_ξ Ratio of identified to theoretical damping ratios

ARMA Autoregressive moving average

BSS Blind source separation

CAD Computer aided design

CMIF Complex mode indicator function

eFDD Enhanced frequency domain decomposition

EMA Experimental modal analysis

eMIF Enhanced mode indicator function

ERA Eigensystem realization algorithm

EVD Eigenvalue decomposition

FDD Frequency domain decomposition

FE Finite element

FFT Fast Fourier transform

FOBI Fourth-order blind identification

FRF Frequency response function

HHT Hilbert-Huang transform

IC Independent component

ICA Independent component analysis

IFFT Inverse fast Fourier transform

IRF Impulse response function

ITD Ibrahim time domain

IV Instrumental variable

JADE Joint approximate diagonalization of eigenmatrices

LSCE Least squares complex exponential

MAC Modal assurance criterion

MDOF Multi-degree of freedom

MIMO Multi-input multi-output

ML Maximum likelihood

NExT Natural excitation technique

NMSE Normalized mean-square error

OMA Operational modal analysis

PCA Principal component analysis

POD Proper orthogonal decomposition

PolyMAX Polyreference least square complex frequency-domain

POM Proper orthogonal mode

PP SDOF Peak picking

PSD Power spectral density

PTD Polyreference time domain

RD Random decrement

RMS Root mean square

SDOF Single degree of freedom

SIMO Single-input multi-output

SISO Single-input single-output

SOBI Second-order blind identification

SOD Smooth orthogonal decomposition

SSI Stochastic subspace identification

SSI-COV Covariance-driven stochastic subspace identification

SSI-DATA Data-driven stochastic subspace identification

SVD Singular value decomposition

Introduction

Be it for economic concerns, safety matters or merely enhancement of the products, structural dynamics analysis is of prior importance for engineers. Vibrations are inherent phenomenon of elastic structures, and can cause unpleasant repercussions, including the reach of serviceability limit states, high damages and structural failures, if they are not severely controlled.

Technology developments, emergence of new materials and modern architecture trends have increased the complexity of structures. Current challenging engineering projects commonly demand lighter and more impressive structures leading, in parallel, to much more complex operational loading conditions. Of course, during the last few decades, the development of powerful predictive tools, such as finite element softwares, have facilitated the task of predicting the dynamical behavior of such structures. Nevertheless, although it can be expansive and time consuming, experimental testing is still required to reassure the confidence in the numerical models before to be used for advanced calculations.

Damage detection, health monitoring, design and safety of aeronautical components, evaluation of damping capacity for existing structures are some of the domains where modal analysis proved to be useful. This work, involved in this context, mainly deals with the experimental part of dynamical studies consisting of modal testing and modal parameter estimation.

The major cause for concern throughout the thesis is to simplify the data post-processing in order to shorten the design phase and to minimize the subjective part of the result interpretation. The present document is divided into five parts describing the reference methods and their implications, the new methodology developed in the frame of this research, its application for comparison purpose with another well-established method and one last important part addressing the problem of interpretation of the results.

It should be noted that this research was made possible by the financial support of the Walloon Government and Techspace Aero company, as part of the FIRST DEI project (num. 516108) dealing with the validation of structural models in presence of nonlinear phenomena [Pon09].

Most of the developments and applications contained in this thesis have also

been presented in international conferences and then published in reviewed papers. The interested reader can refer to [KPG07, PKGV07, PKGM07].

Outline of the Thesis

As previously mentioned, this dissertation principally focuses on modal parameter estimation using experimental measurements. In this context, the fundamentals of modal testing are discussed in **Chapter 1**. Because the accuracy of the results is highly related to the quality of the information contained in the dynamic signals, vibration testing techniques, including setup basics and measurement precautions, are first reviewed. This first stage is referred to as data acquisition in the present study. Second, these data have to be processed to estimate the modal parameters. Numerous techniques were developed and some of them, based on output-only information, are surveyed. Finally, the covariance-driven stochastic subspace identification method, that is used as a reference method throughout the work, is detailed.

The main objective of the thesis is to use the so-called blind source separation techniques to estimate the modal parameters using output-only signals. **Chapter 2** introduces the theoretical foundations of blind source separation, leading to the concepts of sources, mixtures, mixing matrix and statistical independence. Numerous reference techniques are available in the literature for source separation, and they are briefly surveyed. Two of them, namely the independent component analysis and the second-order blind identification, are considered for modal identification, and are described in more details. Similarities between source separation and other empirical and statistical approaches are also investigated.

In **Chapter 3**, both modal identification and blind source separation are combined, and a new methodology is developed to estimate the modal parameters from free and random forced responses. The theoretical developments demonstrate a one-to-one relationship between the so-called mixing matrix and the vibration modes, and an automated procedure is proposed to identify and automatically select the genuine results.

Next, in order to validate the proposed methodology for free and random responses, discrete and distributed-parameter systems, for which exact solutions exist, are considered in **Chapter 4**. Both ICA and SOBI algorithms are compared and their performance is evaluated with respect to noise, damping and non-deterministic excitation. The proposed automated mode selection is also illustrated when the number of active modes is lower than the number of identified sources.

Finally, **Chapter 5** demonstrates the utility of SOBI for output-only modal analysis in practical applications. Three structures are considered dealing with

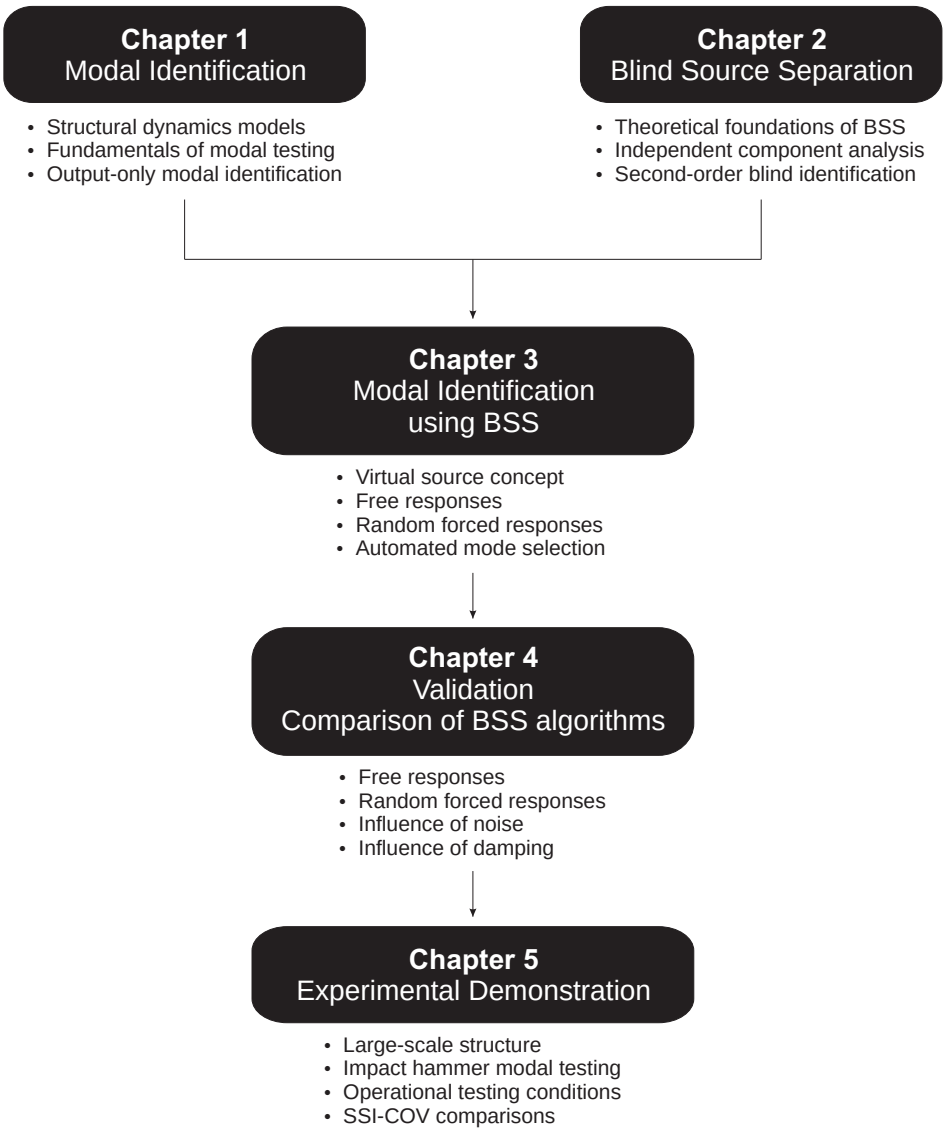

Figure 1: **Outline of the thesis.** SSI-COV: Covariance-driven stochastic subspace identification. BSS: Blind source separation.

a large number of active modes, typical impact hammer modal testing, and operational testing conditions, respectively. The identified modal parameters are compared to those obtained using the well-established stochastic subspace identification method.

Chapter 1

Experimental Modal Analysis in Structural Dynamics

Abstract

This chapter introduces the fundamentals of modal testing. Two specific aspects are underlined, dealing with data acquisition and processing respectively. The main features and limitations of commonly-used techniques are reviewed.

First, three models used to describe the mechanical system dynamics are presented (Sec. 1.1).

Section 1.2 gives an overview of vibration testing techniques (i.e., data acquisition). These techniques are classified according to the testing objectives, and several important aspects of the setup preparation are emphasized.

The next section presents the modal parameter estimation techniques (i.e., data processing) used to obtain dynamic models from experimental measurements. A general classification is proposed for the identification methods (Sec. 1.3).

Section 1.4 briefly reviews the existing output-only based methods, which are the focus of this work.

Finally, the covariance-driven stochastic subspace identification is described in more details in Sec. 1.5 since this well-established modal parameter estimation method is used as a reference method for comparison throughout this work.

1.1 Structural Dynamics Models

The modeling of mechanical system dynamics can take different forms. Numerical models, based on computer-aided design (CAD), are usually considered during the design phase. They require a complete description of the system including geometrical and material characterization. Reduced models, only comprising few parameters, facilitate the comprehension of the system dynamics. They also enable the numerical predictions to be compared to experimental results. Besides numerical and reduced models, models using the transfer function concept can evaluate the structural dynamic response to given excitations.

In the scientific literature, those models are referred to as spatial, modal and response models, respectively. Figure 1.1 presents the relations that exist between the three models for an undamped system, and the next sections describe them.

1.1.1 Spatial Model

Mechanical engineers usually model structures using finite element (FE) models. The continuous systems are then discretized into multi-degree-of-freedom (MDOF) systems.

In the case of linear-dynamics assumption, the response of the undamped system is governed by the equation of motion

$$\mathbf{M}\ddot{\mathbf{y}}(t) + \mathbf{K}\mathbf{y}(t) = \mathbf{f}(t), \tag{1.1}$$

where $\mathbf{y}(t)$ and $\mathbf{f}(t)$ are the time-varying displacement response and applied force, respectively. The structural matrices $\mathbf{M}$ and $\mathbf{K}$ are referred to as the mass and stiffness matrices respectively. A velocity term appears for the viscously-damped system

$$\mathbf{M}\ddot{\mathbf{y}}(t) + \mathbf{C}\dot{\mathbf{y}}(t) + \mathbf{K}\mathbf{y}(t) = \mathbf{f}(t). \tag{1.2}$$

where $\mathbf{C}$ is the damping matrix.

Structural hysteretic damping can also be considered by introducing the imaginary term $i\mathbf{D}\mathbf{y}(t)$ in the left-hand member of Eqn. (1.1).

The three matrices $\mathbf{M}$, $\mathbf{K}$ and $\mathbf{C}$ represent the spatial distribution of the system mechanical properties and form the so-called *Spatial Model*.

Although this modeling approach contains most of the interesting information about the system, the dynamic properties are buried within complex structures (i.e., the *structural matrices*) which can quickly become obscure for large MDOF systems. For daily engineering practice, these properties are thus extracted, leading to the modal parameters and, therefore, the modal model.

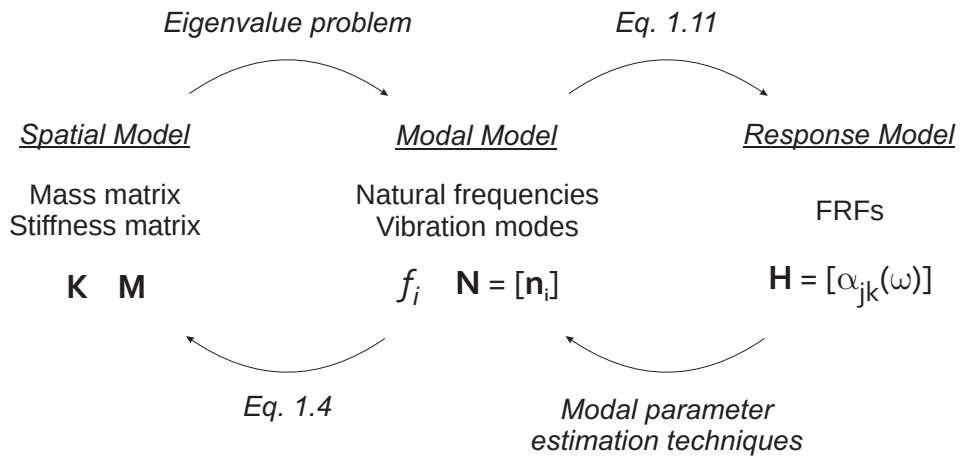

Figure 1.1: **Dynamic models interrelation for the undamped system.** The spatial and response models are linked together with the modal model.

1.1.2 Modal Model

The so-called *Modal Model* is a synthesized model that summarizes the dynamical information in a few parameters, called *modal parameters*. This term encompasses the natural frequencies $\mathbf{f} = [\cdots f_i \cdots]^T$ or pulsations $\boldsymbol{\omega} = [\cdots \omega_i \cdots]^T$, the vibration modes $\mathbf{N} = [\cdots \mathbf{n}_i \cdots]$ and the damping ratios $\boldsymbol{\xi} = [\cdots \xi_i \cdots]^T$.

Thanks to its simplified form, the triplets $(\omega_i, \mathbf{n}_i, \xi_i)$, evaluated from different sources (i.e., experimentally or theoretically), can be compared easily making the modal model really powerful for structural dynamic analysis.

Spatial and modal models can be related to each other, as illustrated in Fig. 1.1. For example, in the case of undamped systems, the modal parameters can be computed from the structural matrices by solving the eigenvalue problem

$$\mathbf{K}\mathbf{n}_i = \omega_i^2 \mathbf{M}\mathbf{n}_i. \tag{1.3}$$

Recovering the spatial model from the modal parameters is also possible. Thanks to the orthogonal properties of the modal matrix, the relation between the structural matrices and the modal parameters is provided by

$$\mathbf{M} = \mathbf{N}^{-T}\mathbf{N}^{-1} \text{ and } \mathbf{K} = \mathbf{N}^{-T}\left[\diagdown\omega_r^2\diagup\right]\mathbf{N}^{-1}, \tag{1.4}$$

where $\left[\diagdown\omega_r^2\diagup\right]$ is a diagonal matrix containing the squared pulsations ω_r^2. If conceivable, this process can quickly become complicated for damped or large-scaled structures. Note also that in case of nonlinear systems, the modal model, as such, is no longer applicable.

1.1.3 Response Model

Analyzing the dynamic response of a system subjected to a given excitation is of great interest during a structural dynamic analysis. This can be either theoretically or experimentally based.

The dynamic response mainly depends on two factors: the system dynamic characteristics and the imposed excitation. Consequently, the system is completely characterized by computing its response for a standard excitation. The standard signal commonly used for this purpose is the unit impulse function $\delta(t)$, also referred to as Dirac's delta. The resulting time response is called the Impulse Response Function (IRF) and denoted $\mathbf{h}(t)$. The IRF function relates the given input excitation to the time response signals using a convolution product through

$$\mathbf{y}(t) = \mathbf{h}(t) \otimes \mathbf{f}(t). \tag{1.5}$$

In the frequency domain this leads to the concept of *Frequency Response Function* (FRF), denoted $\mathbf{H}(\omega)$. The FRF is the transfer function of the system for dynamics, and it comes

$$\mathbf{Y}(\omega) = \mathbf{H}(\omega)\mathbf{F}(\omega) \tag{1.6}$$

where $\mathbf{Y}(\omega)$ and $\mathbf{F}(\omega)$ are the Fourier transforms of the time response and excitation signals, respectively.

Thus, knowing the IRF or the FRF, the dynamic response $\mathbf{y}(t)$ can be computed for any particular given excitation.

The *Response Model* usually comprises a set of FRFs defined over the frequency range of interest. Those FRFs can be directly computed from the experimental results, if both response $\mathbf{Y}(\omega)$ and excitation $\mathbf{F}(\omega)$ signals are recorded during the vibration testing. But noise often perturbs the measured responses and input forces, as illustrated in Fig. 1.2 and such that

$$\mathbf{x}(t) = \mathbf{y}(t) + \boldsymbol{\sigma}_{noise} \tag{1.7}$$

$$\widetilde{\mathbf{f}}(t) = \mathbf{f}(t) + \boldsymbol{\sigma}_{noise} \tag{1.8}$$

where $\boldsymbol{\sigma}_{noise}$ is the noise signal. Thus, the transfer function $\mathbf{H}(\omega)$ cannot be computed directly from Eqn. 1.6 and it is necessary to use one of the following estimators

$$\mathbf{H}_1(\omega) = \frac{\mathbf{S}_{\widetilde{\mathrm{f}}\mathrm{x}}(\omega)}{\mathbf{S}_{\widetilde{\mathrm{f}}\widetilde{\mathrm{f}}}(\omega)} \tag{1.9}$$

$$\mathbf{H}_2(\omega) = \frac{\mathbf{S}_{\mathrm{xx}}(\omega)}{\mathbf{S}_{\mathrm{x}\widetilde{\mathrm{f}}}(\omega)} \tag{1.10}$$

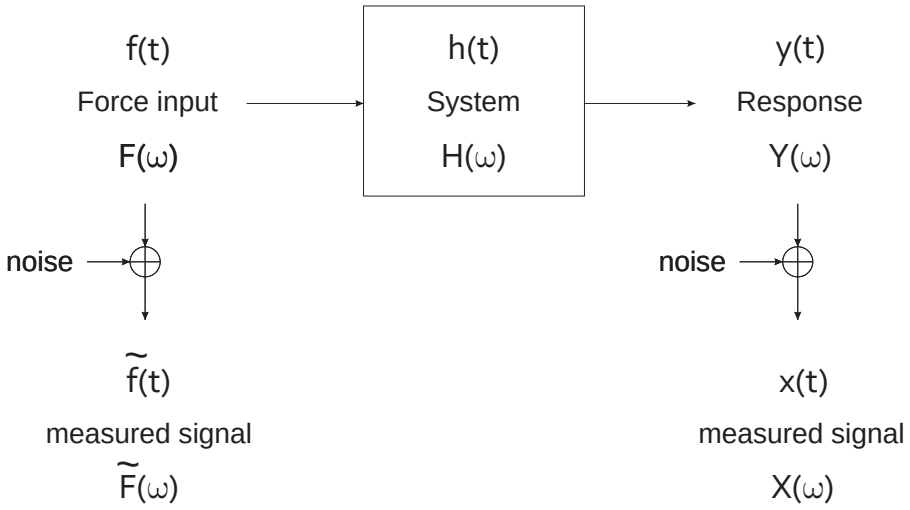

Figure 1.2: **Traditional measurement system model.** During data acquisition, the signals are perturbed by noise. The measured signals slightly differ from the real input and output signals.

where $\mathbf{S}_{xx}$ and $\mathbf{S}_{\tilde{f}\tilde{f}}$ are the auto-spectral densities of the response and excitation signals, respectively, and $\mathbf{S}_{x\tilde{f}}$ is the cross-spectral densities between both signals [Ewi00, MS97].

To obtain the response model from the modal parameters, a unit-amplitude sinusoidal force $\mathbf{f}(t) = \mathbf{F}e^{i\omega t}$ is introduced in the equation of motion (1.1). For the undamped MDOF system, the FRF is directly linked to the modal parameters using

$$\mathbf{H}(\omega) = \boldsymbol{\alpha}(\omega) = \mathbf{N}\left[\diagdown(\omega_r^2 - \omega^2)\diagdown\right]^{-1}\mathbf{N}^{-1}. \tag{1.11}$$

The modal model can be deduced from the response model using modal analysis techniques such as explained in Sec. 1.3. Those techniques are usually used to extract the modal parameters from experimental data.

Unfortunately, some structures are subjected to unknown and unmeasurable excitations. This is the case for civil engineering structures subjected to wind or traffic loads or mechanical engines under operational conditions. In this case, the response model cannot be evaluated and the modal parameters need to be estimated without FRF data. The modal parameters are directly estimated from the time response signals ; this process is referred to as **Operational Modal Analysis** in the literature.

1.2 Data Acquisition

The last decades witnessed significant progress regarding computational capacity. Nowadays, advanced virtual prototyping, using CAD and other numerical techniques such as the FE method, is commonly used to predict the system dynamics.

CAD techniques have been developed to make the design phase shorter and consequently to reduce the cost of the prototyping phase. Unfortunately some features (damping for example) cannot be accurately predicted. Furthermore, uncertainties related to material behavior, boundary conditions or joint modeling reduce the predictive capability of the numerical results. A thorough design and prototyping phase should include an experimental step, such as vibration testing. The experimental results can be compared to the numerical predictions and used to update and validate the model [FM95]. This experimental validation reassures the confidence in the model before using it for advanced calculations, such as the evaluation of the response levels to complex excitations.

Both theoretical and experimental approaches are closely related and provide complementary information. The comparison is usually achieved using modal models. Figure 1.3 presents these two routes to vibration analysis.

The experimental phase aiming at establishing the modal model is referred to as **Modal Testing**. According to Ewins [Ewi00], modal testing approach *"encompasses the processes involved in testing components or structures with the objective of obtaining a mathematical description of their dynamic or vibration behaviour"*.

1.2.1 Classification of the Testing Procedures

The vibration testing procedures can be classified in three categories, according to the testing objectives:

Modal testing. The modal testing approach aims at determining the modal model of the structure subjected to a monitored excitation. Both dynamic responses and input excitations are measured, and the experimental conditions are such that any undesired and unmeasurable excitation is avoided. The post-processing is usually based on the acquired sets of FRFs.

Operational testing. If the tested structure cannot be extracted from its operational environment, the only signals that can be measured are the responses to an unknown and unquantifiable excitation. In the case of operational testing, the extraction of the modal parameters is based on output-only methods (i.e., operational modal analysis).

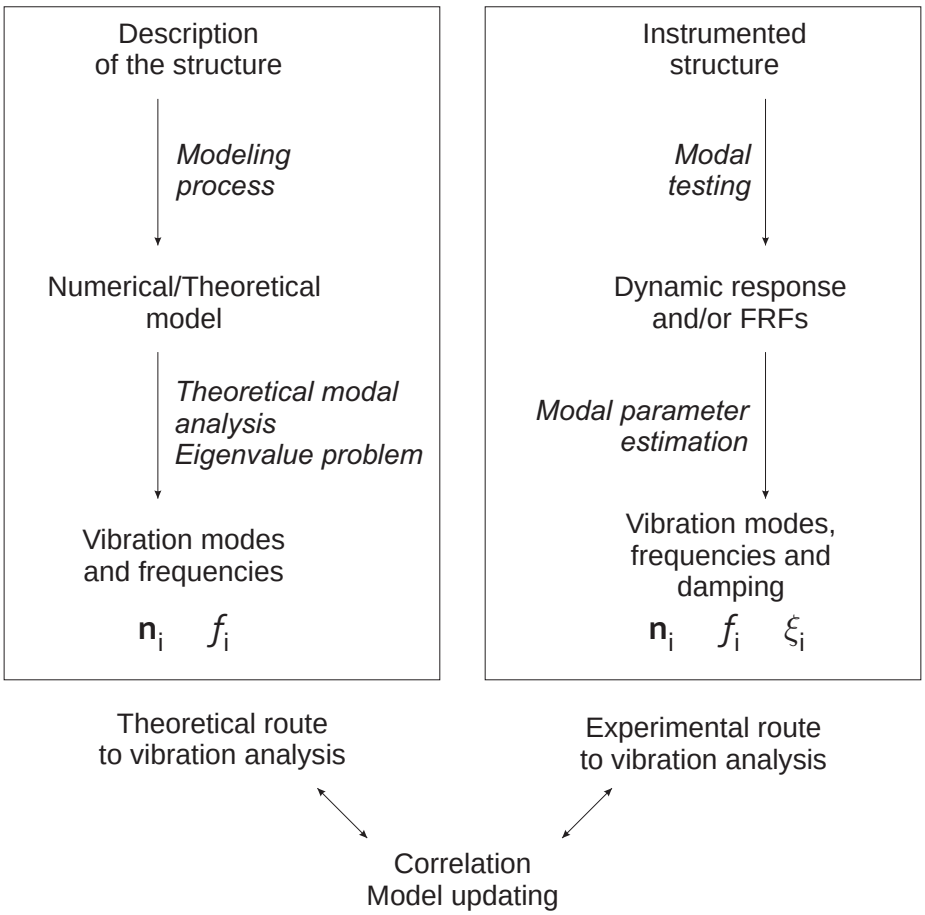

Figure 1.3: **Comparison of the two routes to vibration analysis.** The theoretical route starts from the geometrical and physical description of the structure and uses numerical techniques to estimate the modal parameters. The experimental route starts from experimental measurements and uses modal analysis techniques in order to determine the modal model. Both set of modal parameters can be compared and the theoretical model can thus be updated.

Environmental testing. Another outcome of vibration testing is the qualification of assemblies for their future operational vibratory environment. During these environmental tests, the structure is subjected to vibration of a specified form and amplitude for a certain period of time in order to assess its operational integrity.

The present work focuses on the extraction of modal parameters directly from the measured responses ; the *excitation is then assumed to be unknown*. The corresponding testing conditions are then those of the *operational testing*.

1.2.2 Setup Basics and Measurement Precautions

A particular attention has to be paid to the testing phase to ensure the acquisition of high-quality data. Precautions should be taken regarding several aspects of the procedure from the supporting conditions to the signal processing including the transduction of the measured quantities. The experimental process is schematized in Fig. 1.4. Some of these aspects are briefly summarized hereafter but the interested reader can refer to Refs. [McC95, Ewi00, HLS02, MS97] for further information.

Supporting conditions

Depending on how the resulting information will be used, the supporting conditions can be of different kinds. *Free conditions* are achieved by suspending the structure by means of very soft springs or by simply laying it on a piece of soft foam. This option is foreground in the case of correlations with FE predictions since free boundary conditions are much easier to simulate.

Another classical way of mounting an experimental setup is to *rigidly clamp* the testpiece at given locations. This can be a good approximation of the operational conditions and might facilitate the measurements.

Finally, some testpieces cannot be extracted from their operational environment and have to be tested *in situ*. This is the case for mechanical pieces of running machines for instance. The connection of such samples to some other structures or components presents a semi-rigid behavior that is, however, more complex to assess and model. These supporting conditions are closely related to the aforementioned operational testing procedure.

Applied excitation

The quality of the information contained in the measured responses is directly related to the way of applying the input force. Thus the mechanics of the excitation is an important parameter of vibrating tests. Many configurations are

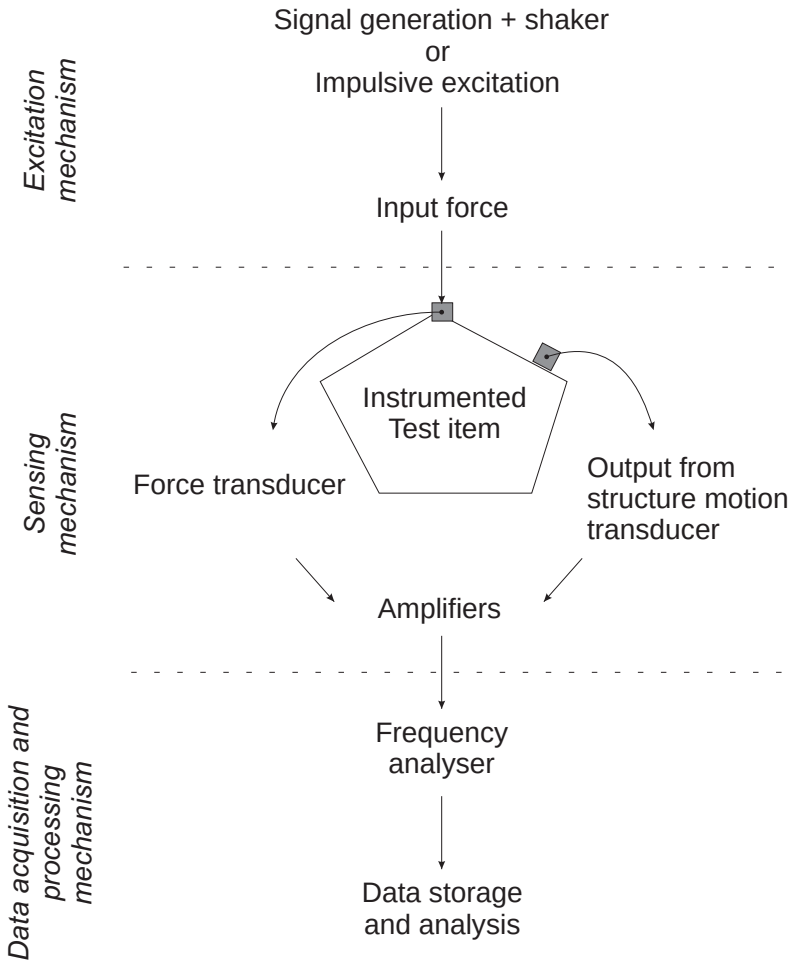

Figure 1.4: **Generic test item for vibration testing.** Three mechanisms are identified for a vibration test: the excitation mechanism, the sensing mechanism and finally the data acquisition and processing mechanism.

possible, and a thorough study should be completed for each particular case before testing. But, basically, three ways of applying the force are available: the impact hammer, the shakers or vibration generators and finally the operational environment.

The *impulse response* corresponds to the free vibrations occurring after a small perturbation. This can, for instance, be achieved using a small force-transducer hammer blow. This technique is cheaper, easier and quicker than any others but, because the input energy is very localized in space and in time (the excitation approximates the Dirac delta function), the amount of energy contained in the impact pulse is low. Thus, this approach is particularly appreciated for modal parameter identification of lightly damped structures. For large and highly damped structures, the excitation energy can be quickly dissipated before propagating far within the structure and is consequently useless.

In order to obtain a recording time long enough for post-processing, the highly damped structures can be excited during the measurement window using *vibration generators* (or *shakers*). These devices permit the application of different kinds of input signals in a specific range of frequency (such as random, chirp or harmonic excitation to cite a few).

Using several shakers on the same structure, a multi-point testing is also possible. In this particular case, the energy can be fed in the structure more uniformly. It is possible to perform phase-resonance testing using several shakers. A single mode of vibration is then excited at a time. This kind of tests, even if quite heavy to implement, is popular for very large structures such as aircraft structures, because it makes possible the measurement of real normal modes for direct comparison with FE results [VDAOLB91, BCLF95, BGFG06, PCdD$^+$08].

Finally, in case of operational testing, the input force is, totally or partially, introduced in the system through the *operational environment* preventing the recording of the input force.

Transduction of the signals

Besides the previous considerations, other parameters such as the *sampling frequency* or the *frequency range* of interest must be carefully chosen. Those parameters also influence the choice of the *transducers* on which the accuracy of the measurements depends. Moreover, the modification of the tested structure due to the instrumentation should be as limited as possible.

Transducers are commonly made of piezoelectric elements directly connected to the structure and aim at detecting forces and acceleration signals. But according to the weight of the testpiece, non-contact measurement tools (such as laser vibrometers) could profitably be used in some cases.

The force and motion transducers generate analog time signals, and they have

to be converted into digital data for computer processing. Some acquisition systems also automatically convert the time signals into the frequency domain using analyzers based on the Fast Fourier Transform (FFT) [CT65]. If both response and excitation signals are measured, the FRFs are then directly provided for post-processing.

Note that the number and placement of sensors on the structure highly influence the quality of the measurements. An inappropriate location can lead to data containing few information on the system dynamics. Some techniques have been developed and should be used for complex structures in order to optimize the sensor placement [Kam91].

The accuracy of the measured data is of great interest, because they are subjected to many analysis procedures to extract the underlying information (i.e., data processing). The numerical techniques providing this information are addressed in the next sections.

1.3 Data Processing

1.3.1 Modal Parameter Extraction

Mechanical engineers started to use modal analysis in the 40's for better understanding the dynamic behavior of aircrafts. Over the years, modal analysis became more powerful and popular for structural dynamic studies. The real advent of experimental dynamic techniques came out forty years ago thanks to the introduction of new signal processing methods such as the FFT algorithm, published in 1965 by Cooley et al. in [CT65]. Since then, its fundamental role in structural dynamics has never lessened, and modal analysis became more and more popular following the development of instrumentation, spectrum analyzers and computational capacities.

Nowadays, the so-called *Modal Analysis* is a more generic term covering a large range of engineering areas, from modal testing to structural modification including, among others, correlation and model updating techniques, and one can count numerous publications on this topic.

The present work focuses on the part of modal analysis referred to as *Modal Parameter Estimation*, performed by post-processing the measured experimental data. Many methods are available to deal with large-scale and industrial structures. They proved to be useful for complex systems such as civil engineering structures [MCC08, WLL$^+$07], complete aircraft or ship structures [AGB$^+$99, BGFG06, BG08, RS08], other motorized vehicles [SSAC08, BCG$^+$09] or launch vehicles [CMPC08].

All the systems considered in this work for modal analysis are assumed to

be linear. Nonlinear system modal analysis is not discussed herein. Additional information on this topic can be found in Refs. [KWVG06, WT01].

1.3.2 Classification of Methods

A large selection of techniques is available for the extraction of modal parameters from experimental measurements. Every single method possesses its own characteristics, and a thorough inspection should be considered in order to adopt the most appropriate technique for each specific case. A classification of the existing methods is proposed hereafter in order to help the user identifying their essential features.

Basically, modal parameter extraction aims at identifying theoretical model parameters such that they match the experimental measurements. Curve-fitting methods can either be applied in the frequency domain or in the time domain. A first level of distinction is based on the application domain:

- **Frequency domain**: The modal parameter extraction techniques are based on the experimental *FRFs signals*. These methods permit the identification on a limited frequency range and are generally used for a relatively small number of modes;

- **Time domain**: Either the IRFs (directly deduced from the FRFs using the Inverse Fast Fourier Transform, i.e., IFFT) or the *time response histories* are used to determine the modal parameters. This tends to provide the best results when a large number of modes are active within the frequency range.

A second classification emerges when focusing on the kind of parameters used for the fitting:

- **Indirect**: The term 'indirect' signifies that the identification is based on the *modal model*. This means that the natural frequencies, the damping ratios and the modal constants are used as fitting parameters;

- **Direct**: The fitting techniques can also rest on the *spatial model* and thus on the matrix equations of dynamic equilibrium.

One can also consider the frequency range over which each individual analysis is performed. This creates two new categories, according to the number of modes that can be analyzed:

- **SDOF**: In single degree of freedom (SDOF) analysis, each mode is *studied separately*. SDOF techniques are available neither for time domain nor direct methods, but only for indirect frequency-domain based methods.

- **MDOF**: For larger frequency ranges, *several modes* are extracted at a time, and this corresponds to MDOF methods.

Section 1.2 showed different possibilities for the testing procedures. The measured signals can be recorded simultaneously or not; several, or only one, responses can be recorded at a time; and the excitation can be strictly controlled or simply due to the operational conditions. These options also introduce a new categorization, according to the number of signals that can be treated at the same time:

- **SISO**: Some of the modal analysis methods, that can only be applied to *a single FRF* at a time, are called single FRF or single-input-single-output (SISO) methods;

- **SIMO**: Based on the assumption that the natural frequencies and the damping ratios do not vary from one FRF to another FRF, global or single-input-multi-output (SIMO) methods are conceivable. They process several FRFs at a time. The FRFs are obtained using a single *excitation point* but correspond to different response locations on the structure;

- **MIMO**: Finally, more complex methodologies have been implemented in order to simultaneously deal with all the available FRFs (from *various excitation and response locations*). They are called polyreference or multi-input-multi-output (MIMO) methods.

To summarize, Figure 1.5 summarizes all the possible combinations.

Because this work uses IRFs or time responses, the identification techniques considered herein are then *time domain and MDOF methods. Both direct and indirect methodologies are considered* for modal analysis. For instance, the blind source separation based techniques, developed in this work, are direct methods while the well-established stochastic subspace identification method, used as a reference technique, is an indirect one.

1.4 Output-Only Based Techniques

Besides the previous classification, modal parameter estimation methods can be divided into two other large classes: *Operational Modal Analysis* (OMA) and *Experimental Modal Analysis* (EMA). OMA is an output-only based modal parameter estimation technique and is used in case of operational testing conditions (cf. Sec. 1.2.1). It does not require the input load to be recorded in contrast with EMA for which both excitation and response signals are necessary.

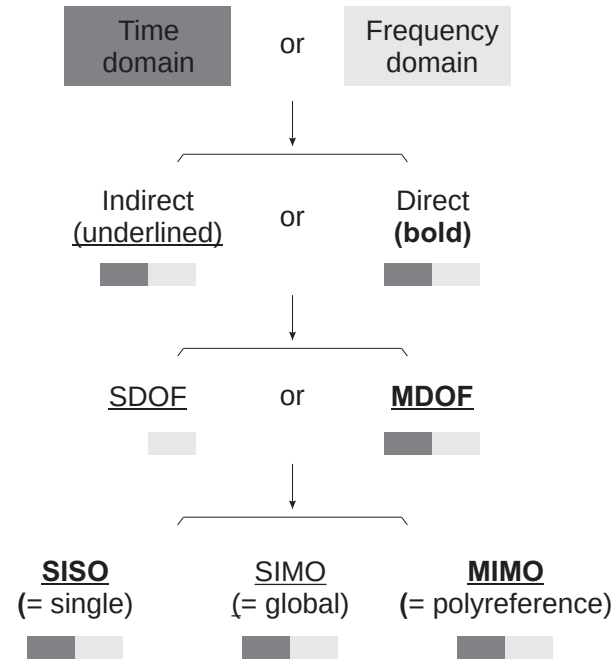

Figure 1.5: **Classification of modal parameter extraction methods.** Various classification can be applied to these methods according to the application domain, the kind of parameters used for the fitting, the number of degrees of freedom or the number of considered input and output signals.

Many methods have been proposed to solve the so-called OMA problem. Some of the most used techniques are presented hereafter, focusing on time-domain techniques. A complete description of the methods is beyond the scope of this work, nevertheless the identification techniques are listed according to their principal features.

In case of OMA, the excitation process being unknown, the response signals must be recorded simultaneously to assure the same testing conditions. The deterministic knowledge of the input is usually replaced by the assumption that the input is a realization of a stochastic process (i.e., a white noise uniformly exciting the structure over the complete frequency range). The related methods are referred to as stochastic system identification methods.

Last, the measurements considered herein are the time-dependent dynamic responses that can be either displacement, velocity or acceleration responses.If the identification method requires a pre-processing phase to remove the redundant information from the signals, the time data are then transformed to covariances or to a frequency-domain representation, provided by the power spectrum. The power spectrum is defined as the discrete-time Fourier transform of the covariance sequence. Those concepts are defined by Peeters in Refs. [Pee00, PDR01]. Therefore, the output-only identification methods can be either *spectrum-driven* or *covariance-driven* according to the data pre-processing that has to be performed or simply *data-driven* if no pre-processing is required.

1.4.1 Spectrum-Driven Methods

Single-DOF Peak Picking method (PP)

One of the first procedure used to estimate modal parameters is the so-called *SDOF Peak Picking* method (PP). The method is originally based on FRFs curves and consists in identifying the eigenfrequencies as the peaks of the curves. A damping estimate is obtained using the half-power bandwidth method, and the FRFs amplitude at the peak can be considered as an estimate of the mode shape.

The method is probably the easiest and the most widely-used technique for fast modal parameter estimation and has been successfully applied to civil engineering structures, for instance [CCCD99]. Unfortunately, PP method is only effective for low damping and well separated frequencies, and leads to erroneous results in case of violation of these basic requirements. Furthermore, the improvement of the estimation results requires a large amount of interactions with the operator which tends to offset the simplicity of the implementation. These drawbacks exclude the PP method for commercial or industrial purposes.

The method is detailed in most of scientific publications addressing structural dynamics, such as Refs. [MS97, Ewi00]. The PP method is extended to OMA by

using output response power spectra instead of FRFs as proposed in Refs. [BP93, Fel93].

Complex Mode Indicator Function (CMIF)

The *Complex Mode Indicator Function* (CMIF) is a popular spatial-domain modal parameter estimation technique. It utilizes the eigenvalue or Singular Value Decomposition (SVD) of the FRF matrix in order to evaluate the proper number of normal modes that are included in the measurement data ; the idea is developed in [STAB88, PAF98, AB06]. The CMIF method can be considered as the multi-input extension of the PP method and is commonly followed by the *enhanced Mode Indicator Function* (eMIF) to obtain a more accurate estimate of the modal frequencies as well as the corresponding damping ratios, which are not provided by CMIF.

The corresponding extensions of these methods for OMA are the so-called *Frequency Domain Decomposition* (FDD) and *enhanced Frequency Domain Decomposition* (eFDD) methods where output response power spectra simply replace the FRF matrix [BZA00, LFPB98].

Maximum Likelihood identification (ML)

Classical optimization techniques have also been used for modal parameter estimation. The idea is to identify the modal information by minimizing the error norm between a parametric frequency-domain model and the measured data. The methods vary with the objective functions and the optimization algorithms. The use of *Maximum Likelihood* (ML) estimators for this purpose is discussed in Refs. [PGR$^+$94, SP91].

As the aforementioned techniques, the ML method was originally intended for application to FRFs but was extended for output-only cases using power spectra [HGVDA98, GHVDA99]).

If resting on solid mathematical background, the method requires an iterative procedure leading to a high computational load and furthermore needs good initial guesses to avoid local minima, usually obtained by a least squares approach [Ver02]. Its use for large-scale industrial applications might not be advised.

1.4.2 Covariance-Driven Methods

Random decrement (RD)

The *Random Decrement* technique (RD) was introduced in the late 60's by Cole [Col68] and already applied to aerospace structures for failure detection in

the 70's by the American Space Agency [Col71, Col73]. Many civil engineering applications have also been studied using RD [Asm97]. This algorithm is not a modal parameter estimation technique but preprocesses the data in order to feed traditional IRF-based time-domain techniques.

The idea is to average a large number of signal segments, all of them having the same initial displacement, and to assume that both random and impulse responses due to the initial velocity average out. The obtained RD functions are related to output covariances and traditional covariance-driven identification methods can then be applied [Asm97]. For the implementation, the interested reader can refer to [Ibr77].

Natural excitation technique (NExT)

One of the earliest OMA technique, the so-called *Natural Excitation Technique* (NExT), was proposed by James et al. in the 90's for modal testing of vertical-axis wind turbines [JCL93, JCL95]. The objective of NExT is the same as the RD technique, i.e., to convert forced responses due to unknown stationary input to free decays, and is consequently not a proper modal parameter identification technique.

Similarities exist between the mathematical expression of impulse responses and output covariances resulting from a white noise excitation. Indeed, both signals can be expressed as the sum of decaying sinusoids possessing the same modal information [BP93]. Thus, the NExT algorithm uses the auto and cross-correlation functions to produce free decaying responses of the system.

A successful application of NExT requires first that all the modes be sufficiently excited by the unknown input, and second that the acquisition time be long enough. NExT is still used today, as proved by some recent publications [GSDC09, MBCH07, CHT09], and a detailed description of the algorithm is proposed in Chapter 3.

Instrumental variable method (IV)

The *Instrumental Variable* method (IV) is derived from the AutoRegressive Moving Average models (ARMA, see [MS97] for some details). The method is closely related to a well-known EMA technique, the so-called Polyreference Time Domain (PTD) technique, where the impulse responses are substituted by the output covariances [VKRR82].

The PTD method is one of the most widely used output-input based techniques, and contains the Least Squares Complex Exponential (LSCE) [BAZM79] and the Ibrahim Time Domain (ITD) methods as particular cases [IM77].

Unfortunately, the fitting technique used for the PTD identification (and so for the IV method as well) introduces some spurious modes in addition to the genuine ones. A post-processing tool is then required to eliminate these modes before any advanced analysis is done.

Covariance-driven stochastic subspace identification methods (SSI-COV)

The *Stochastic Subspace Identification* methods (SSI) address the so-called stochastic realization problem by identifying a stochastic state-space model from output-only data. These methods identify the modal parameters in an indirect way: a state-space model is characterized, and the modal parameters are derived from the identified system matrices.

Several variants of SSI have been proposed in the literature differing from each other by data pre-processing. For details on the state-space models and their use in modal analysis, the interested reader may refer to [VODM96].

The *Covariance-driven Stochastic Subspace Identification* method (SSI-COV) is one of the most powerful identification techniques using output-only data. Thanks to its remarkable sensitivity and good performance regarding the noise problem, the SSI-COV has been used for many industrial applications, as illustrated in [HVDA99, PDR01, HVDAAG98, GQ04]. The SSI-COV is then used as the reference method in this work in order to evaluate the efficiency of the proposed method. The methodology is described in more details in Sec. 1.5.

It is worth pointing that, as for the IV method, all SSI methods require a post-processing phase to eliminate the numerically-generated spurious modes.

1.4.3 Data-Driven Methods

Data-driven stochastic subspace identification methods (SSI-DATA)

The *Data-driven Stochastic Subspace Identification* method (SSI-DATA) is also a state-space model-based method for output-only modal parameter estimation. As opposed to SSI-COV, SSI-DATA does not require the computation of covariances as data pre-processing. It identifies the model directly from the raw output response time histories. However, a data reduction is obtained by projecting the row space of the future outputs into the row space of the past outputs, which finally makes the SSI-COV much faster than SSI-DATA [PDR01].

The SSI-DATA algorithm was proposed during the early 90's by Van Overschee and De Moor in [VODM93]. Additional information can be found in [VODM96, PDR99, ZBA05, PDR01, Pee00].

The method can be applied to large-scale systems for which the dimension of the matrices is reduced by introducing the idea of the reference sensors [PDR99,

Pee00]. A spectrum-driven variant of SSI was also proposed [VODMD97].

Other time-driven methods

Traditional time-domain algorithms such as the Least Square Complex Exponential (LSCE) [BAZM79]), the Ibrahim Time Domain (ITD) [Ibr77]), the Polyreference Time Domain (PTD) [VKRR82], and the Eigensystem Realization Algorithm (ERA) [JP85, LJ89] can also be used for OMA. In this case, preprocessing methods transforming the forced responses under random excitation into free decays (i.e., NExT or RD techniques for example) have to be considered.

1.4.4 Drawbacks

Most of the widely-used OMA techniques are based on overspecified models in order to fit the data. This overspecification usually leads to better modal parameter estimation, but it also introduces spurious computational modes. A tool is then required to eliminate these spurious modes from the genuine ones.

The *stabilization diagram*, commonly used in commercial softwares, is a traditional way of picking out the genuine modes. The basic idea is to perform several identifications for different model orders. For each considered order, the identified eigenfrequencies are plotted in the diagram in which they can be compared to the poles of the lower-order models. If the variations of the eigenfrequencies, the damping ratios and the mode shapes are lower than preset values, the poles are said to be 'stable'. Finally a pole is identified as genuine if it is stable for several consecutive system orders [MS97, Ewi00].

Even though it is widely used, the stabilization diagram possesses important drawbacks. First, it requires several modal identifications, the number of computed orders being directly related to the number of active modes in the frequency range. Second, the selection of the stabilized modes is time consuming and requires good user's expertise. Therefore the results might vary according to the user interpretation. Figure 1.6 presents an example of a confusing stabilization diagram. As illustrated in recent publications such as [PLLVDA08], finding an automatic procedure for the selection of the modal parameters remains a challenging issue for dynamics operators.

In the last few years, a new frequency-domain-based method has been proposed for OMA purpose. Frequency-domain algorithms are usually not dedicated to OMA, however an output-only variant of the LSCE algorithm, termed the *Polyreference Least Square Complex Frequency-domain* method (PolyMAX), emerged.

The method, originally implemented for experimental modal analysis, was applied to traditional FRF-based experimental data [GVV$^+$03, PVDAG04] and then

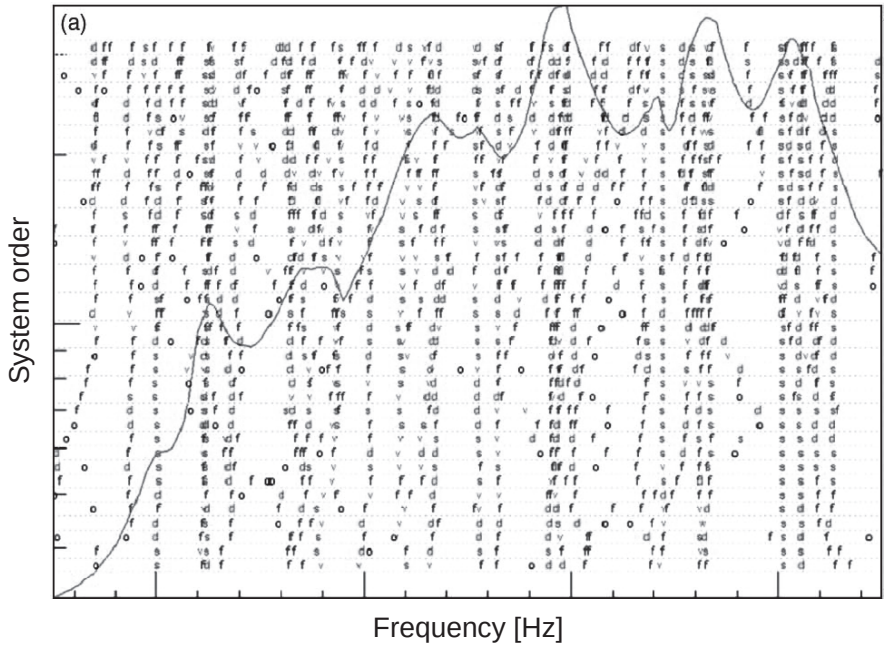

Figure 1.6: **Example of a stabilization diagram** [PLLVDA08]. The stabilization diagram is a post-processing tool for modal analysis. It makes the distinction between genuine and spurious computational modes possible but becomes unclear for high orders and/or systems containing numerous natural frequencies.

extended to OMA [PVDA05]. The objective is to clarify the stabilization diagrams by improving numerical conditioning facilitating their interpretation. Consequently, the method is certainly the most powerful commercial frequency-domain modal analysis algorithm, which is available today.

1.5 Covariance-Driven Stochastic Subspace Identification Method

As already underlined in Sec. 1.4, the SSI-COV method is well-established and is used herein as a reference method in order to evaluate the quality of the results provided by other innovative identification techniques. This section aims at describing the method in more details.

The only information required for the use of SSI-COV method is the recorded time response histories which can be either free or random forced response. The latter simply assumes that the unknown and unmeasurable external forces are uncorrelated random signals. The discrete-time output is provided as n_y-dimensional vector series $\mathbf{y}_k$ where n_y is the number of measured response signals (or sensors), and $\mathbf{y}_k = \mathbf{y}(t_k)$ is the system response measured at the time t_k.

A detailed description of the method can be found in [VODM96, HVDAAG98, HVDA99, AVVODM98, KG05].

1.5.1 State-Space Model

The dynamic behavior of a structure can be described by a stochastic state-space formulation of the form:

$$\begin{aligned} \mathbf{r}_{k+1} &= \mathbf{A}\mathbf{r}_k + \mathbf{w}_k \\ \mathbf{y}_k &= \mathbf{B}\mathbf{r}_k + \mathbf{v}_k \end{aligned} \tag{1.12}$$

where $\mathbf{r}_k$ represents the state vector and $\mathbf{w}_k$ and $\mathbf{v}_k$ are the process and measurement noises (assumed to be zero-mean white Gaussian noise). Matrices $\mathbf{A}$ and $\mathbf{B}$ are the state-space and output matrices, respectively, and completely characterize the system dynamics.

Assuming the knowledge of the matrix $\mathbf{A}$, its eigendecomposition provides the two matrices $\mathbf{\Lambda}$ and $\mathbf{\Phi}$:

- The diagonal matrix $\mathbf{\Lambda}$ contains the discrete eigenvalues $\lambda_r = e^{\mu_r \Delta t}$ from which the system poles μ_r can be extracted;
- The matrix $\mathbf{\Phi}$ contains the system eigenvectors $\boldsymbol{\phi}_r$.

The modal parameters are directly related to these two matrices. The natural frequencies ω_r and the damping ratios ξ_r can be computed directly from the system poles μ_r using

$$\mu_r = \frac{1}{\Delta t} \ln \lambda_r = \sigma_r + i\omega_r \tag{1.13}$$

$$\xi_r = \frac{-\sigma_r}{\sqrt{\omega_r^2 + \sigma_r^2}} \tag{1.14}$$

where σ_r is the damping factor. The shape vector $\mathbf{n}_r$ of the r-th structural mode is deduced from the system eigenvector $\boldsymbol{\phi}_r$

$$\mathbf{n}_r = \mathbf{B}\boldsymbol{\phi}_r \tag{1.15}$$

using matrix $\mathbf{B}$ of the state-space model (1.12).

1.5.2 SSI-COV Implementation

The identification problem consists in estimating the two matrices $\mathbf{A}$ and $\mathbf{B}$ only using the output measurements $\mathbf{y}_k$.

The success of SSI-COV depends first on the quality of the covariance matrices estimation. Since, in practice, the true correlation functions are unknown, empirical values need to be used. A finite set of data samples $\mathbf{y}_k$ at the discrete time instants $k = 1, ..., n_{ts}$ (where n_{ts} represents the number of considered time samples) is used to estimate these matrices. The proposed estimation of the $n_y \times n_y$ correlation matrix $\mathbf{R}_k$ is given by

$$\mathbf{R}_k = \frac{1}{n_{ts} - k} \sum_{m=1}^{n_{ts}-k} \mathbf{y}_{k+m} \mathbf{y}_m^{\top}. \tag{1.16}$$

Once the correlation matrices $\mathbf{R}_k$ are computed, the model order has to be chosen. This order equals the number of frequencies that should be computed in the considered frequency range and depends on the number of blocks of the Hankel matrix.

Indeed, the following block-Hankel matrix

$$\mathbf{H}_{pq} = \begin{bmatrix} \mathbf{R}_1 & \mathbf{R}_2 & \cdots & \mathbf{R}_q \\ \mathbf{R}_2 & \mathbf{R}_3 & \cdots & \mathbf{R}_{q+1} \\ \cdots & \cdots & \ddots & \vdots \\ \mathbf{R}_p & \mathbf{R}_{p+1} & \cdots & \mathbf{R}_{p+q-1} \end{bmatrix} \tag{1.17}$$

is filled up with p block rows and q block columns (with $p \geqslant q$) of the correlation matrices $\mathbf{R}_k$. The numerical system order is given by $(p \cdot n_y)$.

In [HVDA99], it is shown that the observability matrix $\mathbf{O}_p$ is directly related to the matrices resulting from the SVD of this Hankel matrix, namely $\mathbf{U}$ and $\mathbf{S}$

$$\mathbf{H}_{pq} = \mathbf{U}\ \mathbf{S}\ \mathbf{V}^T \tag{1.18}$$

and

$$\mathbf{O}_p = \mathbf{U}\ \mathbf{S}^{1/2}. \tag{1.19}$$

Finally, the definition of the observability matrix

$$\mathbf{O}_p = \mathbf{U}\ \mathbf{S}^{1/2} = \left[\ \mathbf{B} \quad \mathbf{BA} \quad \cdots \quad \mathbf{BA}^{p-1}\ \right]^T \tag{1.20}$$

permits the evaluation of the two state-space matrices $\mathbf{A}$ and $\mathbf{B}$ and the relations between the state-space and the modal models (Sec. 1.5.1) provide the modal parameters.

1.6 Concluding Remarks

The objective of vibration testing is usually twofold. On the one hand, environmental testing encompasses the experimental processes through which an engineering structure is qualified for its future operational environment. On the other hand, modal or operational testing aims at developing a reliable model of the structure matching the experimental measurements for advanced calculations.

While modal testing meets ideal experimental conditions where both output responses and input excitation are measurable, operational conditions assume an unknown and unmeasurable excitation. Numerous techniques have been proposed in the scientific literature since the 40's, each of them including interesting features as well as limitations. The modal parameter estimation techniques based on output-only data, namely operational modal analysis (OMA) are the methods on which this work focuses and some of the most used or well-known OMA techniques have been presented in this chapter. Unfortunately, most of them are based on overspecified system orders to assure a good correlation with the experimental measurements, introducing numerical spurious modes. Therefore, the methods require an interactive post-processing of the results that complicates the identification.

The most generalized post-processing technique, that is commonly used in commercial softwares, is the stabilization diagram. This approach helps the operator to separate the genuine modes from the spurious ones. Nevertheless, the stabilization diagram possesses three main drawbacks:

- First, the modal parameters are computed and identified as many times as considered system orders. This iterative process may lead to high computational load.

- Second, the stabilization diagram analysis can quickly become fastidious in case of complex industrial structures containing numerous natural frequencies.
- Finally, because the user's interpretation is required to extract the genuine modes, an inconsistency between estimates of different operators according their expertise may appear.

In view of the intrinsic limitations of the stabilization diagram approach, the main objective of this doctoral dissertation is to develop a new technique facilitating modal parameter estimation. The proposed methodology is based on blind source separation techniques, detailed in the next chapter.

Chapter 2

Blind Source Separation

Abstract

This chapter introduces the concept of blind source separation. Source separation techniques are based on statistical concepts and aim at revealing the independent components hidden within a set of measured signal mixtures. The theoretical foundations are presented, and two of the algorithms utilized in the next chapters are discussed.

First, Section 2.1 describes the blind source separation problem. The theoretical model is presented and illustrated using simple examples. The related assumptions are then detailed.

Blind source separation techniques have been applied to numerous applications, and many algorithms have been proposed. This is briefly presented in Sec. 2.2.

The following two sections describe two specific techniques, namely the independent component analysis (Sec. 2.3) and the second order blind identification (Sec. 2.4). These methods are used in the following chapters in order to develop new modal parameter estimation methodologies.

Finally, Section 2.5 presents the similarities between blind source separation and proper orthogonal decomposition, that has been previously applied to structural dynamics in the scientific literature.

2.1 Theoretical Background

2.1.1 Concept and Notations

Blind Source Separation (BSS) techniques were initially developed in the early 80's for signal processing in the context of neural network modeling. During the last two decades, numerous studies were achieved on this topic diversifying the application fields. This success certainly comes from two of the BSS intrinsic features:

- First, the ambition of any BSS technique is to reveal the underlying structure of a set of observed phenomena (e.g., random variables, measurements or signals). Recovering initial (and unobservable) signals from measured data is a generic problem in many domains.
- Secondly, a small number of assumptions is required about the signals. The term 'blind' means that the source signals are extracted from the rough data even though very little, if anything, is known about the nature of those initial components. The methods are said to be versatile in the sense that the analyzed data can originate from various domains, and that no a priori knowledge is required about the physical phenomenon of interest.

The desired signals, denoted **s**, are named *sources* or *components* of the system. They are of primary interest because they concentrate the valuable information of the system. Unfortunately, this information is diluted within the measured signals, denoted **x**, that are essentially *mixtures* of the sources.

The simplest BSS model assumes the existence of n_s sources $\{s_1(t)...s_{n_s}(t)\}$ and the observation of as many mixtures $\{x_1(t)...x_{n_x}(t)\}$, where $n_x = n_s$. This is illustrated in Fig. 2.1.

The next paragraph presents the theoretical BSS model but the interested reader could find a nice introduction to BSS and ICA techniques in [Sto04]. Some additional information is also provided in Refs. [HKO01, HO00, CDLD05].

2.1.2 The BSS Model

Although convolutive and nonlinear mixtures can be considered, this work focuses on linear and static mixtures for which BSS is well established. Mathematically, a generative model can be defined as follows

$$\mathbf{x}(t) = \mathbf{A}\mathbf{s}(t), \tag{2.1}$$

where the observed data $\mathbf{x}(t)$ are assumed to be linear combinations of unknown sources $\mathbf{s}(t)$. The matrix $\mathbf{A}$ is referred to as the *mixing matrix*. Using the subscript

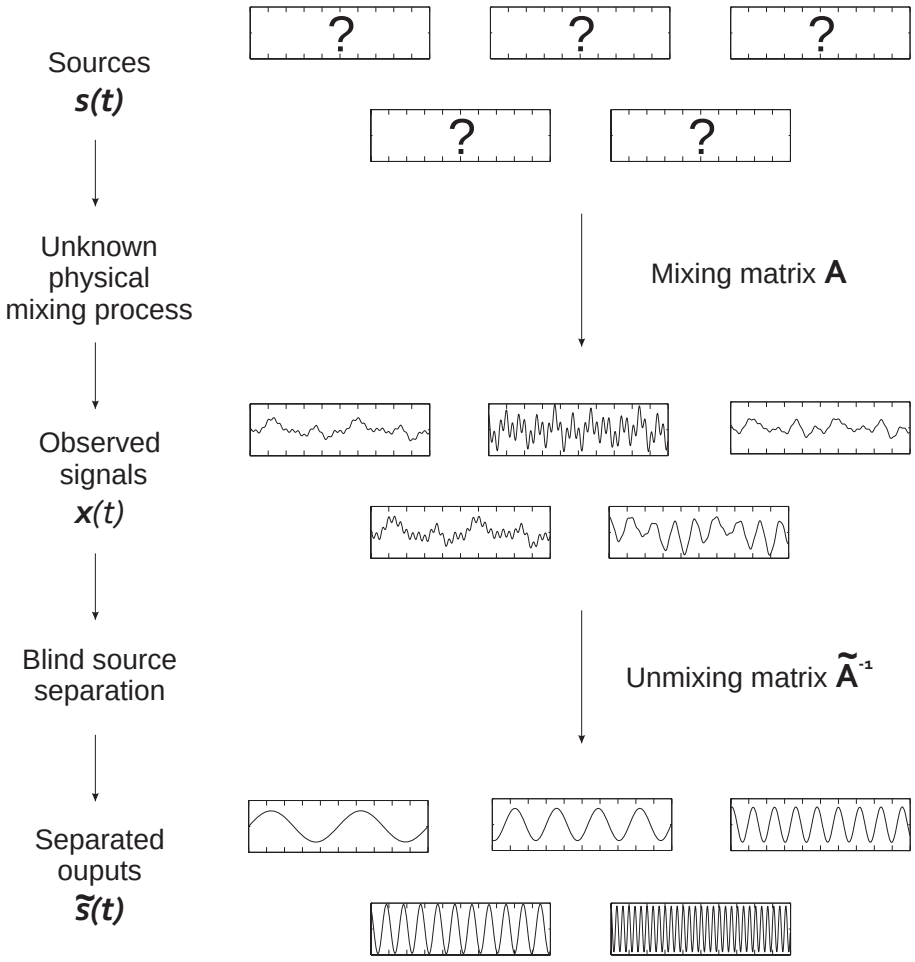

Figure 2.1: **Illustration of a generic BSS process**. Independent sources are mixed through unknown physical process. The resulting mixtures are the observable information. BSS techniques tempt to recover the initial signals using very few information about the sources and the mixing process.

notation, (2.1) can be written as

$$x_i(t) = \sum_{j=1}^{n_s} a_{ij} s_j(t). \tag{2.2}$$

Knowing the signals $\mathbf{x}(t)$, the BSS problem then consists in estimating the sources. Because both mixing coefficients a_{ij} and sources s_i are unknown, the estimation problem is considerably more difficult.

Noise may also corrupt the data and, in this case, the noisy model can be expressed as

$$x_i(t) = \sum_{j=1}^{n_s} a_{ij} s_j(t) + \sigma_{noise,i}(t) \quad i = 1, ..., n_x, \tag{2.3}$$

or, in matrix form,

$$\mathbf{x}(t) = \mathbf{y}(t) + \boldsymbol{\sigma}_{noise}(t) = \mathbf{A}\,\mathbf{s}(t) + \boldsymbol{\sigma}_{noise}(t), \tag{2.4}$$

where $\boldsymbol{\sigma}_{noise}$ is the noise vector corrupting the data.

By way of generalization, note that BSS techniques are not restricted to time variables, any random distribution can be considered. Nevertheless, all the variables of interest in this dissertation are time-dependent.

2.1.3 Illustration of the BSS Objective

The objective of the BSS techniques can be adequately illustrated with the so-called *cocktail party* example. The problem is illustrated in Fig. 2.2 and consists in several people speaking at the same time in a room where microphones are installed. Every single microphone records a mixture of the speech signals (i.e., a mixture of independent physical sources).

Discerning a specific sound in a noisy environment is a practical example of the BSS concept and is a common task that humans naturally apply all along the day. The BSS-algorithm job is then to imitate the human ear's capability of isolating a specific voice from the others.

It is physically realistic to assume that if different signals originate from different physical processes, they are unrelated. Mathematically, the property of 'unrelatedness' can be captured in terms of *statistical independence*. Two random variables x_1 and x_2 are said to be independent if the value of any one of them cannot be inferred from the value of the other one. In other terms, their joint density function factorizes into the product of their marginal densities such as

$$p_{x,y}(x, y) = p_x(x) p_y(y). \tag{2.5}$$

The key strategy for separating the signal mixtures is based on the fact that:

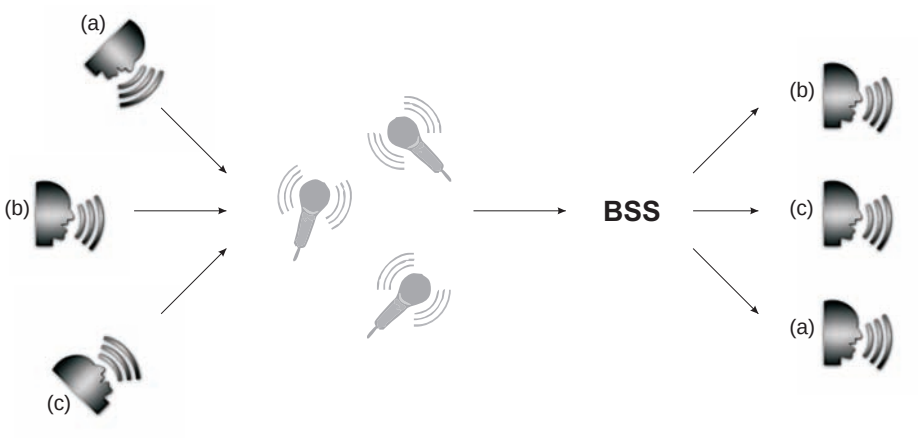

Figure 2.2: **BSS applied to the cocktail party problem.** Three people speaking at the same time in a room are recorded using three microphones. The recorded signals are mixtures of the individual voices. BSS techniques are able to separate the initial signals from the recorded mixtures.

	f_i [Hz]	A_i [-]	ϕ_i [s]
Sine 1	1.000	$5 \cdot 10^{-6}$	1.88
Sine 2	2.300	$5 \cdot 10^{0}$	0.58
Sine 3	4.100	$5 \cdot 10^{0}$	0.75
Sine 4	4.105	$5 \cdot 10^{0}$	0.23
Sine 5	15.000	$5 \cdot 10^{0}$	1.93

Table 2.1: Parameters of the five sine curves used as sources for the BSS problem illustration.

> *if different physical sources lead to statistically-independent signals then the signals extracted from the mixtures that verify the statistical independence property should be issued from different physical processes.*

In other words, using the microphone records, if an algorithm is able to extract statistically-independent signals, they should be the speech signals emitted by different speakers.

This new assumption, which sets the foundation of all BSS methods, is not mathematically demonstrated and is consequently unwarranted, but nevertheless works in practice.

By way of clarification, BSS techniques aim at separating signal mixtures into statistically independent signals, and each of them is a desired interpretable signal because it is generated by a different physical process.

Numerical example

For illustration, a BSS algorithm, namely the Second-Order Blind Identification, is applied to a simple numerical example: a signal that is a mixture of five sine curves expressed as

$$s_i = A_i \cdot \sin(2\pi f_i t + \phi_i). \tag{2.6}$$

The sine parameters are provided in Table 2.1 and were chosen to emphasize some interesting features of the methodology.

First, in order to prove the accuracy of the method even in the presence of similar signals, some of the sine frequencies f_i are chosen to be very close to each other (e.g., the relative distance between f_3 and f_4 is lower than 0.13%).

Second, one of the considered sources (sine 1) has an amplitude A_1 much lower than the other signals. The participation of this source is then very low (i.e., 10^6 times less than the others). This should underline the high sensitivity of BSS methods for weakly-participating signals.

Figure 2.3 presents both mixtures and identified sources where it can be noticed that all the sources are accurately separated. However, neither the source order nor the source amplitude is correctly identified. These indeterminacies are addressed in the next paragraphs.

2.1.4 Assumptions and Restrictions

According to the previous considerations, the separation processes considered in this work are restricted to the following assumptions:

- The sources are assumed as *statistically independent*. The mathematical definition of statistical independence, based on the joint probability density functions, is recalled in Eqn. (2.5).

- The unknown *mixing matrix is usually assumed to be square*. The number n_x of sensors is then assumed to be equal to the number n_s of sources. Note that this assumption could be relaxed [DLDMVC03, JML00].

2.1.5 Indeterminacies

Because both sources $\mathbf{s}$ and mixing matrix $\mathbf{A}$ are unknown, the following two indeterminacies remain after applying a separation algorithm.

- The effect of any scalar multiplier α_j applied to one of the sources $s_j(t)$ can always be canceled by scaling the corresponding column $\mathbf{a}_j$ of the mixing matrix using the inverse parameter $1/\alpha_j$. Mathematically, this means that Eqn. (2.2) can be identically transformed as

$$x_i(t) = \sum_{j=1}^{n_s} \left(\frac{1}{\alpha_j} \cdot a_{ij} \right) (\alpha_j \cdot s_j(t)) \,. \tag{2.7}$$

  Therefore, *the variance of the sources cannot be determined and is usually normalized* assuming unit-variance sources (i.e., $E\left[s_i^2(t)\right] = 1$, $i = 1, ..., n$).

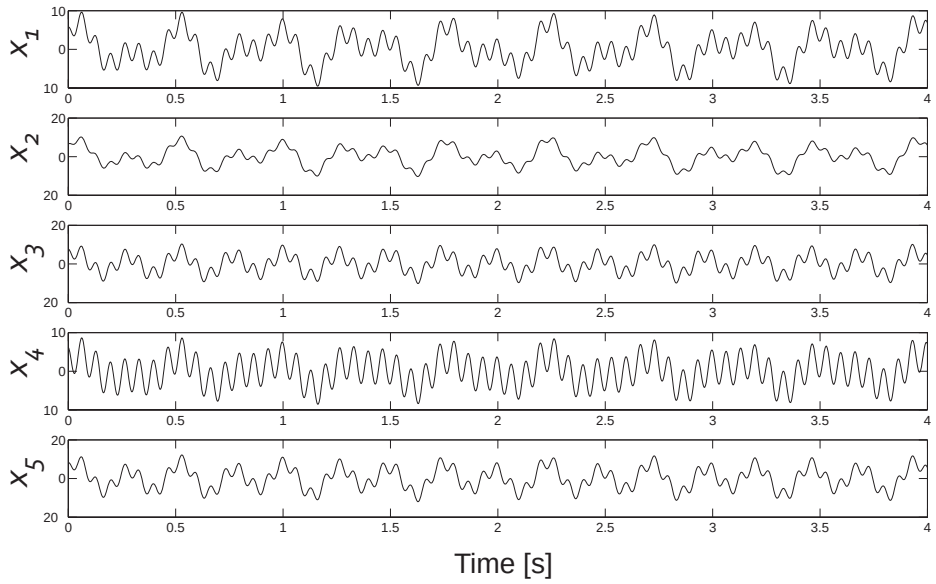

(a) Observed mixtures

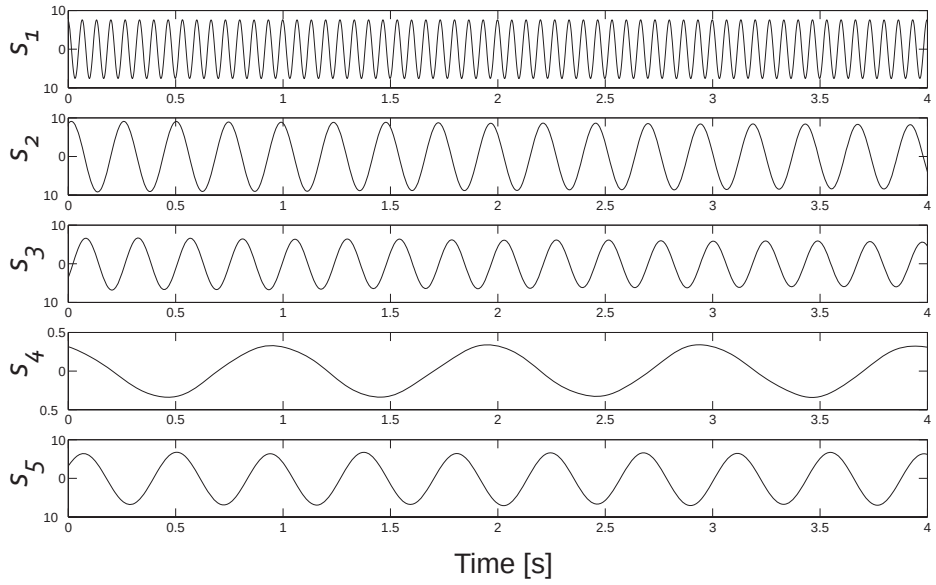

(b) Identified sources

Figure 2.3: **BSS example** using the Second-Order Blind Identification algorithm. The five sources are sines with the following frequencies: 1, 2.3, 4.1, 4.105 and 15 Hz.

- Similarly, any permutation $\mathbf{P}$ of the columns of the mixing matrix can be balanced by a permutation of the source order

$$\mathbf{x} = \mathbf{A}\mathbf{s} \quad \Longleftrightarrow \quad \mathbf{x} = \mathbf{A}\mathbf{P}^{-1}\mathbf{P}\mathbf{s}. \tag{2.8}$$

  The *order of the sources* is then also *undetermined*.

2.2 Literature Survey

2.2.1 Application Fields

Due to its general formulation, BSS has been applied to diverse kinds of problems. According to Hyvärinen et al. [HKO01] and Jutten [Jut00], the problem first came out in 1982 in a neurophysiological environment. Since then, many signals issued from medical applications were analyzed using BSS. For instance, brain imaging applications, in which many sources in the brain emit signals that are mixed up in the sensors outside the head, are studied by Jung et al. in [JMM$^+$01] (for hemodynamic recordings from the human brain) and by Vigãrio et al. in [VSJ$^+$00] (for electroencephalography and magnetoencephalography signal separation).

BSS techniques also performed well for the analysis of multivariate data sets such as financial time series (in order to minimize the risk in the investment strategy [BW97]), astrophysical data sets (helping the detection of Cosmic Microwave Background fluctuations [PDC04]), telecommunication signals [FK99] and digitized natural images [HO00].

Of course, BSS similarly benefits to mechanical engineering, where the issue of determining the nature of unknown sources from exogenous measurements has always been a major concern. A special issue dealing with BSS was published in 'Mechanical Systems and Signal Processing' in 2005 where several applications of BSS are presented [AB05]. Rotating machines and bearing diagnostics [ERFGD05, PBZ05], non-destructive control [SVIG05], online monitoring [PSL05] or noise analysis of diesel engine [EBDGS05] are some of these interesting applications.

Even though BSS techniques proved useful in numerous application domains, they were quite underused for many years in structural dynamics. If it is promising, the application of BSS in structural dynamics still remains a challenge, as pointed out by Antoni in Ref. [Ant05]. The reason is that the time response of mechanical systems is related to the physical excitation through a convolutive mixture, contrary to the static mixtures usually studied, cf. Eqn. (2.1). This particular case of source separation is much more difficult to treat than the usual static mixture and is addressed, among others, in Refs. [TJ95, BAK05, BAK04].

Some applications were naturally carried out such as damage detection [ZFI04], condition monitoring [RES02, SF04] and discrimination between pure tones and sharp-pointed resonances [AGMS04]. Nevertheless, the modal parameter estimation remained quite marginal in these studies.

2.2.2 Algorithms

A complete overview of the existing BSS techniques is beyond the scope of this work. A brief survey of the subject is only proposed in this section, but the interested reader may consult Refs. [CCPL05, RE01, Sto04] for more details.

The few number of assumptions over the recorded channels and the sources makes the methodology very attractive, and several approaches have been proposed. They differ from each other, on the one hand, by the objective function, the so-called 'contrast' function, representing the independence of the identified sources and, on the other hand, by the algorithm used to optimize this function. However, as it is the case of tensorial methods, the algorithm and the estimation function may be difficult to separate.

A fundamental approach to BSS is given by the principle of non-Gaussianity, providing a representation of the signals independence as explained in [HKO01]. Statistical concepts such as kurtosis and negentropy (or any approximate of them) can estimate the non-Gaussianity [DL95, Hyv99] ; gradient methods or fixed-point algorithms can thus profitably be used to maximize the latter. For instance, algorithms such as Independent Component Analysis (ICA) or FastICA can be based on these notions [HO97, CDLD05, LKL07].

Maximum likelihood estimation, that is a fundamental method of statistical estimation, is a popular approach for estimating the BSS model. Maximization techniques such as the Bell-Sejnowski or the natural gradient algorithms can be used for the separation [HKO01] but FastICA could also be considered. Algorithms using this approach are detailed and explained notably in [Car97, OD98, PP97, PG97].

Mutual information is a natural information-theoretic measure of dependence and its minimization leads to estimate the independent components. The variant of ICA used in this work is based on the mutual information minimization (see Sec. 2.3). The concept has first been proposed by Common in Ref. [Com94], but originally comes from neural network studies, and was then developed in [YA97, OD98].

BSS models may also be obtained by making zero the higher-order cumulants. Cumulant tensors used in this case can be considered as generalizations of the covariance matrix and then leads to higher-order decorrelation of the signals. The Fourth-Order Blind Identification (FOBI) is probably the simplest method for performing blind source separation and is very efficient, but it suffers some limitations

[Car89, CM96]. The Joint Approximate Diagonalization of Eigenmatrices (JADE) partially fixes them [CS93].

Finally, as it is the case for the Second-Order Blind Identification (SOBI), the BSS problem may be simplified by taking into account the time structure of the data. SOBI is based on a joint diagonalization of time-lagged covariance matrices. The AMUSE algorithm is a simplified version of SOBI where only one time-lag is considered [TLSH91, MS94].

Extended methodologies dealing with over-completed bases (i.e., the number of mixtures is smaller than the number of independent sources), noisy data or convolutive mixtures have also been developed in the scientific literature. More information on these subjects can be found in [HKO01, RE01].

In order to test the BSS techniques in the field of modal analysis, two specific algorithms are considered herein: ICA and SOBI.

- Most BSS approaches are based on a model in which the sources are independent and identically distributed variables. *Independent Component Analysis* (ICA) algorithm detailed by Comon in [Com94], is one of them. One of its characteristics is that the sample order has no importance in the method.

- The objective of the *Second-Order Blind Identification* (SOBI) method is to take advantage, whenever possible, of the temporal structure of the sources for facilitating their separation. The SOBI algorithm consists in constructing several time-lagged covariance matrices from the measured data and to find a matrix which jointly diagonalizes them.

2.3 Independent Component Analysis (ICA)

2.3.1 Concept and Notations

ICA was first introduced by Jutten and Herault in 1991 [JH91]. The method is arguably the most popular in the scientific literature for performing source separation. To alleviate the lack of a priori knowledge about the mixtures, ICA assumes that the observed data are linear combinations of statistically independent (or as independent as possible) sources.

The method uses high-order statistical concepts to separate the independent components and estimate the ICA model. Because higher-order cumulants are known to be zero for Gaussian distributions, ICA-based separation is mostly impossible if the observed variables have such a statistical distribution. Thus, the sources must have *non-Gaussian distributions* to be able to separate the signals.

If some of the components are Gaussian, they are simply not separated from the others.

The sources $\mathbf{s}$ are termed *Independent Components* (ICs), and the ICA basis vectors (i.e., the columns of the mixing matrix $\mathbf{A}$) are referred to as *ICA modes* in the present study. ICA modes are linearly independent, but their orthogonality is not enforced. This contrasts with other well-known separation methods in structural dynamics such as the Proper Orthogonal Decomposition [HLB96]. A comparison between both methodologies is proposed in Sec. 2.5.

Note that various algorithms have been developed for ICA in the literature. They differ mainly by the contrast function. This contrast function can be based on kurtosis, negentropy, likelihood or mutual information to cite a few [Com94, PGJ92, BS95, DLDMV96, HKO01].

The interested reader may consult Refs. [HKO01, HO00, Sto04, Com94, Car98] for the implementation of ICA and the practical estimation of the ICs.

2.3.2 Maximization of non-Gaussianity

Non-Gaussianity and statistical independence are closely related to each other. This is the reason why the maximization of non-Gaussianity is one of the way of estimating ICA models. The motivation of this idea comes from the central limit theorem:

> *"Under certain conditions, the distribution of a sum of independent random variables tends toward a gaussian distribution"*

The ICA principle can be explained as follows. Considering a linear combination of the observed data

$$\alpha = \mathbf{w}^T \mathbf{x}, \tag{2.9}$$

if these observed data are assumed to respect the BSS formulation (2.1), they can be expressed as

$$\alpha = \mathbf{w}^T \mathbf{A} \mathbf{s} = \mathbf{z}^T \mathbf{s}, \tag{2.10}$$

where $\mathbf{z} = \mathbf{A}^T \mathbf{w}$, and the combination $\mathbf{w}$ is to be determined.

According to the central limit theorem, a sum of two independent random variables is more Gaussian than any of the two original random variables. It follows that $\mathbf{z}^T \mathbf{s}$ is more Gaussian than any of the sources, except when $\mathbf{z}$ has only one nonzero element. Consequently, by maximizing the non-Gaussianity of $\mathbf{z}^T \mathbf{s}$, or equivalently of $\mathbf{w}^T \mathbf{x}$, the convergence toward one of the ICs is guaranteed.

Subsequently, the use of the previous principle to separate the ICs requires a quantitative measure of the non-Gaussianity. The traditional fourth-order cumulant, namely the kurtosis, is one of the simplest statistical instruments indicating

the non-Gaussianity of a random variable. The value of the kurtosis is zero for a Gaussian distribution and nonzero for non-Gaussian random variables.

The kurtosis of a random variable y is simply a normalized version of the fourth moment $E\{y^4\}$, and is denoted kurt(y):

$$\text{kurt}(y) = E\{y^4\} - 3\left(E\{y^2\}\right)^2 \tag{2.11}$$

Unfortunately, the kurtosis is not a robust measure of non-Gaussianity, because it is very sensitive to outlier values and to erroneous or irrelevant observations. Furthermore, its evaluation requires a high computation load preventing it to be used within an iterative process.

2.3.3 Minimization of Mutual Information

The ICA algorithm used in the present study is based on the mutual information minimization philosophy. It can be shown that mutual information is a natural measure of the dependence between random variables. It takes into account the whole dependence structure of the variables.

Hyvärinen et al. demonstrate in Ref. [HKO01] that the minimization of mutual information is equivalent to maximizing the sum of non-Gaussianities of the ICs estimates. However, the estimates $\tilde{s}_i$ are constrained to be uncorrelated. The mutual information is usually easier to compute than kurtosis and its minimization provides accurate results.

A complete description of the "information theory" is not the goal of this work but additional information can be found in Ref. [CDLD05].

2.4 Second Order Blind Identification (SOBI)

2.4.1 Formulation of the Problem

Most BSS approaches are based (explicitly or not) on a model in which the sources are independent and identically-distributed variables. Therefore, the sample order has no importance. Shuffling them does have effect neither on the estimation method nor on the accuracy of the model. The problem is quite different if the sources are time-dependent signals, because they may contain much more structure than simple random variables.

If the time structure is considered, a different approach is then possible. The objective of SOBI algorithm is to take advantage, whenever possible, of this structure to facilitate the signal separation. SOBI is therefore an interesting alternative to ICA for sources with different spectral contents, and this is usually the case in

structural dynamics. As suggested by its name, the method is based on second-order statistical data that are the covariances. As opposed to the case of pure random variables, the autocovariance properties are well-defined for time signals.

Considering a set of observed signals $\mathbf{x}(t)$, the *covariances* between two different signals $x_i(t)$ and $x_j(t)$

$$\mathrm{cov}\left(x_i(t+\tau)\ x_j(t)\right) \text{ where } i \neq j \tag{2.12}$$

and the *autocovariances*, which are the covariances between the values of the same signal $x_i(t)$ at different time steps,

$$\mathrm{cov}\left(x_i(t+\tau)\ x_i(t)\right) \tag{2.13}$$

are two basic information about the time structure, where τ is the time-lag or delay.

The so-called *time-lagged covariance matrix* combines all these quantities for a given time-lag τ and is defined as

$$\mathbf{C}_\tau^{\mathrm{x}} = E\left\{\mathbf{x}(t+\tau)\ \mathbf{x}^\star(t)\right\} \tag{2.14}$$

where the superscript $\star$ denotes the conjugate transpose of the vector $\mathbf{x}$.

Since SOBI is based on the diagonalization of time-lagged covariance matrices, it relies entirely on second-order statistics. This is an advantage compared to ICA techniques, because higher-order statistics computation is known to be time consuming and even misleading in the case of scarce data. Moreover, the introduction of the time structure by means of the autocovariance properties relaxes the assumption of non-Gaussian distribution for the ICs, meaning that autocovariances are a simple option replacing non-Gaussianity [HKO01]. Of course, some alternative assumptions (differing from non-Gaussianity and based on the time structure of the ICs) are required for the estimation. In the case of SOBI, each source must have different and nonzero autocovariances.

A complete description of the method is proposed by Belouchrani et al. in Ref. [BAMCM97].

A simple decorrelation of the observed signals $\mathbf{x}(t)$ can be assured simply by imposing the instantaneous covariances (i.e., covariances where $\tau = 0$) to be zero. The resulting signals are then such that

$$\mathbf{C}_\tau^{\mathrm{x}} = 0 \qquad \text{for } \tau = 0 \tag{2.15}$$

Nevertheless, just the correlation matrix $\mathbf{C}_{\tau=0}^{\mathrm{x}}$ (i.e., a zero-lagged covariance matrix) does not contain enough information for the separation. In fact, due to the independence property of the ICs, all their lagged covariances, and not only one, should be zero according to

$$\mathbf{C}_\tau^{\mathrm{x}} = 0 \qquad \forall\tau \tag{2.16}$$

The SOBI problem is then to find a matrix $\mathbf{B}$ which can be applied to the observed measurements $\mathbf{x}(t)$ in such a way that

$$\mathbf{z}(t) = \mathbf{B}\mathbf{x}(t) \tag{2.17}$$

so that all the lagged covariances are zero as well. That means:

$$E\left\{z_i(t+\tau)\ z_j(t)\right\} = 0 \text{ for all } i, j \text{ and } \tau. \tag{2.18}$$

2.4.2 Algorithm Description

The starting point of the method is still Eqn. (2.4) which is recalled hereafter:

$$\mathbf{x}(t) = \mathbf{y}(t) + \boldsymbol{\sigma}_{noise}(t) = \mathbf{A}\,\mathbf{s}(t) + \boldsymbol{\sigma}_{noise}(t). \tag{2.19}$$

When the sources are stationary, mutually uncorrelated and scaled to have unit variance, their covariance matrix is provided by

$$\mathbf{C}_0^{\mathrm{s}} = E\{\mathbf{s}(t)\mathbf{s}^{\star}(t)\} = \mathbf{I}. \tag{2.20}$$

The covariance matrix of the observed mixtures is then provided by

$$\begin{aligned} \mathbf{C}_0^{\mathrm{x}} &= E\left\{\mathbf{x}(t)\mathbf{x}^{\star}(t)\right\} \\ &= \mathbf{A}\mathbf{C}_0^{\mathrm{s}}\mathbf{A}^H + E\left\{\boldsymbol{\sigma}_{noise}(t)\boldsymbol{\sigma}^{\star}_{noise}(t)\right\} \\ &= \mathbf{A}\mathbf{A}^H + \sigma^2_{noise}\mathbf{I} \end{aligned} \tag{2.21}$$

where the superscript H denotes the complex conjugate transpose of the matrix $\mathbf{A}$. The additive noise $\boldsymbol{\sigma}_{noise}$ is assumed to be a stationary, temporally and spatially white random process independent of the source signals.

Thus, there must be two steps in the SOBI algorithm [BAMCM97]:

- The *whitening* preprocesses the observed data in such a way that whitened data are uncorrelated and have a unit variance;
- The *estimation of the mixing matrix* $\mathbf{A}$ allows the sources $\mathbf{s}(t)$ to be identified.

Whitening

Traditionally the data are likewise preprocessed for all source separation algorithms. This phase is strongly recommended because reducing the number of free parameters and increasing the performance of the methods, especially for high-dimensional data.

Whiteness is a slightly stronger property than uncorrelatedness. The whitening transformation consists in transforming a data vector $\mathbf{q}$ by linearly multiplying it with a matrix $\mathbf{W}$ such that a new vector $\mathbf{q}_w$ is obtained

$$\mathbf{q}_w = \mathbf{W}\mathbf{q}. \tag{2.22}$$

The random vector $\mathbf{q}_w$ is white if its components are uncorrelated and their variance equal to unity, mathematically

$$E\left\{\mathbf{q}_w\ \mathbf{q}_w^\star\right\} = \mathbf{I} \tag{2.23}$$

Thus, if the linear transformation $\mathbf{W}$ is applied to the observed data $\mathbf{y}(t)$ where noise is assumed to be nonexistent, the resulting whitened data $\mathbf{y}_w(t)$ are uncorrelated and have unit variance. They verify

$$\begin{aligned} \mathbf{C}_0^{\mathrm{y}_w} &= E\{\mathbf{y}_w\mathbf{y}_w^\star\} \\ &= E\left\{\mathbf{W}\mathbf{y}(t)\mathbf{y}^*(t)\mathbf{W}^H\right\} \\ &= \mathbf{I}. \end{aligned} \tag{2.24}$$

Whitened data facilitates the mixing matrix identification. Indeed, thanks to Eqns. (2.4) and (2.20), it comes

$$\begin{aligned} \mathbf{C}_0^{\mathrm{y}_w} &= E\left\{\mathbf{W}\mathbf{y}(t)\mathbf{y}^*(t)\mathbf{W}^H\right\} \\ &= \mathbf{W}\mathbf{A}E\left\{\mathbf{s}(t)\mathbf{s}^*(t)\right\}\mathbf{A}^H\mathbf{W}^H \\ &= \mathbf{W}\mathbf{A}\mathbf{C}_0^{\mathrm{s}}\mathbf{A}^H\mathbf{W}^H \\ &= \mathbf{W}\mathbf{A}\mathbf{A}^H\mathbf{W}^H \end{aligned} \tag{2.25}$$

If $\mathbf{y}_w(t)$ are whitened, Eqn. (2.24) is verified, and it follows that

$$\mathbf{W}\mathbf{A}\mathbf{A}^H\mathbf{W}^H = \mathbf{I} \tag{2.26}$$

Because an identity matrix $\mathbf{I}$ can always be expressed in terms of a unitary matrix $\mathbf{U}$ such as $\mathbf{I} = \mathbf{U}\mathbf{U}^H$, it comes

$$\mathbf{W}\mathbf{A}\mathbf{A}^H\mathbf{W}^H = \mathbf{U}\mathbf{U}^H. \tag{2.27}$$

Finally, it can be concluded that, for any whitening matrix $\mathbf{W}$, there exists a unitary matrix $\mathbf{U}$ such that

$$\mathbf{U} = \mathbf{W}\mathbf{A}. \tag{2.28}$$

Two straightforward solutions for whitening are the Principal Component Analysis (PCA) expansion [Jol86] and the Eigenvalue Decomposition (EVD). Starting

from the matrix $\mathbf{C}_0^{\mathrm{y}}$ (i.e., the instantaneous covariance matrix of the observed data $\mathbf{y}(t)$), the EVD provides the matrix $\mathbf{V}$ whose columns are the unit-norm eigenvectors and the diagonal matrix $\mathbf{D}$ of the eigenvalues according to

$$\mathbf{C}_0^{\mathrm{y}} = E\left\{\mathbf{y}\ \mathbf{y}^{\star}\right\} = \mathbf{V}\mathbf{D}\mathbf{V}^{H}. \tag{2.29}$$

The whitening matrix is then provided by

$$\mathbf{W} = \mathbf{D}^{-1/2}\mathbf{V}^{H}. \tag{2.30}$$

The matrix $\mathbf{W}$ applied to $\mathbf{y}(t)$ creates a set of whitened data $\mathbf{y}_w(t)$. This can be proved as follows

$$\begin{aligned} E\left\{\mathbf{y}_w\mathbf{y}_w^{\star}\right\} &= \mathbf{W}E\left\{\mathbf{y}\mathbf{y}^{\star}\right\}\mathbf{W}^{H} \\ &= \mathbf{W}\mathbf{V}\mathbf{D}\mathbf{V}^{H}\mathbf{W}^{H} \\ &= \mathbf{D}^{-1/2}\mathbf{V}^{H}\mathbf{V}\mathbf{D}\mathbf{V}^{H}\mathbf{V}\mathbf{D}^{-1/2} \\ &= \mathbf{I}. \end{aligned} \tag{2.31}$$

When noise is present, i.e. when $\mathbf{x}(t) \neq \mathbf{y}(t)$, and is such that Eqn. (2.21) is valid, the whitening process $\mathbf{x}_w(t) = \mathbf{W}\mathbf{x}(t)$ is such that

$$\begin{aligned} E\left\{\mathbf{x}_w(t)\mathbf{x}_w^{\star}(t)\right\} = \mathbf{C}_0^{\mathrm{z}} &= E\left\{\mathbf{W}\mathbf{x}(t)\mathbf{x}^{\star}(t)\mathbf{W}^{H}\right\} \\ &= \mathbf{W}\mathbf{A}\mathbf{A}^{H}\mathbf{W}^{H} + \mathbf{W}\sigma_{noise}^2\mathbf{W}^{H} \\ &= \mathbf{W}\left(\mathbf{C}_0^{\mathrm{x}} - \sigma_{noise}^2\mathbf{I}\right)\mathbf{W}^{H} + \mathbf{W}\sigma_{noise}^2\mathbf{W}^{H} \\ &= \mathbf{W}\mathbf{C}_0^{\mathrm{x}}\mathbf{W}^{H} \end{aligned} \tag{2.32}$$

This shows that a whitening matrix $\mathbf{W}$ can be determined from the covariance matrix $\mathbf{C}_0^{\mathrm{x}}$ under the assumption that the noise is spatially white. As explained in [BAMCM97], this assumption is not crucial and the determination of a whitening matrix is still possible even in the case of an unknown noise covariance matrix.

Mixing matrix estimation

The goal of the second step is the estimation of the unitary matrix $\mathbf{U}$, and consequently the mixing matrix $\mathbf{A}$, thanks to the relation (2.28). To this end, time-lagged covariance matrices based on the whitened data are considered

$$\begin{aligned} \mathbf{C}_{\tau}^{\mathrm{x}_w} &= E\left\{\mathbf{x}_w(t+\tau)\mathbf{x}_w^{\star}(t)\right\} \\ &= \mathbf{W}E\left\{\mathbf{x}(t+\tau)\mathbf{x}^{\star}(t)\right\}\mathbf{W}^{H} \\ &= \mathbf{W}\mathbf{A}E\left\{\mathbf{s}(t+\tau)\mathbf{s}^{\star}(t)\right\}\mathbf{A}^{H}\mathbf{W}^{H} \qquad \forall\tau \neq 0 \end{aligned} \tag{2.33}$$

leading to

$$\mathbf{C}_{\tau}^{\mathrm{x}_w} = \mathbf{U}\mathbf{C}_{\tau}^{\mathrm{s}}\mathbf{U}^{H} \qquad \forall\tau \neq 0 \tag{2.34}$$

where $\mathbf{C}_\tau^{\mathrm{s}} = E\left\{\mathbf{s}(t+\tau)\mathbf{s}^\star(t)\right\}$ is the time-lagged covariance matrix of the sources $\mathbf{s}(t)$.

Because $\mathbf{U}$ is a unitary matrix and $\mathbf{C}_\tau^{\mathrm{s}}$ is diagonal, the relation (2.34) shows that *any whitened covariance matrix* $\mathbf{C}_\tau^{\mathrm{x}w}$ *is diagonalized by the unitary transform* $\mathbf{U}$ [BAMCM97]. It turns out that the matrix $\mathbf{U}$ can be determined through an eigenvalue decomposition of the time-lagged whitened covariance matrix.

The mixing matrix $\mathbf{A}$ is easily computed, since $\mathbf{U} = \mathbf{WA}$, and so are the sources, since $\mathbf{x}(t) = \mathbf{A}\mathbf{s}(t)$.

The diagonal elements of $\mathbf{C}_\tau^{\mathrm{s}}$ must be different in order that $\mathbf{C}_\tau^{\mathrm{x}w}$ have distinct eigenvalues and uniquely defined eigenvectors. Therefore, the time lag τ must be chosen carefully. Cardoso et al. have shown that robustness of the method is significantly increased when several time lags τ are considered [BAMCM97]. On the one hand, an unfortunate choice of the time lag is less probable. On the other hand, the matrix $\mathbf{U}$ is inferred from a larger set of statistics.

As a result, during the second step of the SOBI algorithm, several time-lagged covariance matrices $\mathbf{C}_\tau^{\mathrm{x}w}$ are jointly diagonalized. For information, the simultaneous diagonalization is carried out using an extension of the Jacobi technique [CS96].

For further details about the mathematical development of the SOBI method, the reader can refer to Ref. [BAMCM97]. If only one time lag τ is considered, the SOBI method reduces to the AMUSE method, introduced by Tong et al. in Ref. [TLSH91].

2.5 BSS and Other Statistical Approaches

Besides BSS techniques, empirical statistical approaches have been used over the last years in the field of structural dynamics. The Proper Orthogonal Decomposition technique (POD), that is a variant of PCA for dynamical systems [KGVB05], is one of them and can be closely related to the BSS approach.

In fact, POD and BSS are two different ways of solving the same basic problem

$$\mathbf{x} = \mathbf{A}\mathbf{s} \tag{2.35}$$

but both techniques are simply based on different assumptions. POD could be considered as a blind technique assuming that the original sources $\mathbf{s}$ are uncorrelated whereas BSS assumes their statistical independence.

The basic idea of POD is to reduce the large number of the observed interdependent variables $\mathbf{x}(t)$ to a more readable and eventually smaller number of uncorrelated variables, while retaining as much as possible of the information present in the original variables.

The transformation is performed using an orthogonal transformation to the basis of the eigenvectors of the sample covariance matrix. The data are projected onto the subspace spanned by the eigenvectors corresponding to the largest eigenvalues.

The main property of the POD is its optimality in the sense that it minimizes the average squared distance between the original signal and its reduced linear representation. As opposed to ICA separation, the method is suitable for variables with Gaussian distribution. In this case, the contours of the joint probability density function consist of ellipsoids, and the Proper Orthogonal Modes (POM) are the principal axes of these ellipsoids.

Considering two variables x_1 and x_2 with Gaussian distribution, Figure 2.4 represents the distribution in the 2D space. The figure shows clearly that the POMs align the two principal axes of the distribution.

However, in the presence of non-Gaussian data, the uncorrelated variables computed through POD are not statistically independent, which may represent a limitation in some cases. For instance, when considering two variables with uniform distribution, Figure 2.5 clearly shows that POD is unable to recover the underlying structure in the data unlike ICA. POD assumption is too weak to get a good separation in practical problem.

2.6 Concluding Remarks

Blind source separation (BSS) problems first emerged in the context of neural network but share concerns with many other research fields. During the last decades, BSS techniques became more and more mature, and important applications have been considered in various domains, from medical applications to telecommunication including structural dynamics. However, dynamicists restricted the use of BSS to specific applications (such as damage detection or condition monitoring). This certainly comes from the fact that time response and excitation signals are linked together by convolutive mixtures.

The objective of the chapter was to introduce BSS concepts and techniques, allowing us to point out some of the BSS main interesting features:

- Only fairly general assumptions about the sources are necessary to consider source separation which makes the methodology usable for many applications.
- No a priori knowledge is required about the physical phenomenon of interest or even about the system excitation.
- Separation methods for static mixture described by (2.1) are well established and have proved success in various domains.

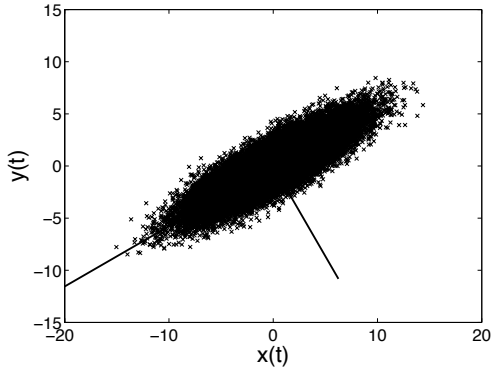

Figure 2.4: **Proper Orthogonal Decomposition (POD) applied to two variables with Gaussian distribution.** The Proper Orthogonal Modes (POMs) accurately align with the two principal axes of the distribution.

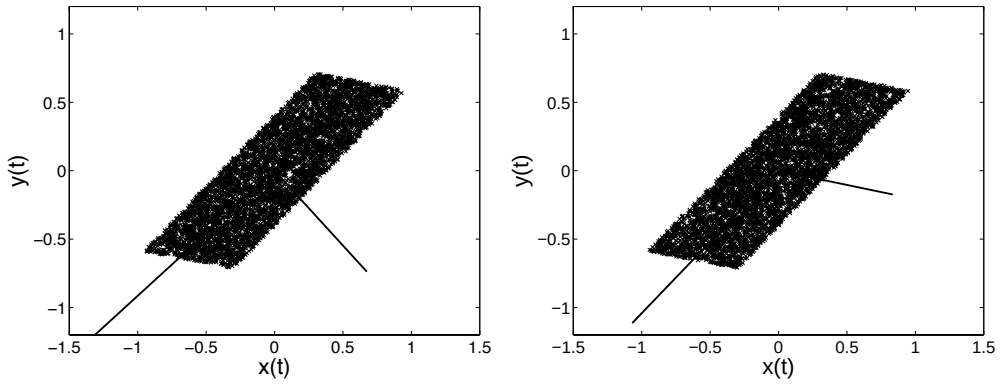

(a) POD (b) ICA

Figure 2.5: **Proper Orthogonal Decomposition (POD) and Independent Component Analysis applied to two variables with uniform distribution.** POD is unable to recover the two principal axes of the distribution whereas ICA performs accurately.

- Methods such as SOBI provide very accurate results even in case of weakly-participating or close-frequency signals.

Considering the previous features and the success of BSS in other domains, it appears that BSS is a promising methodology. This prompts us to carry on in the dynamics field, and especially for modal parameter estimation. Two of the well-known BSS algorithms are considered for this purpose in this dissertation.

The ICA algorithm, firstly used in this work, is based on the mutual information approach. The original components are assumed to be statistically independent and must have non-Gaussian distribution.

The second technique, named SOBI, takes advantage of the temporal structure of the sources for separating them. This approach is a second-order based technique, which facilitates its implementation. The sources are assumed to have different spectral contents.

Despite these advantages, ICA and SOBI possess some weaknesses that might become problematic in some cases:

- First, even though this hypothesis can be relaxed, the basic BSS model assumes that the number of mixture equals the number of sources.

- Second, some statistical distributions might not be accurately separated. This is the case for Gaussian signals (using ICA) and for signals with overlapping spectral contents (using SOBI).

- Finally, because both sources and mixing matrix are unknown, BSS methods possess two indeterminacies related to the amplitude and the order of the sources.

These aspects are addressed in the following chapters where both ICA and SOBI techniques are considered to identify modal parameters using only the structural time-response data, such as acceleration, velocity or displacement histories.

Chapter 3

Modal Parameter Estimation using Blind Source Separation Techniques

Abstract

This chapter proposes to use BSS techniques to estimate the modal parameters of mechanical systems using output dynamic time histories only.

First, Section 3.1 presents the specific features of the proposed methodology compared to classical output-only modal parameter estimation techniques. The utility of statistical techniques for modal identification is also demonstrated.

Section 3.2 introduces the concept of virtual sources for BSS when applied to dynamics. A one-to-one relationship between the BSS modes contained in the identified mixing matrix and the vibration modes is developed.

The following two sections propose a procedure for modal analysis based on BSS using structural dynamic responses. Modal parameter estimation based on the free responses (Sec. 3.3) is first detailed. A specific procedure is then proposed to deal with random forced responses (Sec. 3.4).

Finally, an automated post-processing is introduced for the separation of genuine and spurious modes appearing when the number of sensors is larger than the number of active modes in the frequency range (Sec. 3.5).

3.1 Motivation

Beside the fact that new techniques are always welcome, the motivation for the use of BSS techniques for modal analysis basically comes from the following two ideas. First, statistical and empirical techniques have been extensively used during the last years in dynamics, and the extension to BSS seems to be well-advised. Second, despite of the high number existing techniques, few of them, if none, are able to perform modal parameters estimation without the assistance of an operator.

BSS-based identification possesses some of these interesting features. This dissertation does not pretend to provide a generic solution for all practical applications, but it proposes an additional method in the set of existing methods. The most suitable technique is then left to the user's expertise and preference.

3.1.1 Statistical and Empirical Techniques for Modal Analysis

In Chapter 1, it has been shown that linear system identification is a discipline that has evolved considerably for the last thirty years. Over the past few years, a special attention has been paid to statistical signal processing techniques. As is the case for BSS, they can be applied to various kinds of signals and, by force, to simple dynamic responses, providing the underlying information based on few assumptions.

As it has been shown in Sec. 2.5, BSS is closely related to other statistical techniques. POD is one of them, and it has been proved useful for modal analysis in the past. The relation between the normal modes and the POMs (i.e., the modes extracted using POD) was demonstrated in [FK98, KG02]. Therefore, POD was proposed as the tool for computing the normal modes directly from the measured data [HF02, IMD06]. Some additional information related to the use of POD can be found in Refs. [KG02, CZ06, Fee02].

One intrinsic limitation of POD is that the knowledge of the mass matrix is required. To address this issue, Chelidze and Zhou introduced a new multivariate data analysis method called Smooth Orthogonal Decomposition (SOD) in Ref. [CZ06].

In Ref. [HSL$^+$98], another statistical technique, namely the Hilbert-Huang transform (HHT), has been shown to be effective for characterizing a wide range of non-stationary signals in terms of elemental components through what has been called the empirical mode decomposition. Since then, HHT has been widely used, as it provides a concise basis for the analysis of non-linear systems [KVL$^+$08]. As demonstrated in Refs. [YLPH03a, YLPH03b], this technique is also useful for linear system identification.

3.1.2 Automated post-processing

Many numerical techniques have been proposed for modal parameter extraction from experimental vibration measurements. Some of them are listed in Sec. 1.4 for operational modal analysis. The user can find in this set of methods the one that best fulfills the assumptions corresponding to his experimental conditions.

However, the lack of a priori knowledge about the number of active modes within the studied frequency range may lead to problematic situations. This number is a parameter of prior importance because it is directly related to the complexity of the dynamic model. This uncertainty usually prevents the classical modal analysis methods from being used for automated modal parameter estimation.

As mentioned in Chapter 1, the order of theoretical models is commonly overestimated in modern techniques so as to accurately match the experimental signals. This generates unexpected fictitious modes that have to be separated from the genuine modes.

One of the most widely-used tools performing mode selection is the aforementioned stabilization diagram. Unfortunately, the tool requires a great deal of expertise because an interaction with the experimenter is required. Moreover, in the absence of automated signal processing, discrepancies may appear in the results ensuing from different operators.

Even though numerous modal analysis methods exist, the development of a method combining an automated selection process and a physical interpretation of this choice remains a challenging task as proved by recent developments, such as Ref. [PLLVDA08].

3.2 Interpretation of the BSS Sources in Structural Dynamics

The objective of this section is twofold. First, BSS techniques are proved to be useful for modal identification, even in the absence of external forces, which might, at first, appear paradoxical. Second, it is shown how time responses of mechanical systems can be interpreted as a static mixture of sources.

3.2.1 Physical Excitation Loads as Sources of the BSS Problem

BSS techniques are able to separate the different excitation sources of a system. But the question is now to investigate how those techniques could be exploited for structural modal analysis.

The dynamic response of a linear undamped mechanical system is described by Eqn. (1.1), i.e.,

$$\mathbf{M}\ddot{\mathbf{y}}(t) + \mathbf{K}\mathbf{y}(t) = \mathbf{f}(t), \tag{3.1}$$

where $\mathbf{M}$ and $\mathbf{K}$ are the mass and stiffness matrices, respectively. The physical excitations that are applied on the structure are represented by the vector $\mathbf{f}(t)$ and the system responses $\mathbf{y}(t)$ are the measured output data.

Looking for statistical independence to apply the BSS problem to dynamic systems, a natural way is to consider the applied forces, which are physically independent, as the sources of the system. As already developed in Eqn. (1.5), the system response $\mathbf{y}(\mathbf{t})$ can be written as a convolution product between the IRF $\mathbf{h}(t)$ and the external force vector $\mathbf{f}(t)$

$$\mathbf{y}(t) = \mathbf{h}(t) \otimes \mathbf{f}(t), \tag{3.2}$$

where $\otimes$ denotes the convolution product.

In contrast to the basic equation of BSS (2.1), this relationship involves a dynamic mixture of sources. Unfortunately, as stated in Ref. [AB05] and already explained in Sec. 2.2.1, the separation of sources mixed through a convolution product is not yet completely well-established and raises several problems. Moreover, the solution of this problem does not lead directly to the desired modal parameters.

3.2.2 Virtual Sources Concept

An interesting alternative for expressing the response of a mechanical system is based on the modal expansion. By definition of the normal modes, a n_{DOF} mechanical system possesses n_{DOF} normal mode vectors, denoted $\mathbf{n}_i^{(n_y \times 1)}$, where n_y represents the number of observed signals. Because normal modes are linearly independent they provide a complete set for the expansion of an arbitrary vector $\mathbf{q}^{(n_y \times 1)}$.

Then the $(n_y \times 1)$ system response vector $\mathbf{y}(t)$ defined in Eqn. (3.1) may be written as a modal expansion (i.e., a modal superposition), according to

$$\begin{aligned} \mathbf{y}(t) &= \sum_{i=1}^{n_{DOF}} \mathbf{n}_i \eta_i(t) \\ &= \mathbf{N}\,\boldsymbol{\eta}(t) \end{aligned} \tag{3.3}$$

where the coefficients $\eta_i(t)$ are the so-called normal coordinates and represent the amplitude modulation of the corresponding normal modes $\mathbf{n}_i$.

Expression (3.3) shows that

> *when expanding the system response in terms of the vibration modes, the normal coordinates act as virtual sources regardless of the number and type of the physical excitation forces.*

Furthermore, the time response can be interpreted as a static mixture of these virtual sources, which renders the application of the BSS techniques conceivable.

3.2.3 Normal Coordinates: the Good BSS-source Candidates?

Thanks to Eqn (3.3), the structural dynamics problem can be stated in such a way that it corresponds to the BSS formulation. In order to consider BSS for modal identification, the experimental conditions for which the methodology is applicable have to be defined.

If a necessary condition, the formulation of a problem under the form $\mathbf{x}(t) = \mathbf{A}\mathbf{s}(t)$ is not sufficient to use BSS techniques. The sources $\mathbf{s}(t)$ are also required to be statistically independent, as detailed in Sec. 2.1.4. It should then be determined under what assumptions the normal coordinates $\eta_i(t)$ are statistically independent sources.

The statistical independence has to be verified for all experimental cases. In the following, it is demonstrated that the normal coordinates ensuing from free and random forced responses can be considered as independent for undamped and moderately damped systems.

3.3 Modal Identification using Free Responses

3.3.1 Modal Coordinates and Statistical Independence

Let us first consider the free response of the undamped system (3.1), where the input forces are set to zero (i.e., $\mathbf{f}(t) = 0$). In this case, according to Geradin and Rixen in Ref. [GR94], the normal coordinates are

$$\eta_i(t) = \alpha_i \cos \omega_i t + \beta_i \sin \omega_i t, \tag{3.4}$$

i.e., simple harmonic functions with different spectral contents where ω_i represents the i-th natural pulsation of the system, and α_i and β_i are constant parameters depending on the initial conditions.

The harmonic functions are independent as long as their frequencies are incommensurable. This is illustrated in Fig. 3.1 depicting two sinusoidal functions, $s_1(t) = \sin t$ and $s_2(t) = \sin \pi t$. The knowledge of the value of s_1 does not help in predicting the value of s_2.

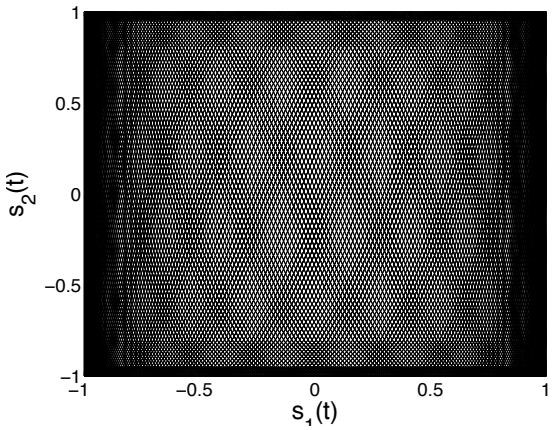

Figure 3.1: **Two sinusoidal functions with irrational ratio of their frequencies.** Both signals are independent and the value of one signal does not provides any information about the value of the second one.

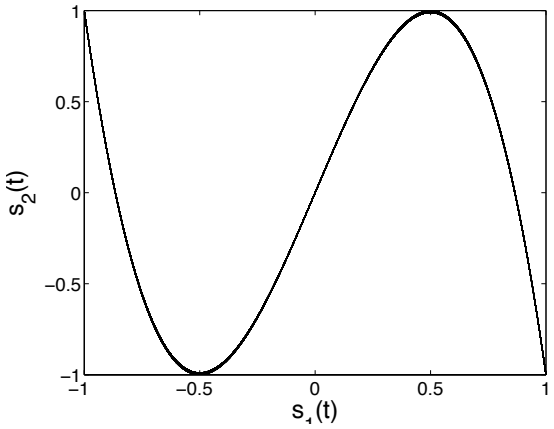

Figure 3.2: **Two sinusoidal functions with rational ratio of their frequencies.** Both signals are not independent as their values are linked. The value of s_1 entirely determines the value of s_2.

In this case, the sources identified using BSS algorithm provide the statistically independent normal coordinates, and, according to Eqn. (3.3), each column of the mixing matrix corresponds to one of the structural vibration modes:

$$\mathbf{A} = \mathbf{N} = [\mathbf{n}_1 \mathbf{n}_2 \cdots \mathbf{n}_{n_s}] \text{ and } \mathbf{s}(t) = \boldsymbol{\eta}(t). \tag{3.5}$$

These relations easily lead to a direct modal parameter identification from a BSS signal separation.

It should be noted that the normal coordinates are no longer independent in case the ratio of their frequencies is an integer, as depicted in Fig. 3.2. In this particular case, there may be a mismatch between the vibration modes and the BSS modes. Fortunately, this possibility is rarely encountered in practice. Nevertheless, it might become problematic for numerical examples containing geometrical symmetries.

Moving to the damped analog of system (3.1), the equations of motion become

$$\mathbf{M}\ddot{\mathbf{y}}(t) + \mathbf{C}\dot{\mathbf{y}}(t) + \mathbf{K}\mathbf{y}(t) = \mathbf{f}(t) \tag{3.6}$$

where $\mathbf{C}$ is the damping matrix. If the right-hand member of the equation is still set to zero ($\mathbf{f}(t) = 0$) and if only proportional damping is considered, the corresponding normal coordinates are exponentially damped harmonic functions:

$$\eta_i(t) = Y_i \cdot \exp\left(-\xi_i \omega_i t\right) \cdot \cos\left(\sqrt{1-\xi_i^2}\omega_i t + \alpha_i\right) \tag{3.7}$$

where ω_i and ξ_i are the natural frequency and damping ratio of the i-th mode, respectively. The amplitude Y_i and the phase α_i are constant parameters depending on the initial conditions. The modal coordinates are still monochromatic with different spectral contents.

One may run into difficulty applying the above ideas in case of high damping because the virtual sources are active only during a limited time window. However, if the damping ratios are low enough, several cycles of vibration may be observed, and we speculate that BSS techniques are able to identify the normal coordinates as the identified sources.

3.3.2 Modal Parameter Estimation

The goal of modal identification is to determine the three modal parameters, namely the normal modes $\mathbf{n}_i$, the natural frequencies, f_i and the damping ratios ξ_i.

As detailed in the previous section, the BSS output data are the mixing matrix $\mathbf{A} = \mathbf{N} = [\mathbf{n}_1 \mathbf{n}_2 \cdots \mathbf{n}_{n_s}]$ and the normal coordinates $\mathbf{s}(t) = \boldsymbol{\eta}(t)$. The mode

shapes are thus directly provided by the columns of the mixing matrix but a post-processing is required for the identified sources in order to evaluate the other modal parameters.

In case of free vibrations, the theoretical expression of the normal coordinates is well-known and given by . This signal is monochromatic, and a simple way for identifying the frequency would be to apply the FFT algorithm. An estimate of the damping ratio can also be provided using the half power method, for instance. Nevertheless, these values are only approximates of the modal parameters and should be refined.

Realizing that Equation (3.7) only depends on four parameters (i.e., the amplitude Y_i, the pulsation ω_i, the damping ratio ξ_i and the phase α_i), it is straightforward to identify the natural frequencies and damping ratios, one by one for each normal coordinate. Starting from initial guesses close to the solution thanks to the FFT process, this is carried out by fitting the time series of the sources $s_i(t)$ with exponentially damped harmonic functions using classical optimization codes.

3.3.3 Proposed Methodology

The key idea is to interpret the normal coordinates of a dynamic system as virtually independent sources. This assumption is valid when the free or random responses of weakly damped systems is considered, and, in this case, there is a one-to-one mapping between the mixing matrix and the vibration modes of the structure. This idea forms the basis of a truly simple modal analysis procedure, detailed in the flowchart of Fig. 3.3. The procedure is as follows:

1. Perform experimental measurements (i.e., a modal testing, cf. Sec. 1.2) to obtain the time series $\mathbf{y}(t)$ at different sensing locations.

2. Apply BSS (ICA or SOBI) directly to the measured time series $\mathbf{y}(t)$ to estimate the mixing matrix $\mathbf{A}$ and the sources $\mathbf{s}(t)$.

3. The mode shapes $\mathbf{n}_i$ are simply contained in the columns of the mixing matrix $\mathbf{A}$.

4. A first approximation of the frequencies and damping ratios is obtained using FFT and half power method for example. Afterwards, these values are refined by fitting the time series of the identified sources $s_i(t)$ with the theoretical expression of the normal coordinates η_i of Eqn. (3.7).

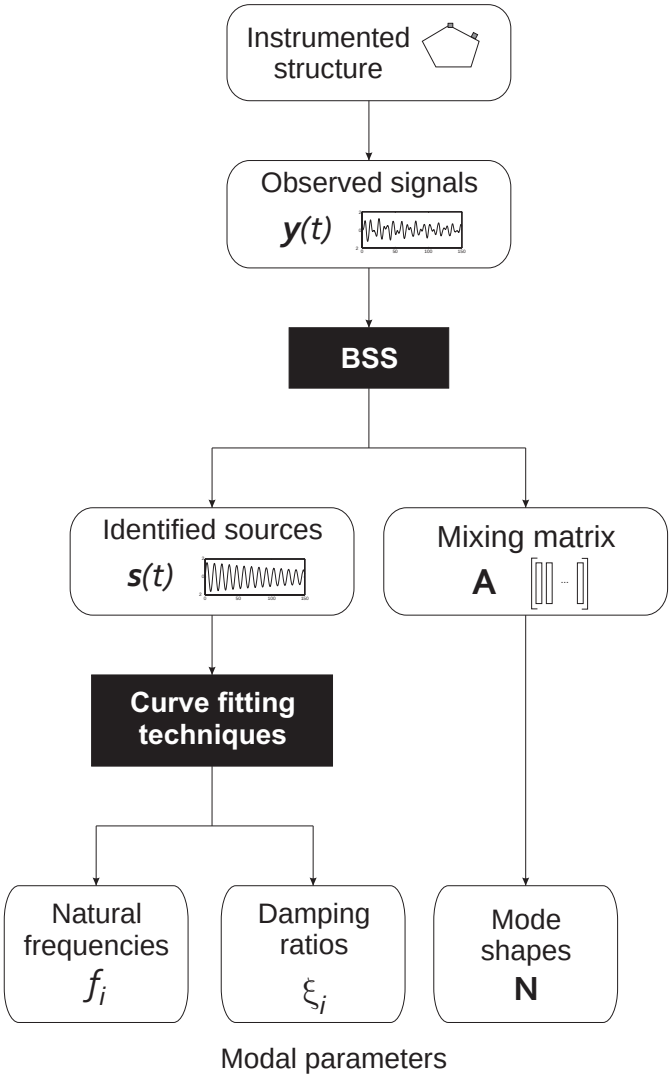

Figure 3.3: **Flowchart for modal identification from free responses** of structures using BSS techniques

3.4 Modal Identification using Forced Responses

3.4.1 Virtual Sources for Forced Systems

In the case of a random excitation, an exact deterministic analytic system response cannot be computed. However, the undamped system, governed by Eqn. (3.1), mainly responds at frequencies equal to its natural frequencies and the system response can still be expressed as a sum of monochromatic functions, to a first approximation.

According to Ref. [GR94], the approximation of the random forced response of an undamped system is provided by the mathematical expression

$$\mathbf{y}(t) \approx \sum_{i=1}^{n_s} \mathbf{n}_i \cdot [e_i(t)(\alpha_i \cos \omega_i t + \beta_i \sin \omega_i t)] \,, \tag{3.8}$$

showing that the normal coordinates can be approximated by harmonic functions modulated by a slowly-varying envelope, denoted $e_i(t)$, depending on the input force amplitude variation.

As is the case for the free response, if the natural frequencies are distinct and incommensurable, the modes extracted from the BSS algorithm and contained in the mixing matrix should therefore provide a good and direct approximation of the natural vibration modes.

In case of damped systems (3.6), the approximation (3.8) holds if light or moderate damping is considered. Indeed, if the damping ratios are still low enough (i.e., there is minimum spectral overlap between the virtual sources) the normal coordinates mostly remain monochromatic. Note that the sustained random excitation prevents the fast evanishment of the sources that should subsequently contains enough information to be separated.

Moving to the case of harmonic forcing of system (3.1) (i.e., where $\mathbf{f}(t) = \mathbf{p}\cos(\omega t)$), the expression of the forced responses, in terms of normal modes, is the following

$$\mathbf{y}(t) = \left(\sum_{i=1}^{m} \frac{\mathbf{n}_i \mathbf{n}_i^T}{(\omega_i^2 - \omega^2)\mu_i} \right) \cdot \mathbf{p} \cos \omega t \tag{3.9}$$

where μ_i is the generalized mass of the i-th mode. In this case, the BSS techniques are of limited use because the mixing matrix is a combination of all the modes of the structure

$$\mathbf{A} = \sum_{i=1}^{n_s} \frac{\mathbf{n}_i \mathbf{n}_i^T}{(\omega_i^2 - \omega^2)\mu_i} \tag{3.10}$$

and the generalized masses of the modes are a priori unknown in practice.

3.4.2 Modal Parameter Estimation

Compared to the previous case, the estimation of the modal parameters from the forced responses requires an additional step. The mode shapes are still directly provided by the mixing matrix, according to Eqn. (3.8), but the theoretical expression of the identified sources corresponding to the normal coordinates is provided by

$$\eta_i(t) = e_i(t)(\alpha_i \cos \omega_i t + \beta_i \sin \omega_i t), \tag{3.11}$$

where the slowly-varying envelope function $e_i(t)$ is related to the unmeasured input force. The shape of this function is thus completely unknown and fitting the time series with (3.11) is not conceivable.

To overcome these difficulties, the idea is simply to transform the identified normal coordinates into free decaying signals by applying the Natural Excitation Technique (NExT). The NExT algorithm (introduced in Sec. 1.4) was proposed in 1993 to recover the free decaying response of structures subjected to unknown, weakly stationary, broad-band and uncorrelated random excitations [JCL93].

If NExT is applied to the random normal coordinates, the resulting signals are similar to exponentially damped harmonic functions and can be considered as the normal coordinates of the system free response. As is the case for the free response, curve-fitting algorithms are applied for every single signal to extract the natural frequency and the damping ratio. For illustration, the algorithm is applied to a 1DOF system. The initial random response and the free response resulting from NExT are presented in Figs. 3.4(a) and 3.4(b).

The free decaying system response is conventionally obtained by applying the inverse Fourier transform to the FRFs signals. But, because the input excitation is unknown in the case of operational testing, FRFs signals are not computable. The methodology of NExT uses the auto- and cross-correlation functions to recover the free decaying functions.

The correlation functions, that are commonly used to analyze randomly excited systems, are obtained from standard techniques using the time histories. The cross-correlation function, denoted $\mathbf{R}_{xy}(\tau)$, is defined as the expected value of the product of two responses $\mathbf{x}(t)$ and $\mathbf{y}(t)$ evaluated at different time steps t and $t + \tau$ as follows

$$\mathbf{R}_{xy}(\tau) = E\left[\mathbf{x}(t + \tau)\mathbf{y}(t))\right]. \tag{3.12}$$

Let consider the n_{DOF} mechanical system (3.6), assumed to be time-invariant, linear and subjected to random excitations $\mathbf{f}(t)$. It can be proved that the correlation functions are solutions of the corresponding homogeneous system, i.e., solution of the equation of motions (3.6) where $\mathbf{f}(t)$ is set to zero. Consequently,

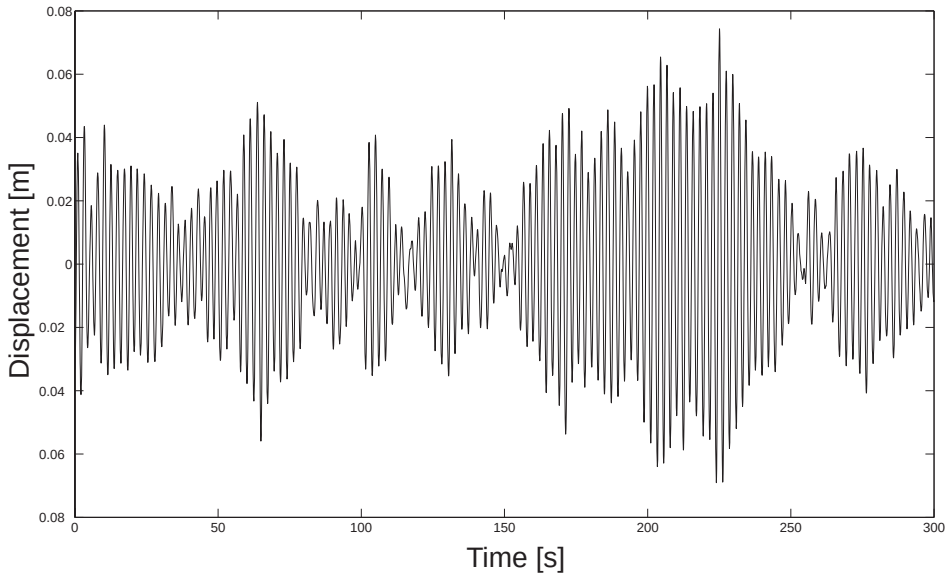

(a) Initial random response

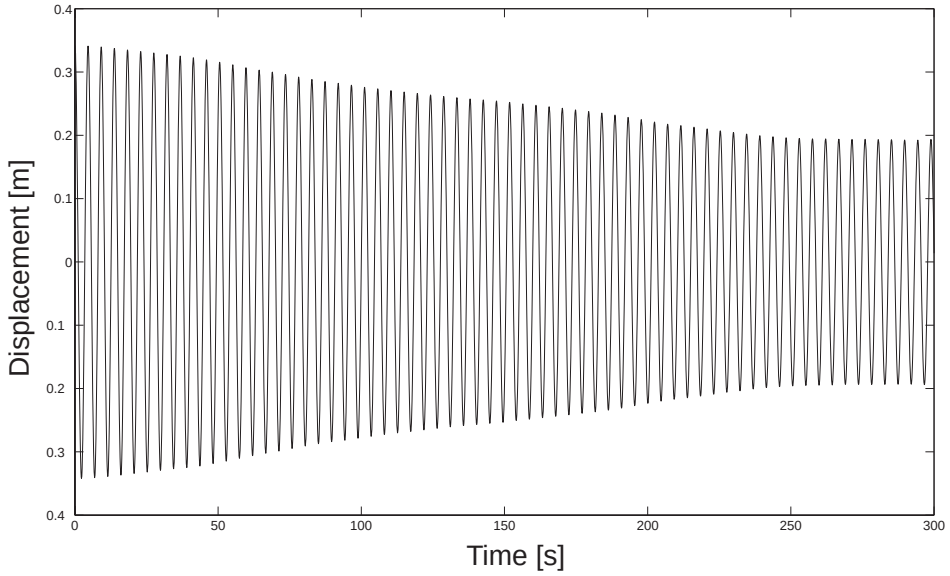

(b) Free response resulting from NExT

Figure 3.4: **Illustration of NExT.** The NExT algorithm is applied to the random forced response of a 1DOF system. The resulting signal approximate the free response of the system.

they correspond to the free response of the system and can be expressed as summations of decaying harmonic functions.

This can be demonstrated as follows. The equation of motion (3.6) can be post-multiplied by a so-called reference signal, denoted $y_i(t-\tau)$, and correlation matrices appear if the expected value of the whole expression is computed:

$$\mathbf{M}\mathbf{R}_{\ddot{y}y_i}(\tau) + \mathbf{C}\mathbf{R}_{\dot{y}y_i}(\tau) + \mathbf{K}\mathbf{R}_{yy_i}(\tau) = \mathbf{R}_{fy_i}(\tau) \tag{3.13}$$

According to Ref. [BP93] where the following relations

$$\dot{\mathbf{R}}_{yy_i}(\tau) = \mathbf{R}_{\dot{y}y_i}(\tau) = -\mathbf{R}_{y\dot{y}_i}(\tau) \tag{3.14}$$

between the correlation functions and their derivatives are demonstrated for weakly stationary processes, Equation (3.13) can easily be modified assuming that the displacement, velocity and acceleration processes are uncorrelated with future disturbances (i.e., $\mathbf{R}_{fy_i}(\tau) = 0$).

Finally, introducing the relations (3.14) in the fourth derivative of (3.13) leads to

$$\mathbf{M}\ddot{\mathbf{R}}_{\ddot{x}\ddot{x}_i}(\tau) + \mathbf{C}\dot{\mathbf{R}}_{\ddot{x}\ddot{x}_i}(\tau) + \mathbf{K}\mathbf{R}_{\ddot{x}\ddot{x}_i}(\tau) = \mathbf{0} \tag{3.15}$$

showing that the cross-correlation function between the structural responses $\ddot{\mathbf{x}}$ and a reference signal $\ddot{x}_i$ satisfies the homogeneous equation of motion and can be treated as free response data.

In the present case, where the signals are monochromatic, the separated signals ensuing from the BSS process can be interpreted as a one-degree-of-freedom system response, and the computation of NExT is highly simplified.

3.4.3 Proposed Methodology

To summarize, the modal parameter estimation process is identical to the free response case but an additional step is introduced between the source separation and the curve fitting. The modal analysis procedure for forced responses of randomly excited structures is detailed in the flowchart of Fig. 3.5 and the procedure is as follows:

1. Perform experimental measurements (i.e., a modal testing, cf. Sec. 1.2) to obtain time series $\mathbf{y}(t)$ at different sensing locations.

2. Apply BSS directly to the measured time series $\mathbf{y}(t)$ to estimate the mixing matrix $\mathbf{A}$ and the sources $\mathbf{s}(t)$.

3. The mode shapes $\mathbf{n}_i$ are simply contained in the columns of the mixing matrix $\mathbf{A}$.

4. The identified monochromatic (random) sources are transformed using NExT algorithm (Sec. 3.4.2) into free decaying harmonic functions that can be interpreted as the normal coordinates of the homogeneous system.

5. A first approximation of the frequencies and damping ratios is obtained using FFT and half power method for example. The values are then refined by fitting the time series resulting from the NExT application with the theoretical expression of the normal coordinates η_i of Eq. (3.7).

3.5 Mode Selection Criteria

It has been shown in Sec. 3.1 that modern structural identification methods may introduce some fictitious or computational modes during the data/model matching process. The differentiation between genuine and fictitious modes remains a critical task for many modal tests and usually requires an interaction with the experimenter, as is the case if stabilization diagrams are used.

A similar problem may appear with BSS-based methodology in the case of overdetermined systems. This means that the number of sensors (i.e., the number of observed signals) is larger than the number of active modes in the frequency range of interest and, consequently, larger than the number of independent sources.

The use of BSS techniques in this work is restricted to the following assumption (cf. Sec. 2.1.4): it is assumed that the number of identified sources equals the number of observed signals ($n_s = n_x$). If this number is lower than the number of active modes (e.g., the number of normal coordinates), the algorithm tries to identify and separate the sources making them as independent as possible. Some of them are the normal coordinates, and the others are made up of noise and perturbation signals.

Fortunately, BSS methodologies provide us two natural ways to evaluate the reliability of the identified sources:

- First, the quality of the identified sources can be estimated by comparing their shapes with theoretical expressions. This step does not lead to additional computational cost because the source fitting is performed in any case to refine the values of the natural frequencies and damping ratios. It is direct to compute the *fitting error* e_{fit} using the Normalized Mean-Square Error (NMSE) between the identified sources $s_i(t)$ and the fitted curves $s_i^{fit}(t)$:

$$e_{fit} = NMSE = \frac{E\left[\|s_i^{fit}(t) - s_i(t)\|^2\right]}{E\left[\|s_i^{fit}(t) - E\left[s_i^{fit}(t)\right]\|^2\right]}. \tag{3.16}$$

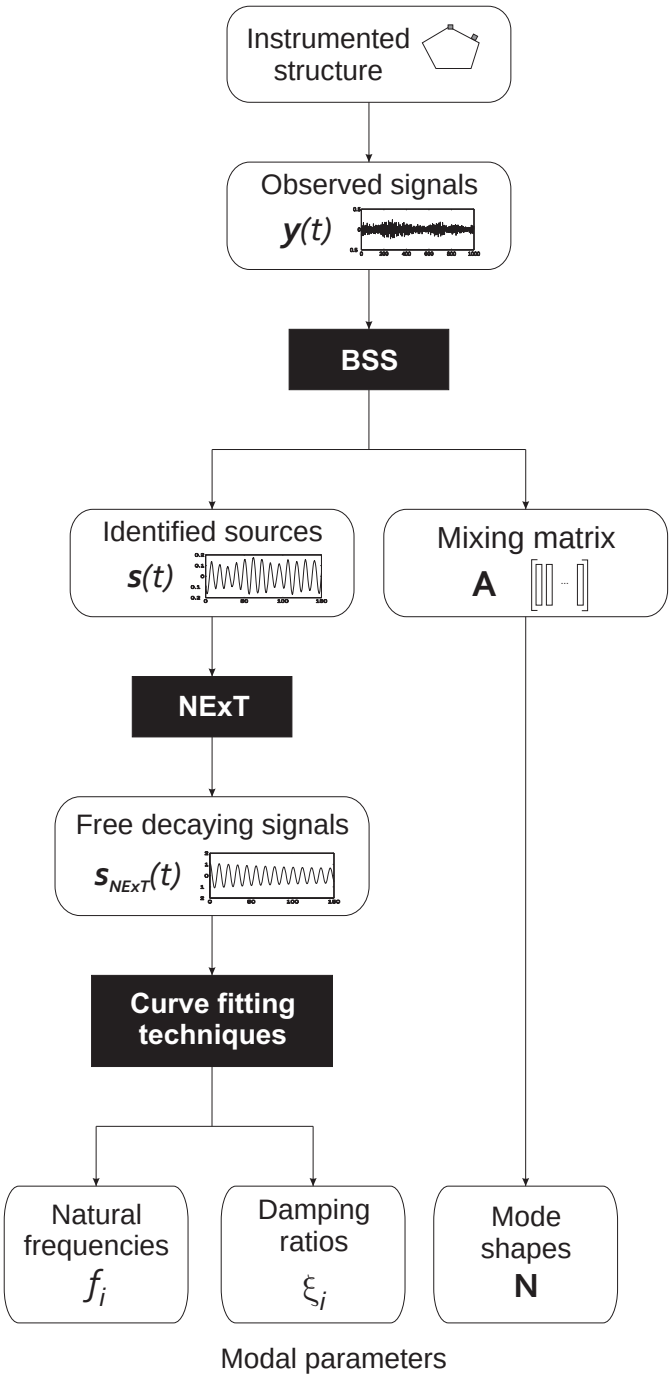

Figure 3.5: **Flowchart for modal identification from forced responses** of randomly excited structures using BSS techniques

The sources can then be considered as genuine if their corresponding fitting errors are low, typically lower than 10 %. The case studies carried out during the research work tend to support this conclusion.

- Second, the observed signals are assumed to be linear mixtures of the sources, it is thus easy to compute an indicator for each identified source, providing a measure of the contribution of the source in the total response signal. This factor can be interpreted as a *participation factor* (PF). Every single source $s_i(t)$ corresponds to a single mode $\mathbf{n}_i$, the relative contribution of which the observed signals $\mathbf{x}(t)$ can be evaluated using the expression

$$PF_i = \frac{\|\mathbf{n}_i \cdot s_i(t)\|}{\sum_{k=1}^{m} (\|\mathbf{n}_k \cdot s_k(t)\|)} \cdot \frac{100}{\max_k (PF_k)} \tag{3.17}$$

where $\| \dots \|$ denotes the Frobenius norm. All the factors are normalized by the highest PF.

This indicator does not properly help during the mode selection but confirm the selection based on the fitting errors. Furthermore, the sum of the selected-mode factors provides information over the quality of the modal analysis process. A high cumulative PF assure that most of the information contained in the initial data has been extracted.

3.6 Concluding Remarks

Over the past few years, statistical and empirical techniques have been extensively used for structural dynamic problems. One major difficulty of using BSS techniques to study the dynamics of mechanical systems concerns the separation of convolutive mixtures. Indeed, the dynamic responses can be related to the physical excitations (i.e., the physical sources of the system) through the IRF using a convolution product. Unfortunately, source separation problem is not yet completely solved for convolutive mixtures.

The proposed methodology overcomes this difficulty by using the concept of virtual sources. When expanding the system response in terms of vibration modes, the normal coordinates, that have been proved to be statistically independent, act as virtual sources of the system regardless of the physical excitations. They can be considered as the sources of a BSS problem in which the normal mode matrix replaces the mixing matrix. This provides a new simple way of identifying the modal parameters using output response data.

The estimation of modal parameters using BSS techniques possesses interesting features:

- The method does not require the measurement of the applied forces and can therefore perform output-only modal analysis.
- BSS can be applied to free as well as random forced responses. In addition, the knowledge of the statistical distribution of the applied forces is not necessary.
- The method is quite simple to implement compared to classical stochastic subspace methodologies, for instance. Because BSS is not based on complex mathematical concepts, the outputs have a physical meaning and are easy to interpret (i.e., the sources are the normal coordinates and the mixing matrix contains the vibration modes).
- The source separation does not require an iterative procedure and has a low computational load. It is thus conceivable to consider large-scaled systems.
- A natural way is provided to determine the accuracy of the results and the relative importance of the sources within the response. When the number of sensors exceed the number of active modes, and so the number of independent sources, an automatic procedure is proposed to extract the genuine modes.

The proposed methodology has also some drawbacks that should be underlined. First, the source separation does not provide a direct access to natural frequencies and damping ratios. Even though it is simple, their evaluation requires a post-processing consisting in fitting the sources with a four-parameter mathematical expression. Second, for random forced responses, the method has to be followed by another signal processing technique (namely NExT) in order to recover the free-decaying normal coordinates. Finally, the number of active sources is assumed to be lower than the number of sensors ; this hypothesis might become problematic in some practical applications.

The methodology therefore needs to be validated against numerical and experimental examples. This is addressed in the following two chapters.

Chapter 4

Validation and Performance of the BSS-based Identification

Abstract

To support the theoretical findings of Chapter 3, the proposed modal parameter estimation method, based on BSS techniques, is applied to simple numerical examples. The objective is twofold. First, free and random forced responses are analyzed in order to validate the method, and second both ICA and SOBI approaches are compared with respect to noise and damping.

First, Section 4.1 describes the considered case studies and presents the indicators used to evaluate the accuracy of the results.

In Sec. 4.2, the proposed methodology is applied to free responses of a discrete system. The influence of the number and the values of the delays considered in SOBI for the separation is also thoroughly studied. Next, modal identification based on random forced responses is investigated (Sec. 4.3). A distributed-parameter system is used to evaluate the robustness of ICA and SOBI with respect to the non-deterministic random excitation.

Section 4.4 illustrates the principle of automated mode selection in case the number of active modes is lower than the number of identified sources.

Finally, Sections 4.5 and 4.6 compare the two BSS algorithms regarding their performance. The robustness with respect to noise and damping is studied in order to identify the more appropriate technique for BSS-based output-only modal analysis.

4.1 Case Studies and Accuracy Indicators

This section describes the discrete and distributed-parameter systems that are used to validate and compare the proposed methodologies. All the case studies considered herein are summarized in Table 4.1, and the indicators used to evaluate the accuracy of the results are defined.

4.1.1 Discrete system

The discrete system considered herein is a three degree-of-freedom (3DOF) system composed of three masses connected in series through linear springs and placed between two rigid walls. The topology of the system is illustrated in Fig. 4.1 and the corresponding equations of motion are

$$\begin{bmatrix} m_1 & 0 & 0 \\ 0 & m_2 & 0 \\ 0 & 0 & m_3 \end{bmatrix} \begin{pmatrix} \ddot{x}_1(t) \\ \ddot{x}_2(t) \\ \ddot{x}_3(t) \end{pmatrix} + \alpha \cdot \begin{bmatrix} c_1 & 0 & 0 \\ 0 & c_2 & 0 \\ 0 & 0 & c_3 \end{bmatrix} \begin{pmatrix} \dot{x}_1(t) \\ \dot{x}_2(t) \\ \dot{x}_3(t) \end{pmatrix} + \begin{bmatrix} k_1 + k_{12} & -k_{12} & 0 \\ -k_{12} & k_{12} + k_{23} & -k_{23} \\ 0 & -k_{23} & k_{23} + k_3 \end{bmatrix} \begin{pmatrix} x_1(t) \\ x_2(t) \\ x_3(t) \end{pmatrix} = \begin{pmatrix} f_1(t) \\ f_2(t) \\ f_3(t) \end{pmatrix}, \tag{4.1}$$

where the mass m_i and the spring stiffness k_i have constant values throughout this work. The masses are set to $m_1 = 2$, $m_2 = 1$ and $m_3 = 3$, and the springs have a unit stiffness ($k_1 = k_{12} = k_{23} = k_3 = 1$). Proportional damping is also introduced by means of the three parameters $c_1 = m_1$, $c_2 = m_2$ and $c_3 = m_3$. The damping properties can then be modified by tuning the α coefficient in Eqn. 4.1.

The system response $\mathbf{x}(t)$ is computed using Newmark's algorithm [GR94]. In order to minimize the computational errors, the sampling frequency must be much higher than the highest natural frequency of the system (0.28522Hz). A sampling frequency of 100 Hz is thus used for the response computation but the signal is then resampled to 10 Hz to mimic experimental conditions.

Unless otherwise informed, and to get closer to realistic conditions, signals are corrupted with white Gaussian noise (5% of the signal RMS value) and the damping coefficient is set to $\alpha = 0.01$. The natural frequencies and the corresponding damping ratios of the system are provided in Table 4.2.

4.1.2 Distributed-parameter system

The second application considered herein consists of a cantilever steel beam modeled using the finite element method. The beam is 0.7 meter length, and its cross section is squared (0.014 meter width). Figure 4.2 illustrates the system.

System	Case study	Objective	Model Parameters	Cf.
3DOF	Free response for lightly damped and noisy system	Validation using free responses	$\alpha = 0.01$; 5% noise; 1500 samples - 10 Hz	Sec. 4.2
	Free response for moderately damped and noisy system	Parametric study of SOBI for the time lag parameters	$\alpha = 0.05$; 5% noise; 1500 samples - 10 Hz and 15000 samples - 100 Hz	Sec. 4.2
	Random forced response for lightly damped and noisy system	Validation using forced responses	$\alpha = 0.01$; 5% noise; 75000 samples - 10 Hz	Sec. 4.3
	Free response corrupted with various levels of white noise	Performance regarding the robustness with respect to noise	$\alpha = 0.01$; $0\% \rightarrow 35\%$ noise; 1500 samples - 10 Hz	Sec. 4.5
	Free response for various damping parameters α	Performance regarding the robustness with respect to damping	$\alpha = 0 \rightarrow 0.15$; 5% noise; 1500 samples - 10 Hz	Sec. 4.6
Beam	Random forced response for moderately damped and noisy system	Performance for the separation of forced responses	$\alpha = 2$; $\beta = 0.2e-5$; 5% noise; 10000 samples - 7500 Hz	Sec. 4.3
	Free response for lightly damped and noisy system	Validation for overdetermined systems	$\alpha = 2$; $\beta = 0.2e-5$; 5% noise; 1500 samples - 2000 Hz	Sec. 4.4

Table 4.1: Summary of the case studies addressed in the present work in order to (i) validate the proposed methodology and (ii) evaluate and compare the performance of the two considered algorithms, namely ICA and SOBI.

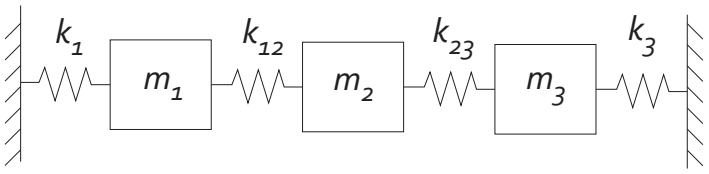

Figure 4.1: **3DOF mass-spring model**. Three masses are connected in series through linear springs and are placed between two rigid walls. Proportional damping is also considered.

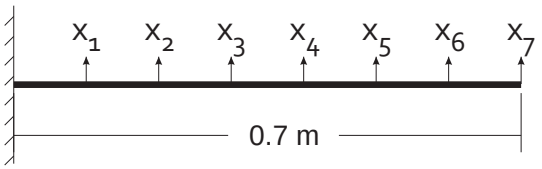

Figure 4.2: **Distributed-parameter system**. The system is a cantilever steel beam. The cross section is a 0.014 meter square and seven locations are considered for the response computation.

	Frequency [Hz]	**Damping Ratio** [%]
Mode 1	0.0895	0.89
Mode 2	0.1458	0.55
Mode 3	0.2522	0.32

Table 4.2: Theoretical modal parameters of the 3DOF system corresponding to a damping coefficient $\alpha = 0.01$.

.

The system response is computed using Newmark's algorithm with a sampling frequency of 100 kHz (the highest considered natural frequency of the system is lower than 3000 Hz). The data used for identification are the vertical accelerations at seven locations that are uniformly distributed along the beam. The signals are then resampled so that the sampling frequency is 2000 Hz or 7500 Hz, according to the frequency range of interest. Proportional damping may also be introduced in the system by means of the coefficients α and β. The ensuing damping matrix used for the simulation is provided by

$$\mathbf{C} = \alpha \cdot \mathbf{M} + \beta \cdot \mathbf{K}. \tag{4.2}$$

As for the 3DOF system, the response signals are corrupted with white Gaussian noise (5% of the signal RMS value) and the damping coefficients are set to $\alpha = 2$ and $\beta = 0.2e-5$, respectively. The first natural frequencies and the corresponding damping ratios of the system are provided in Table 4.3.

4.1.3 Accuracy indicators

Assuming that the structural matrices (**M**, **K** and **C**) are known, the theoretical modal parameters are calculated by solving an eigenvalue problem. The theoretical natural frequencies and the damping ratios (ω_{th} and ξ_{th}) can be compared to the identified parameters (ω_{id} and ξ_{id}) using the normalized ratios

$$r_\omega = \frac{\omega_{id}}{\omega_{th}} \quad \text{and} \quad r_\xi = \frac{\xi_{id}}{\xi_{th}} \tag{4.3}$$

tending to unity in case of perfect correspondence. The accuracy of the identification is also assessed using the Modal Assurance Criterion (MAC)

$$MAC = \frac{\left|\mathbf{n}_{id}^T \mathbf{n}_{th}\right|^2}{\left|\mathbf{n}_{id}^T \mathbf{n}_{id}\right| \cdot \left|\mathbf{n}_{th}^T \mathbf{n}_{th}\right|}, \tag{4.4}$$

	Frequency [Hz]	**Damping Ratio** [%]
Mode 1	23.59	0.69
Mode 2	147.83	0.20
Mode 3	414.30	0.29
Mode 4	814.02	0.53
Mode 5	1353.12	0.86
Mode 6	2038.21	1.29
Mode 7	2845.50	1.79

Table 4.3: Theoretical modal parameters of the distributed-parameter system for the first seven modes corresponding to the damping coefficients $\alpha = 2$ and $\beta = 0.2e - 5$.

comparing the identified $\mathbf{n}_{id}$ and theoretical $\mathbf{n}_{th}$ mode shapes. MAC values range from 0 in case of no correlation to 1 for a complete coincidence.

Besides the classical modal parameters (ω_i, ξ_i and $\mathbf{n}_i$), the exact normal coordinates can also be determined by inverting the modal expansion expression (3.3) or, in other words, by projecting the simulated response $\mathbf{x}(t)$ onto each eigenmode as follows

$$\boldsymbol{\eta}(t) = \mathbf{N}^{-1}\mathbf{x}(t). \tag{4.5}$$

These signals can be used to evaluate the accuracy of the source separation by comparison with the identified normal coordinates. The NMSE, defined in Eqn. (3.16), is then applied between the identified $s_i(t)$ and the theoretical $\eta_i(t)$ according to

$$e_\eta = \frac{E\left[\|\eta_i(t) - s_i(t)\|^2\right]}{E\left[\|\eta_i(t) - E\left[\eta_i(t)\right]\|^2\right]}. \tag{4.6}$$

4.2 Modal Identification using Free Responses

Before considering randomly forced systems, the proposed modal parameter estimation technique is validated for free response signals. Both ICA and SOBI algorithms are tested on the 3DOF system (Eq. (4.1)). The initial conditions are set to zero except for $\dot{x}_3 = 1$ and the excitations $f_i(t)$ are assumed to be zero for any time.

The BSS methodology is applied to the first 1500 samples of the three displacement signals. The observed signals $x_i(t)$ and their Power Spectral Densities (PSD) are presented in Fig. 4.3. The relative participation of each natural frequency in the response signals is represented by the amplitude of the corresponding PSD peak. It can be observed that the first mode is clearly the most important whereas the contribution of the third mode is quite low, providing few information for the separation.

Because the considered BSS problem assumes that the number of sources equals the number of observed signals, the blind separation identifies three sources, that are expected to be monochromatic and to correspond to the normal coordinates of the system. The resulting exponentially damped harmonic signals are presented in Fig. 4.4. The PSDs confirm that a single frequency is active for each identified signal. The dominant frequencies correspond to the three natural frequencies of the 3DOF system, presented in Table 4.2.

The previously-defined accuracy indicators are provided in Table 4.4 for both methods. The low values of the errors indicate the success of the identifications. Both algorithms accurately separate the independent sources $s_i(t)$ providing reliable modal parameters.

As detailed in Sec. 2.4, SOBI is based on the joint diagonalization of several time-lagged covariance matrices and the number of time lags (or delays), as well as their values, have to be fixed before computing the covariance matrices. The selection of the delays τ is a decisive phase in the SOBI-based identification procedure that can impact the accuracy of the results. This selection might be interpreted as a tuning parameter requiring a great deal of expertise from the user, leading to an important drawback.

In order to clarify this point, an extensive study of the robustness of SOBI with respect to the number and the values of the delays is achieved hereafter. For that purpose, several numerical case studies are carried out on the 3DOF system with $\alpha = 0.05$ and with noise corrupting the signals (5 % of the signal RMS value).

The simplest systematic way of selecting the delays is to choose a set of n_τ time step multiples such as $\tau_1 = \Delta t, \tau_2 = 2\Delta t, ...\tau_{n_\tau} = n_\tau \Delta t$. However, if the sampling frequency has been defined much higher than the frequency range of interest, the identification is poor quality. This phenomenon is highlighted in the

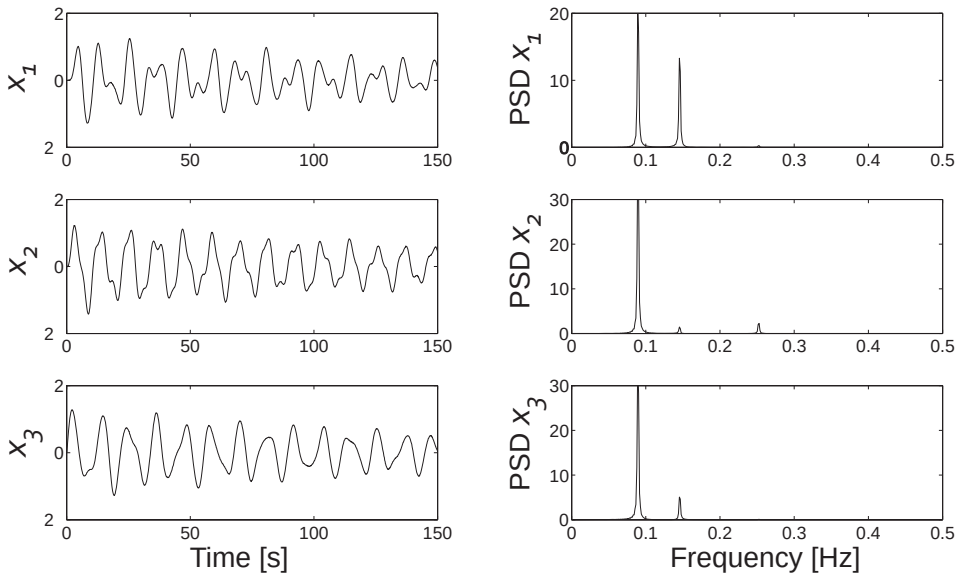

Figure 4.3: **Response signals in terms of displacements on the left and the corresponding PSDs on the right**. The contribution of the modes in the dynamic response is represented by the amplitude of the PSD peaks. The third mode (0.2522 Hz) has a low participation. (3DOF, Free response, $\alpha = 0.01$, 5% RMS noise)

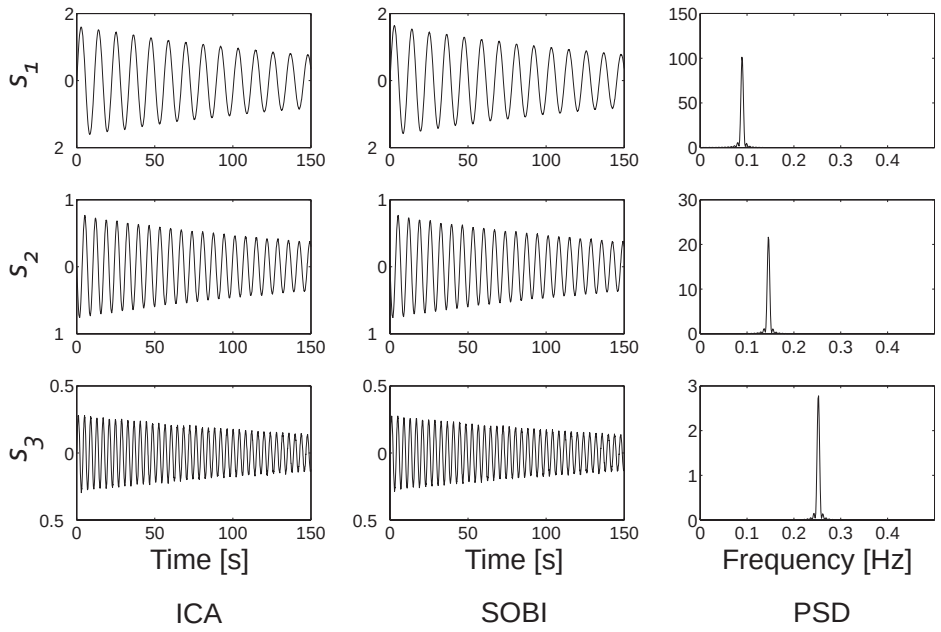

Figure 4.4: **Exponentially damped harmonic signals resulting from ICA and SOBI**. The signals correspond to the system normal coordinates and are monochromatic as highlighted by the PSDs. From the left to the right: sources identified using ICA; sources identified using SOBI; PSDs of the sources. (3DOF, Free response, $\alpha = 0.01$, 5% RMS noise)

		r_ω [-]	r_ξ [-]	MAC [-]	e_η [%]
Mode 1	**ICA**	1.0000	1.0034	1.000	0.114
	SOBI	1.0000	1.0035	1.000	0.015
Mode 2	**ICA**	1.0000	0.9999	1.000	0.011
	SOBI	1.0000	0.9999	1.000	0.015
Mode 3	**ICA**	1.0000	0.9993	0.999	0.026
	SOBI	1.0000	0.9994	1.000	0.006

Table 4.4: Accuracy of the identifications performed using ICA and SOBI. From left to right: identified to theoretical frequencies ratio; ratio of identified to theoretical damping ratios; MAC between mode shapes; NMSE between the fitted and the theoretical sources. (3DOF, Free response, $\alpha = 0.01$, 5% RMS noise)

following examples in which SOBI is applied twice to the same response signals that are first sampled at 10 Hz and next at 100 Hz. In this example, 20 delays are used and the recording time is 150 seconds for both identifications.

Table 4.5 presents the difference between the identifications of both sets of signals. In the case of the 10Hz-sampled signals, (i.e., when the sampling frequency is chosen in accordance with the physics of the problem), the identified modal parameters are extremely good. As for the source separation based on the 100Hz-sampled signals, the accuracy of the results is relatively low. If the identified frequencies and the damping ratios are still very satisfactory, the mode shapes are quite disappointing (less than 0.95 for the MAC) for numerical applications. This comes from the fact that the delays are chosen out of the frequency range containing the natural frequencies.

Consequently, the selection of the delays should be closely related to the physics of the problem, that is represented by the expected natural frequencies. In this dissertation, the delays are uniformly distributed over the time interval $[1/f_{max}; 1/f_{min}]$, in which f_{min} and f_{max} are the smallest and largest eigenfrequencies of the system, respectively. This option prevents the sampling frequency to impacts the results.

The number of delays considered for the identification is another important parameter and its influence is studied in Fig. 4.5 in which the benefit of choosing several time lags is clearly highlighted. However, it can be observed that if the number of time lags increases beyond a certain limit, the accuracy of the identification slightly decreases. Indeed, the number of delays is directly related to

	Sampling Frequency [Hz]	r_ω [-]	r_ξ [-]	MAC [-]	e_η [%]
Mode 1	10	1.0000	0.9951	1.000	0.093
	100	0.9990	1.0257	0.998	1.430
Mode 2	10	1.0000	0.9973	0.998	0.258
	100	1.0008	0.9976	0.941	1.085
Mode 3	10	1.0000	1.0054	0.992	0.198
	100	1.0001	0.9999	0.945	0.529

Table 4.5: Comparison of the SOBI-based identification accuracy for the same signal sampled at 10 and 100 Hz, respectively. From left to right: identified to theoretical frequencies ratio; ratio of identified to theoretical damping ratios; MAC between mode shapes; NMSE between the fitted and the theoretical sources. (3DOF, Free response, $\alpha = 0.05$, 5% RMS noise)

the number of time-lagged covariance matrices that have to be simultaneously diagonalized. Increasing this number leads to computational difficulties and worse results.

In this particular example, the diagonalization of around 10 covariance matrices gives the best results. For practical applications, we recommend to use of 10 to 20 time lags. The case studies carried out during the research work tend to support this conclusion.

It is possible, though not desirable, to carry out source separation with SOBI using a single (and carefully chosen) delay τ. In this case, as previously mentioned, SOBI reduces to the AMUSE method, introduced by Tong et al. in [TLSH91]. Figure 4.6 presents the discrepancy between the results, observed if a single delay is used for the identifications. In this example, 1000 simulations have been performed using a single delay which is randomly chosen within the frequency range of interest. Even though the first mode is most of the time accurately estimated, a large number of identifications fails to recover the second and third theoretical modes. This phenomenon is emphasized in Fig. 4.7 presenting the cumulative probability of obtaining a MAC value lower than a given value, when a single randomly-chosen delay is considered for SOBI. For example, more than 50% of the test-cases provides a MAC value lower than 0.95 for the second and third modes.

In the present study, 20 delays are used throughout the work. They are chosen to be uniformly distributed in the time interval $[1/f_{max}; 1/f_{min}]$.

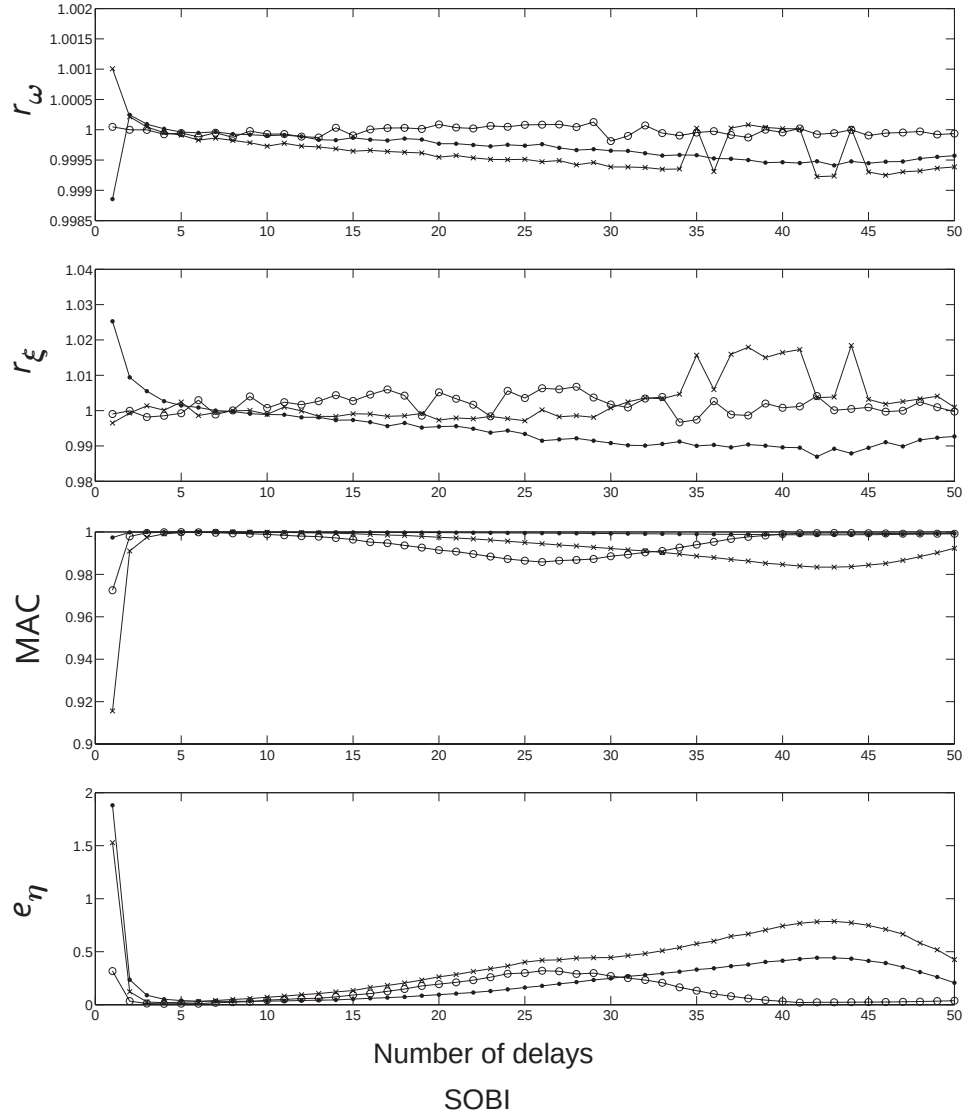

Figure 4.5: **Influence of the number of delays used for SOBI on the accuracy of the identified results**. From top to bottom: identified to theoretical frequencies ratio; ratio of identified to theoretical damping ratios; MAC between mode shapes; NMSE between the separated signals and the theoretical modal coordinates. −•− : mode 1, −×− : mode 2, −○− : mode 3. (3DOF, Free response, $\alpha = 0.05$, 5% RMS noise)

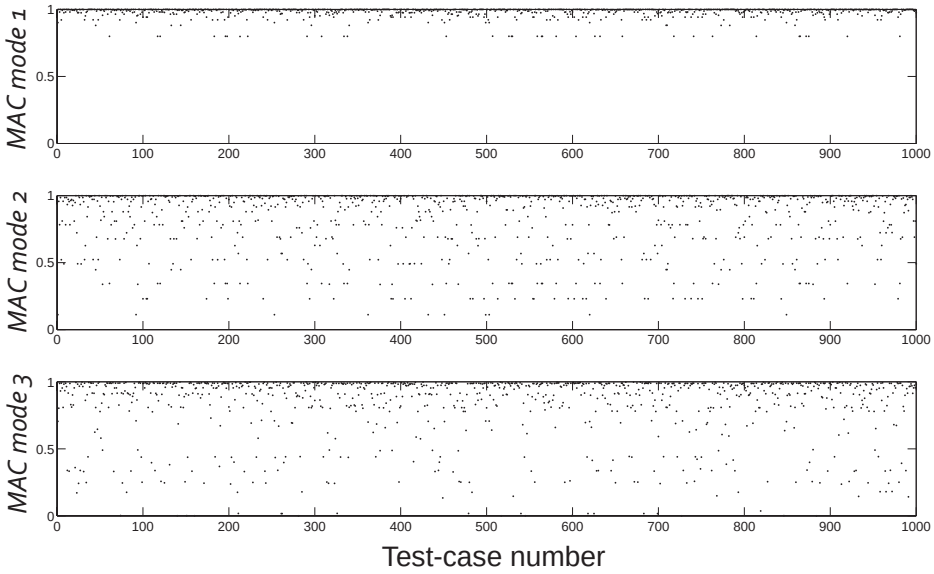

Figure 4.6: **Observed dispersion of MAC values resulting from SOBI in case of single randomly-chosen delay.**. The delays are randomly chosen to belong to the frequency range of interest and 1000 identification have been achieved. The mode identification is clearly not assured as MAC values lower than 0.95 can be obtained. (3DOF, Free response, $\alpha = 0.05$, 5% RMS noise)

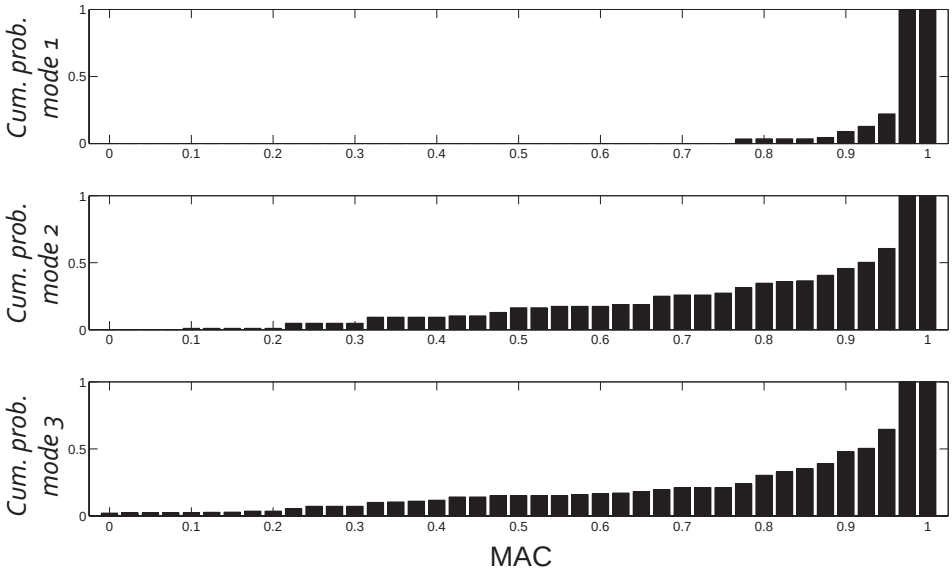

Figure 4.7: **Observed cumulative probability of MAC values resulting from SOBI in case of single randomly-chosen delay.** The delays belong to the frequency range of interest and 1000 identifications have been achieved. The mode identification is not assured as there is 50% probability to obtain MAC values lower than 0.95 for the second and third modes if a single delay is used for the separation. (3DOF, Free response, $\alpha = 0.05$, 5% RMS noise)

4.3 Modal Identification using Random Responses

The case of random forced responses is now considered for modal parameter estimation. To this end, both discrete and distributed-parameter systems are studied first to illustrate the proposed methodology and second to evaluate the robustness of the separation process with respect to random excitations.

BSS identification is then first performed on the forced response of the 3DOF system using ICA and SOBI. A random excitation is applied to the system at the first mass ($f_1 \neq 0$).

As previously mentioned, in case of forced response signals, the identified sources must be transformed into free decaying signals by means of the NExT algorithm before identifying the damping ratios (cf. Sec. 3.3.3). This procedure requires more samples than in the free response case to provide accurate results. Fortunately, because energy is continuously introduced in the system, a long acquisition time is possible even if high damping is considered. The 75000 samples which are considered for the identifications, are presented in Fig. 4.8. The corresponding PSD functions highlight the very low participation of the third mode.

The separation results are given in Fig. 4.9. In the left column the identified sources are presented. They are expected to match harmonic functions modulated by slowly varying envelopes. Both ICA and SOBI provide very similar results. In the middle, PSDs confirm that the sources are mainly monochromatic. Finally, the sources are transformed into free decaying functions using NExT from which the natural frequencies and the damping ratios can be estimated.

The success of the identifications is evaluated using the accuracy indicators, provided in Table 4.6. These results confirm the high accuracy of the identification of the natural frequencies and the mode shapes. It can be observed that the damping ratio evaluation is less efficient. The damping parameter is estimated from the free decaying signals resulting from NExT, and not directly from the normal coordinates of the system. These functions approximate the normal coordinates of the associated free system but deviations can appear in the results. Nevertheless, the relative error remains quite acceptable for damping prediction.

Numerical experiments are then performed using the cantilever beam system subjected to random excitations. The objective is to evaluate the robustness of the method with respect to the excitation and to compare the performances of both ICA and SOBI approaches. The random excitation, $f_7(t)$, is characterized by a uniform random distribution in the interval [-50 N ; 50 N]. The force is applied vertically at the free end of the beam (cf. Fig. 4.2). The theoretical natural frequencies and damping ratios are provided in Table 4.3.

Because of the non-deterministic characteristic of the random excitation, 50 separate identifications resulting from 50 different samples of $f_7(t)$ are carried

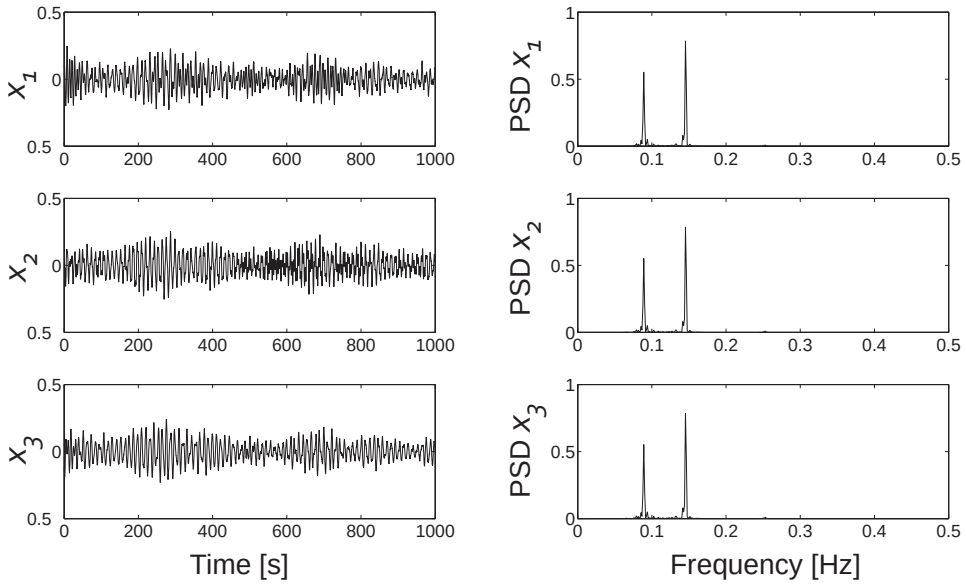

Figure 4.8: **Random forced response signals in terms of displacement on the left and the corresponding PSDs on the right**. The contribution of the modes in the dynamic responses is represented by the importance of the PSD's peaks. Third mode (0.2522 Hz) has a very low participation. (3DOF, Forced response, $\alpha = 0.01$, 5% RMS noise)

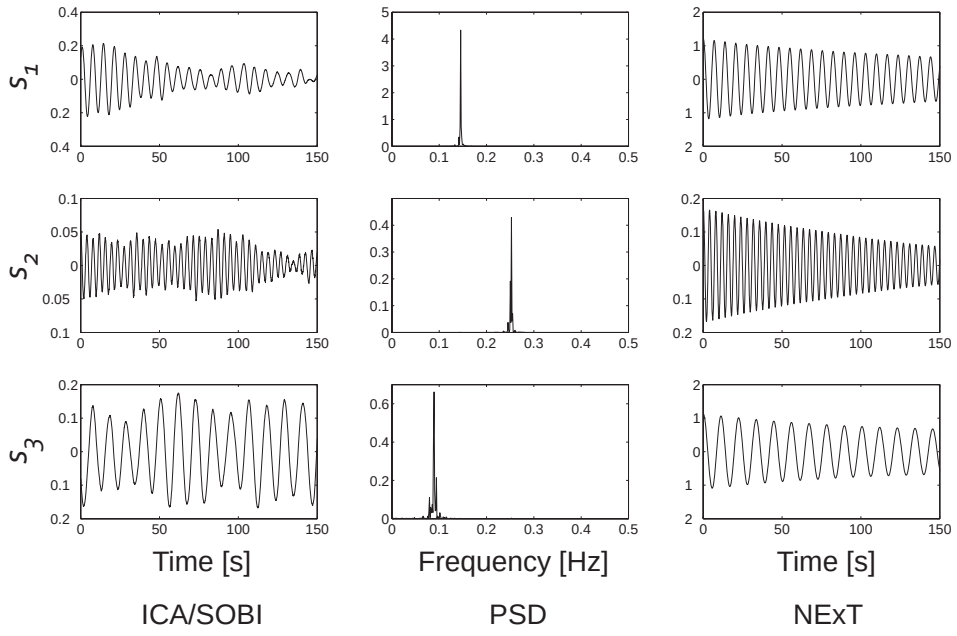

Figure 4.9: **Identified sources resulting from ICA and SOBI and corresponding free decaying signals resulting from NExT.** From the left to the right: sources identified using ICA/SOBI; PSDs of the sources; NExT applied to SOBI sources. (3DOF, Forced response, $\alpha = 0.01$, 5% RMS noise)

		r_ω [-]	r_ξ [-]	MAC [-]	e_η [%]
Mode 1	**ICA**	1.0054	0.9136	0.999	0.521
	SOBI	1.0054	0.9082	1.000	0.007
Mode 2	**ICA**	1.0008	0.9531	1.000	0.018
	SOBI	1.0008	0.9535	1.000	0.007
Mode 3	**ICA**	0.9982	0.8857	0.972	0.705
	SOBI	0.9982	0.8936	1.000	0.001

Table 4.6: Accuracy of the identifications performed using SOBI and compared to theoretical results. From left to right: identified to theoretical frequencies ratio; ratio of identified to theoretical damping ratios; MAC between mode shapes; NMSE between the fitted and the NExT signals. (3DOF, Forced response, $\alpha = 0.01$, 5% RMS noise)

out. In order to enlarge the frequency range of interest and to encompass the seven vibration modes of the beam, the sampling frequency is chosen to be equal to 7500 Hz, and 10000 samples are taken into account for the identification after the transient response damps out. As in the previous cases, noise (5% of the signal RMS value) also corrupts the response signals.

The results are provided in Table 4.7. The identification of a mode is considered successful when its MAC value is higher than 0.98. Table 4.7 presents the number of successful identifications for each mode and the means $\{\mu(r_\omega), \mu(r_\xi), \mu(MAC), \mu(e_\eta)\}$ as well as the standard deviations $\{\sigma(r_\omega), \sigma(r_\xi), \sigma(MAC), \sigma(e_\eta)\}$ are computed for each of the four accuracy indicators, taking into account only the successful identifications.

For ICA, more than half of the identifications fails indicating that the ICA-based modal analysis is not suitable for moderately or highly damped systems. This conclusion is further discussed hereafter. Conversely, SOBI provides accurate results, and, except for the first mode, all the identifications are successful. The accuracy of other parameters such as the frequency and the damping ratio is very good and the variation around the mean, represented by the standard deviation, is very acceptable and much better than the ICA-based one.

As in the free response case, the estimation of the natural frequencies and the mode shapes is straightforward. The estimation of the modal damping ratios requires the prior use of NExT explaining the lower quality of the results when compared to the accuracy of the frequencies or mode shapes.

		Success [-]	$\mu(r_\omega)$ ($\sigma(r_\omega)$) [-]	$\mu(r_\xi)$ ($\sigma(r_\xi)$) [-]	$\mu(MAC)$ ($\sigma(MAC)$) [-]	$\mu(e_\eta)$ ($\sigma(e_\eta)$) [%]
Mode 1	**ICA**	0/50	- (-)	- (-)	- (-)	- (-)
	SOBI	0/50	- (-)	- (-)	- (-)	- (-)
Mode 2	**ICA**	39/50	0.8812 (0.5800)	48.0828 (95.7768)	0.999 (0.0013)	4.6008 (3.5049)
	SOBI	50/50	1.0011 (0.0049)	1.1132 (1.6843)	0.999 (0.0022)	3.2393 (1.8042)
Mode 3	**ICA**	23/50	0.7505 (0.3577)	15.3353 (47.9780)	0.994 (0.0060)	2.0322 (1.0839)
	SOBI	50/50	0.9998 (0.0019)	1.0713 (0.5553)	0.999 (0.0006)	2.2458 (1.1940)
Mode 4	**ICA**	19/50	0.8709 (0.2223)	0.8989 (0.4094)	0.994 (0.0064)	6.6552 (16.7641)
	SOBI	50/50	0.9998 (0.0017)	0.9848 (0.4133)	1.000 (0.0003)	0.5824 (0.2733)
Mode 5	**ICA**	23/50	0.8910 (0.2293)	0.9166 (0.2513)	0.993 (0.0058)	2.8131 (2.3382)
	SOBI	50/50	0.9989 (0.0026)	0.9503 (0.2636)	1.000 (0.0001)	0.6103 (0.2328)
Mode 6	**ICA**	3/50	0.9982 (0.0005)	1.0677 (0.1704)	0.989 (0.0072)	0.3695 (0.1664)
	SOBI	50/50	0.9980 (0.0021)	0.9624 (0.1955)	0.994 (0.0030)	0.1423 (0.0838)
Mode 7	**ICA**	31/50	0.9789 (0.0710)	0.9711 (0.1858)	0.996 (0.0038)	5.5303 (7.6432)
	SOBI	50/50	0.9969 (0.0034)	0.9674 (0.1760)	1.000 (0.0001)	0.2395 (0.2643)

Table 4.7: Accuracy of the identifications performed using ICA and SOBI. From left to right: identified to theoretical frequencies ratio; ratio of identified to theoretical damping ratios; MAC between mode shapes; NMSE between the fitted and the theoretical sources. The means μ and the standard deviations σ are computed for the only successful identification. (Cantilever beam, Forced response, $\alpha = 2$, $\beta = 0.2e-5$, 5% RMS noise)

4.4 Validation of the Automated Mode Selection

The objective of this section is to prove the applicability of the methodology for overdetermined system (i.e., when the number of observed signals is larger than the number of active modes). Chapter 3 proposed to use the fitting error parameter to automatically identify the genuine and meaningful sources. This suggestion is tested hereafter.

The dynamic response of the cantilever beam subjected to a vertical static load (100 N), applied at the free end and suddenly released at time $t = 0$, is computed. Both ICA and SOBI methods are applied to the seven vertical accelerations measured along the beam. The first 1500 samples of the response are considered for the identification, and the corresponding sampling frequency is 2000 Hz. The corresponding frequency range only encompasses four active modes.

The number of separated components is assumed to equal the number of observed signals, and the seven identified sources resulting from the ICA and SOBI are depicted in Fig. 4.10. For illustration, Figure 4.11 depicts the identified and the fitted signals for sources s_1^{SOBI} and s_4^{ICA}.

PSDs provide a visual way of distinguishing the genuine modal coordinates because they are supposed to be monochromatic. Indeed, only the first four sources are purely monochromatic and the respective columns of the mixing matrix should then correspond to physical modes.

Nevertheless the selection is greatly facilitated using the errors that are computed when fitting the source time series with exponentially damped harmonic functions. An automatic selection is then achieved by means of these errors e_{fit} and can be confirmed by the value of the corresponding participation factors PF_i. Both criteria are defined in Sec. 3.5.

The two parameters PF_i and e_{fit} are presented in Figs. 4.12(a) and 4.12(b) for the ICA and the SOBI sources, respectively. These figures demonstrate that the sources s_1 to s_4 combine high PF and low fitting error. As is the case for the previous studies, SOBI provides more accurate results than ICA by avoiding ambiguities for the genuine source selection. The accuracy indicators are provided in Table 4.8. The values of the indicators prove the success of the identification using SOBI while ICA has difficulty to properly separate the four active modes.

The SOBI and ICA mode shapes are also graphically compared to the theoretical modes in Fig. 4.13. SOBI modes perfectly match the theoretical shapes while the third and fourth ICA modes show less accurate results. It is necessary to remind that most of BSS approaches (such as ICA) were developed to deal with identically-distributed variables (i.e., the sample order has no importance). In case of dynamic responses, the signals are time-dependent and contain temporal structure. This additional information is considered in the SOBI approach to facilitate the source separation (cf. 2.4). This may explain the more accurate

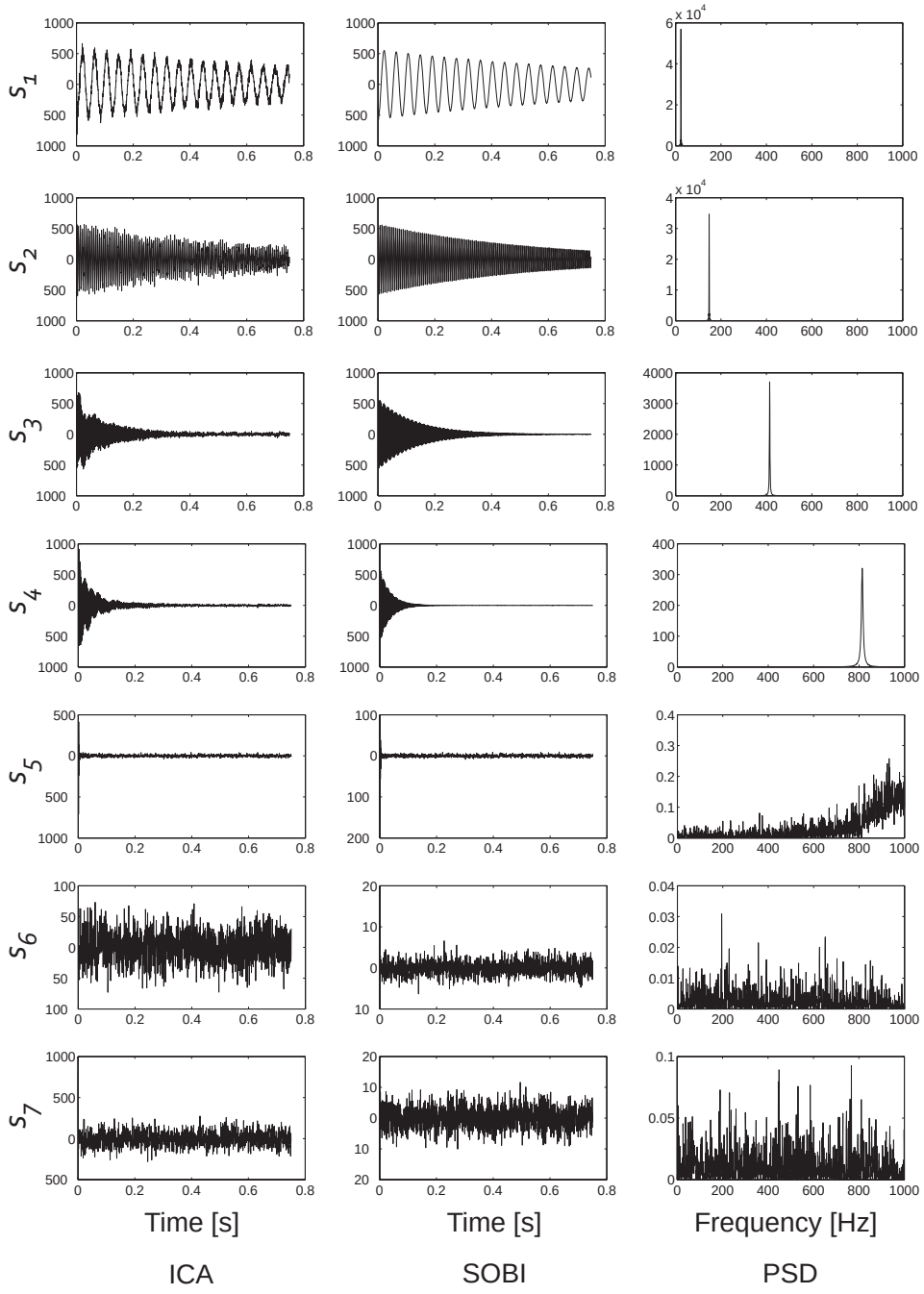

Figure 4.10: **Identified sources resulting from ICA and SOBI**. From the left to the right: sources identified using ICA; sources identified using SOBI; power spectral density of the SOBI sources. (Cantilever beam, Free response, $\alpha = 2$, $\beta = 0.2e - 5$, 5% RMS noise)

		r_ω [-]	r_ξ [-]	MAC [-]	e_η [%]
Mode 1	**ICA**	1.0002	1.1295	0.999	3.519
	SOBI	1.0000	1.0014	1.000	0.024
Mode 2	**ICA**	1.0000	0.9670	0.999	7.193
	SOBI	1.0000	0.9996	1.000	0.026
Mode 3	**ICA**	0.9999	1.0882	0.893	29.633
	SOBI	0.9999	0.9989	1.000	0.102
Mode 4	**ICA**	0.9998	1.0388	0.696	22.567
	SOBI	0.9997	1.0032	1.000	0.044

Table 4.8: Accuracy of the identifications performed using ICA and SOBI. From left to right: relative error on the frequency; relative error on the damping ratio; MAC between mode shapes; NMSE between the fitted and the theoretical sources. (Cantilever beam, Free response, $\alpha = 2$, $\beta = 0.2e-5$, 5% RMS noise)

results.

4.5 Influence of Noise

It has been shown that both ICA and SOBI techniques successfully perform when applied to dynamic responses of weakly damped systems with a low level of noise. To investigate the robustness of the proposed procedure with respect to noise, the displacement signals of the 3DOF system are corrupted by non-Gaussian random white noise (i.e., uniformly distributed). The noise RMS amplitude is gradually increased from 0 % to 35 % of the signal RMS value.

The identifications are carried out on the lightly-damped system considering ICA and SOBI approaches. The first 1500 samples of the signals, corresponding to the first 150 seconds, are used for the analyzes.

Because of the non-deterministic characteristic of noise, 50 separate identifications are performed for each of the 36 levels of noise that are studied. Thus, 1800 identifications have been accomplished for both methods (ICA and SOBI) and, for each of them, a set of four accuracy indicators $\{r_\omega, r_\xi, MAC, e_\eta\}$ is computed.

In order to facilitate the comparison, the mean values $\{\mu(r_\omega), \mu(r_\xi), \mu(MAC), \mu(e_\eta)\}$ and the standard deviations $\{\sigma(r_\omega), \sigma(r_\xi), \sigma(MAC), \sigma(e_\eta)\}$ are estimated for each of the 36 sets of data. An identification is considered successful as soon

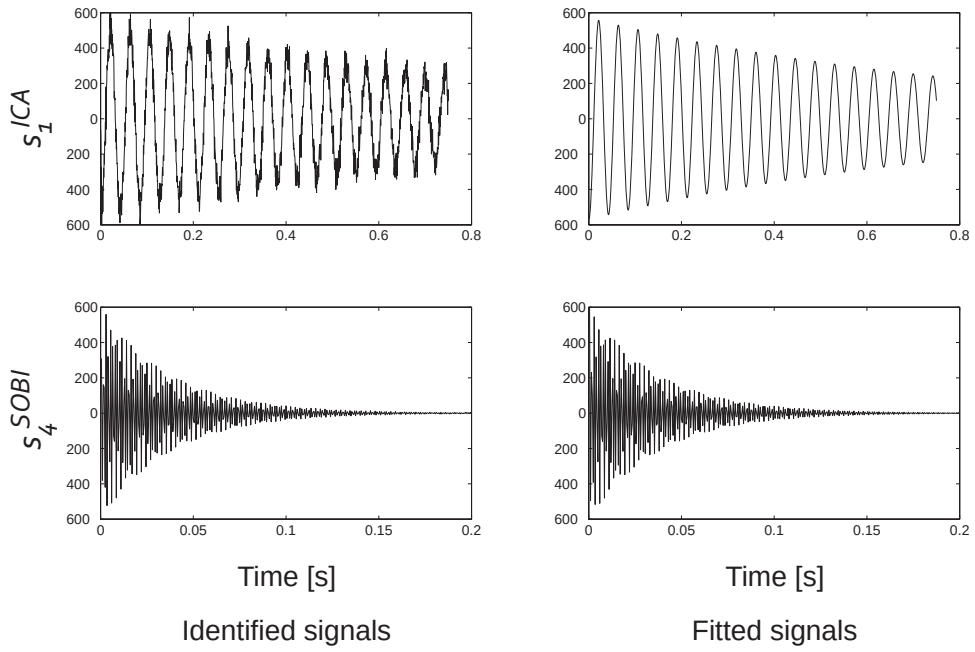

Figure 4.11: **Fitting post-processing for the identified sources**. On the left: two identified sources. On the right; the two corresponding fitted sources. (Cantilever beam, Free response, $\alpha = 2$, $\beta = 0.2e-5$, 5% RMS noise)

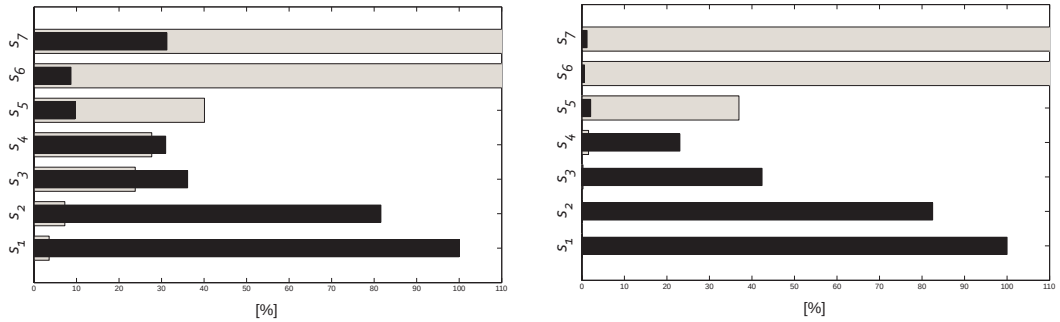

(a) ICA (b) SOBI

Figure 4.12: **Participation factor (in black) and fitting error (in gray) for the seven identified sources resulting from ICA and SOBI**. The first four sources (s_1 to s_4) correspond to the physical modes of the structure. (Cantilever beam, Free response, $\alpha = 2$, $\beta = 0.2e-5$, 5% RMS noise)

Frequency	$0,99 < r_\omega < 1.01$
Damping ratio	$0.8 < r_\xi < 1.2$
Mode shape	$MAC > 0.98$
Normal coordinate	$e_\eta < 5\%$

Table 4.9: Criteria used to evaluate the success of the identifications. (3DOF, Free response, $\alpha = 0.01$, $0\% \rightarrow 35\%$ RMS noise)

as the previous parameters verify the criteria of Table 4.9. Even though very strict conditions are considered for the success of the identifications, both ICA and SOBI methods appropriately identify 100% of the modes, for all of the 1800 identifications.

Figure 4.14 presents the evolution of the mean values regarding the percentage of noise for both identification methods. Since the standard deviations are very low for any level of noise (cf. Table 4.10), the mean values are representative of the general behavior.

It is clear that the mean values of the identified modal parameters are barely affected by the presence of noise. The two ratios $\mu(r_\omega)$ and $\mu(r_\xi)$ are very close to unity (i.e., their relative deviations are than 0.1 ‰ and lower than 1 %, respectively), indicating that the frequencies and the damping ratios are accurately evaluated whatever the level of noise. The MAC values are highly satisfying (much higher than 0.99), and the NMSE $\mu(e_\eta)$ are extremely low (around 0.1 %). These observations are valid for both ICA and SOBI approaches demonstrating very accurate identifications.

As a result, the identification process seems fairly insensitive to the noise in the data, at least under the assumptions considered in the present work. Even though it is not highly significant considering the low level of the errors, it should be noted that SOBI provides slightly better results for each of the four accuracy indicators.

Note that this study was also performed considering white Gaussian noise and led to the same conclusions. Similar results were obtained considering the random forced responses, but, for conciseness, they are not presented here.

	$\sigma(r_\omega)$	$\sigma(r_\xi)$	$\sigma(MAC)$	$\sigma(e_\eta)$
ICA	0.0001	0.05	0.003	0.08
SOBI	0.0001	0.05	0.001	0.02

Table 4.10: Maximum standard deviations corresponding to Fig. 4.14 for the accuracy indicators, for any level of noise and any mode. From left to right: standard deviations of the relative error on the frequency; standard deviation of the relative error on the damping ratio; standard deviation of the MAC between mode shapes; standard deviation of the NMSE between the fitted and the theoretical sources (3DOF, Free response, $\alpha = 0.01$, 0% $\rightarrow$ 35% RMS noise)

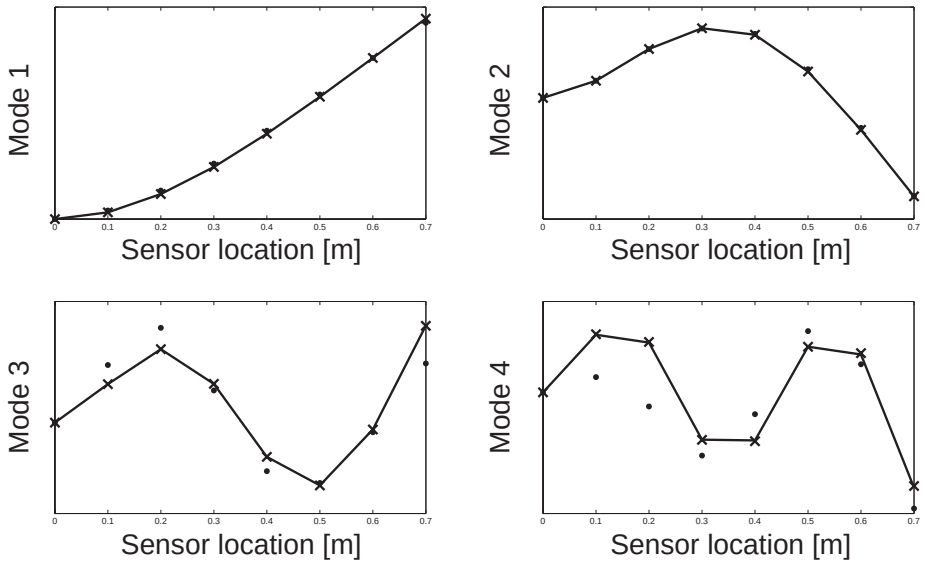

Figure 4.13: **Comparison between the theoretical mode shapes (solid line —), the ICA-based modes (•) and the SOBI-based modes (×)**. (Cantilever beam, Free response, $\alpha = 2$, $\beta = 0.2e - 5$, 5% RMS noise)

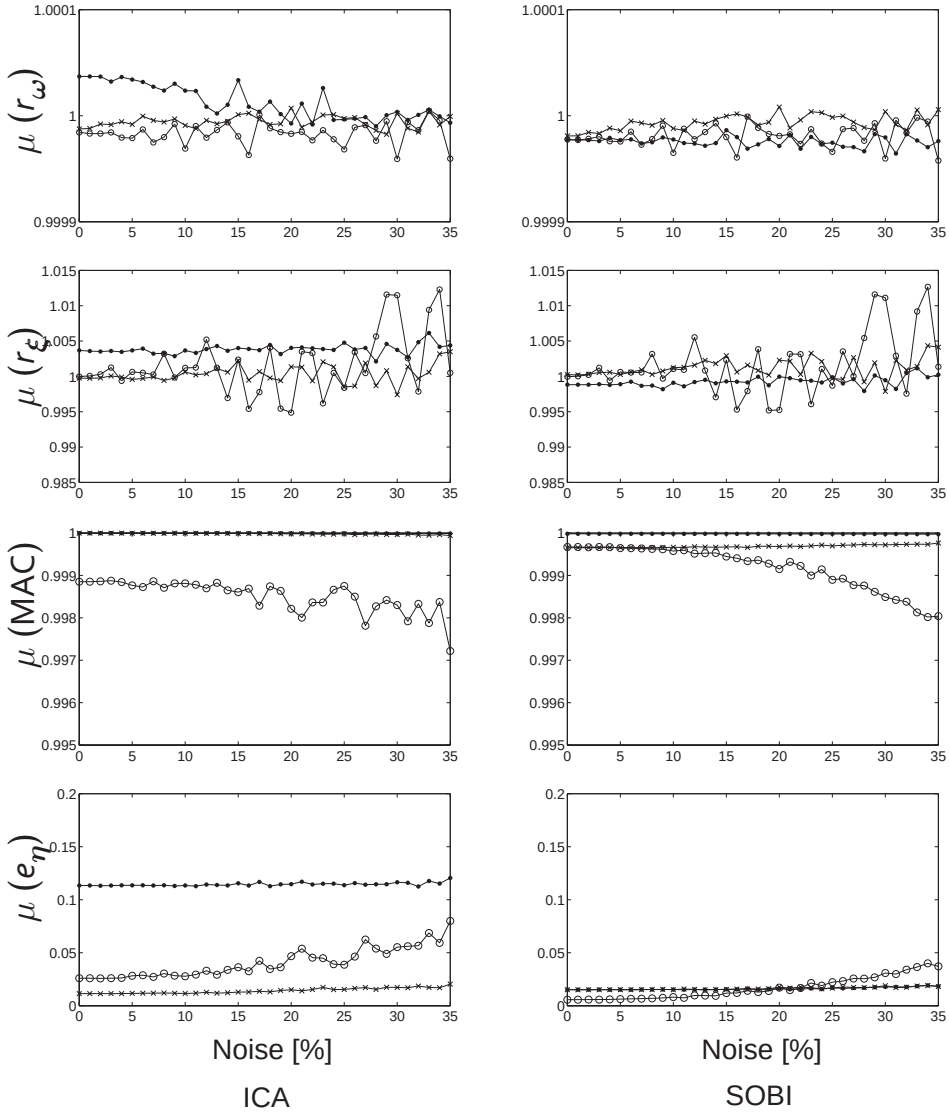

Figure 4.14: **Influence of the percentage of noise corrupting the responses on the accuracy of the identification**. 50 simulations are performed for each level of noise. From top to bottom, the means of the following parameters are presented: identified to theoretical frequencies ratio; ratio of identified to theoretical damping ratios; MAC between mode shapes; NMSE between the separated signals and the theoretical modal coordinates. $-\bullet-$: mode 1, $-\times-$: mode 2, $-\circ-$: mode 3. (3DOF, Free response, $\alpha = 0.01$, $0\% \rightarrow 35\%$ RMS noise)

4.6 Influence of Damping

The robustness of both methods with respect to the amount of damping introduced in the system is investigated in this section. Damping has mainly two effects on the system response. First, in case of free responses, high damping causes the evanishment of the response signals after a short time reducing the amount of available information for the separation. Second, damping may induce overlapping of the frequency spectra ensuing from different natural frequencies. This could be problematic, especially in case the natural frequencies are close to each other.

The free response of the 3DOF damped system is considered herein for values of α ranging from 0 to 0.15. This latter value corresponds to a highly damped system; the damping ratios of the three modes are $\xi_1 = 13.33$ %, $\xi_2 = 8.18$ % and $\xi_3 = 4.73$ %, respectively. As is the case for the reference case study described in Sec. 4.1, Gaussian noise corrupts the signals; the noise RMS amplitude is 5 % of the signal RMS value.

Only the first 1500 samples of the displacements are retained for the identifications. For illustration, the displacement signals corresponding to the highest damping value are presented in Fig. 4.15. The figure shows that the damping reduces the signals to zero after only four or five cycles of the principal natural frequency and the PSD signals present a not insignificant overlap of spectra. These signals have to be compared to those of Fig. 4.3.

ICA and SOBI are then applied to the damped signals, and Figure 4.16 presents the quality of the results in terms of frequencies (r_ω), damping ratios (r_ξ), modes (MAC) and normal coordinates (e_η). The results are depicted with respect to the theoretical damping ratios for each of the three modes, and thus, every single damping parameter α corresponds to three different values of damping ratios ξ_1, ξ_2 and ξ_3 in the graphs.

The first observation is that, as expected, both algorithms perform well for the weakly damped system (i.e., for damping ratios lower than 1 %) but the behaviors differ from one algorithm to the other when damping increases.

Over 1 %, the correspondence between the ICA modes and the vibration modes is no longer assured. Only the first mode, which is dominant if referring to Fig. 4.3, is satisfactorily identified, but ICA clearly fails to separate the sources. Substantial errors appear when looking at the normal coordinates and the mode shapes. For the third mode, MAC values are even close to zero. In addition, ICA presents an erratic behavior regarding the damping, as proved by the presence of gaps in the curves of Fig. 4.16. It is therefore concluded that if ICA is used, high damping causes bad repercussions on the modal parameter estimation.

Contrarily, the SOBI-based method appears more reliable. Whatever the damping ratios, the source separation provides accurate results, as illustrated by the

		r_ω [-]	r_ξ [-]	MAC [-]	e_η [%]
Mode 1	**ICA**	0.9992	1.1729	0.977	74.739
	SOBI	1.0000	0.9975	1.000	0.090
Mode 2	**ICA**	1.0085	1.4935	0.116	282.512
	SOBI	1.0000	1.0002	0.998	0.197
Mode 3	**ICA**	0.5761	0.9993	0.014	73.507
	SOBI	1.0000	0.9990	0.995	0.082

Table 4.11: Accuracy of the identifications (ICA and SOBI) for a damping parameter $\alpha = 0.05$ (corresponding to the damping ratios $\xi_1 = 13.33\%$, $\xi_2 = 8.18\%$ and $\xi_3 = 4.73\%$) compared to theoretical results. From left to right: identified to theoretical frequencies ratio; ratio of identified to theoretical damping ratios; MAC between mode shapes; NMSE between the fitted and the theoretical sources. (3DOF, Free response, $\alpha = 0.05$, 5% RMS noise)

low value of e_η (lower than 5 %). The mixing matrix is also successfully identified, and so are the mode shapes, even in the case of the low-participating third mode (beyond 0.95 for the MAC). It should also be noted that, in contrast with ICA, SOBI has a monotonic behavior regarding damping.

The results are listed in Table 4.11 for a specific value of the damping parameter ($\alpha = 0.05$) and for each of the three modes. These results, representative of the whole system behavior, confirm the efficiency of SOBI in the case of high proportional damping.

Two additional observations, relativizing these conclusions, should be underlined. First, the most important parameter for the accuracy of the SOBI separation is the level of overlap of the frequency spectra. The damping ratio values and the distance between the natural frequencies are thus highly interrelated. For instance, two systems characterized by the same damping ratios can be differently separated according the closeness of their natural frequencies. Second, the damping considered in this work is proportional (i.e., diagonal, cf. 2.4). However, in real applications, high damping is usually non proportional, and this could limit the applicability of the method.

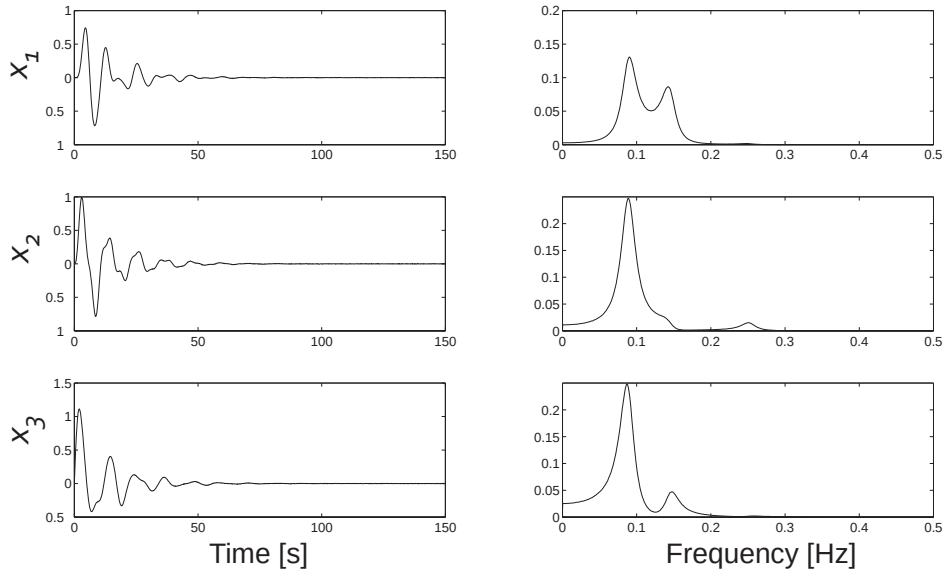

Figure 4.15: **Displacement response for a high damping parameter** $\alpha = 0.15$ **on the left and the corresponding PSDs on the right**. The corresponding damping ratios of the three modes are 13.33 %, 8.18 % and 4.73 %. (3DOF, Free response, $\alpha = 0.15$, 5% RMS noise)

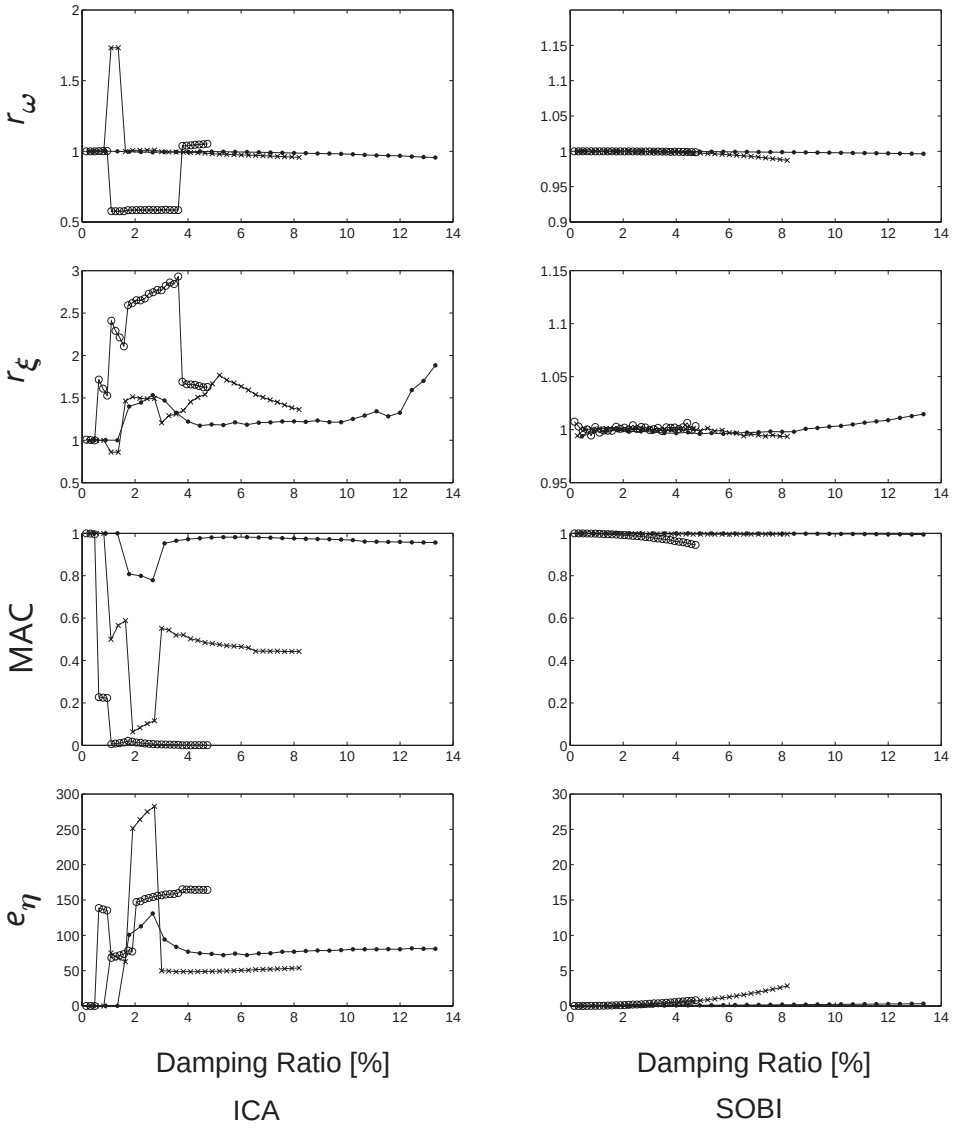

Figure 4.16: **Influence of the percentage of damping ratios on the accuracy of the identification**. From top to bottom: identified to theoretical frequencies ratio; ratio of identified to theoretical damping ratios; MAC between mode shapes; NMSE between the separated signals and the theoretical modal coordinates. $-\bullet-$: mode 1, $-\times-$: mode 2, $-\circ-$: mode 3. (3DOF, Free response, $\alpha = 0 \rightarrow 0.15$, 5% RMS noise)

4.7 Concluding Remarks

BSS techniques such as ICA and SOBI have been theoretically proved to be useful for output-only modal parameter estimation in Chapter 3 and were applied to numerical applications in the present chapter. Besides the numerical validation of these theoretical findings, the objective was to compare the performances of both algorithms in order to identify the most appropriate one for practical applications. For this purpose, several numerical case studies dealing with free or random forced responses, slightly or highly damped systems and noisy data were considered. The proposed automated mode selection, avoiding the use of complex tools such as the stabilization diagram, has also been successfully applied to several examples.

Even though both approaches are BSS techniques, ICA and SOBI behavior differ from each other and the following observations can be highlighted:

- ICA and SOBI have similar performances for slightly damped systems either for free or random forced responses. Modal parameters are very accurately identified.

- No substantial discrepancies can be emphasized between the methods regarding the robustness with respect to noise. Both algorithms are fairly insensitive to temporally and spatially white noise in the data.

- SOBI clearly outclasses ICA in case of non-deterministic random excitation. ICA fails identifying more than half of the considered test-cases and is less robust for practical use.

- In contrast with ICA, the quality of the separation performed using SOBI facilitates the selection of the genuine modes when the number of sources exceeds the number of active modes, by clarifying the accuracy indicators used during the automated mode selection.

- The study of the robustness with respect to damping is clearly in favor of SOBI. Separations based on SOBI provide accurate results, even in case of high damping ratios, whereas ICA behavior is much more erratic.

Besides these considerations, it should be underlined that the quality of the damping ratio estimations slightly decreases in case of random forced responses, though still very satisfactory. It has been shown that this parameter is not directly estimated from the normal coordinates of the system but from the free decaying signals resulting from NExT. This necessary intermediate stage involuntarily deteriorates the damping estimates.

Considering these observations, the proposed methodology based on BSS techniques can be considered as validated for output-only modal analysis. However, SOBI intelligently takes advantage of the temporal structures inherent to dynamical signals and its superiority is clearly established when compared to ICA. Consequently, the only SOBI algorithm is retained in the following chapter. It is also worth pointing that a systematic methodology has been proposed to choose the delays for SOBI. SOBI jointly diagonalizes several time-lagged covariance matrices instead of a single one, and the corresponding delays must be chosen accordingly to the physics of the problem.

Chapter 5

Numerical and Experimental Demonstrations

Abstract

To demonstrate the utility of SOBI for output-only modal analysis in practical applications, the method is applied to the responses of large-scale and real-life structures. Both free and random forced responses are considered and the identified modal parameters are compared to those obtained using the stochastic subspace identification method (SSI-COV), detailed in Chapter 1.

First, a numerical system consisting of a large truss satellite and modeled using the finite element method, is considered (Sec. 5.1). The objective is to validate the proposed methodology for larger systems and for large number of active modes within a small frequency range.

Second, Section 5.2 examines the free response of a real structure. The system is a stator blade extracted from an aeroengine, that is a typical application for modal analysis techniques.

Finally, SOBI is used to identify the modal parameters of a truss structure, modeling a two-story building (Sec.5.3). Free and forced responses are analyzed. For the forced response, the truss is excited through the basement by means of an electrodynamic shaker.

5.1 Truss Satellite

5.1.1 System Description

The structure considered in this section is a large-scale truss satellite. The topology used for the modeling is inspired by the one presented by Salehian et al. in [SCI06]. The central part is a six-meter long cylinder that is stiffened by means of several internal shear panels. Two truss structures (made of tubular longerons, battens and diagonals) are symmetrically placed on both sides of the cylinder. The longerons are parallel to the axial direction of the cylinder (X-axis). Their cross section is tubular, and the corresponding internal and external radiuses equal 37 and 38 mm, respectively. The battens are the triangular structures that link the longerons together, and the diagonal structures prevent the torsion mechanisms. Both have a tubular cross section where the internal radius equals 12.5 with a 0.5 mm thickness.

Reference aluminum elastic material properties are used for all parts. Table 5.1 lists all the material properties and dimensions used for the modeling, and Figure 5.1 illustrates the satellite topology.

5.1.2 Modeling and Simulations

A finite element approach is used to model the structure and simulate the free and forced dynamic responses. Shell elements are used for the shear panels contained in the cylinder whereas beam elements (with tubular cross-section) model the truss.

In order to avoid zero-frequency rigid-body modes which may cause problems during the computation of the dynamic response, eighteen (6 x 3) very soft ground-springs are added along the three principal directions (X, Y and Z) at the three vertices of the sections B and G (see Fig. 5.1). The spring stiffness is chosen such that the six rigid body modes do not interfere with the elastic modes. The corresponding frequencies are around 0.3 Hz, thus much lower than the first non-rigid-body natural frequency that equals 6.55 Hz.

The present analysis focuses on the 20 first elastic modes and this corresponds to the frequency range [0-23Hz]. The corresponding natural frequencies are listed in Table 5.2 and it can be observed that they are very close to each other. The damping ratios are all set to 0.1%.

By way of clarification, the modes are divided into three categories:

- Modes 1V to 8V: bending within the vertical plane (OXZ);
- Modes 1H to 8H: bending within the horizontal plane (OXY0);

Young's modulus	69000 MPa
Poisson's ratio	0.33
Total length	54 m
Internal radius of longerons	37 mm
External radius of longerons	38 mm
Internal radius of diagonals and battens	12.5 mm
External radius of diagonals and battens	13 mm

Table 5.1: Material and geometrical properties of the truss satellite.

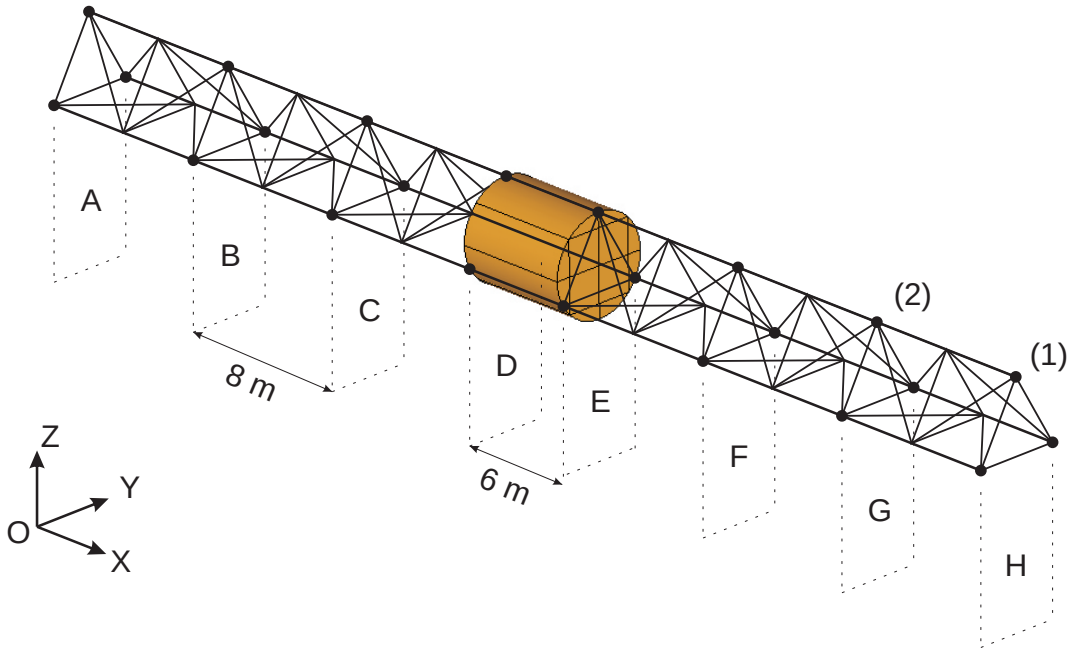

Figure 5.1: **Topology of the considered truss satellite system.** Three locations (•) are defined for each vertical section A to H for the measurement along the two directions Y and Z. The two locations (1) and (2) are the position of the initial non-zero condition (in the case of the free response computation) and of the applied random force (in the case of the forced response computation), respectively.

- Modes 1T to 4T: torsion around the axial direction (OX).

For illustration, one mode shape representative of each category (modes 6H, 3T and 7V) is depicted in Fig. 5.2.

The dynamic responses are computed using the modal superposition principle [GR94]. The first 60 modes are considered for the computation. The generic properties, which are used for all the simulations presented herein, are summarized in Table 5.3. For each simulation, 48 sensor responses are computed; they correspond to the vertical (Z-axis) and horizontal (Y-axis) accelerations at the three vertices of each vertical section A to H (see Fig. 5.1).

The free response is computed by imposing a non-zero velocity initial condition (0.1 m/s). This impulse is applied vertically (along Z-axis) at one extremity of the truss, precisely at the vertex (1) in the section H. For illustration, the response signal at the top vertex of section B is presented in Fig. 5.3.

The forced response is generated by applying a structural loading during all the simulation time. Three different excitations are simultaneously applied to the vertex (2) (cf. Fig. 5.1): a vertical random force along Z-axis, an horizontal random force along Y-axis and finally a random torque around the X-axis. To approximate the experimental conditions, the random Gaussian input is filtered to cover the frequency range from 5 to 30 Hz encompassing the 60 computed FE modes (used for the modal superposition). This should excite all the 20 modes (the vertical and the horizontal bending modes, from 1V to 8V and from 1H to 8H, as well as the torsion modes, from 1T to 4T). For illustration, one representative acceleration signal is presented in Fig. 5.4.

This first test-case is a real challenge for the SOBI-based identification because it combines several major difficulties. First, as indicated in Table 5.2, the number of natural frequencies is relatively high regarding the frequency range of interest. Numerous frequencies are very close to each other and the introduced damping inevitably leads to overlapping of the frequency spectra. Second, due to the single point excitation, some modes might be weakly excited, introducing few information in the responses for the source separation. Finally, due to the spatial resolution, several mode shapes corresponding to different natural frequencies are similar. This phenomenon corresponds to identical columns in the mixing matrix and computational difficulties, and so inaccuracy during the separation.

5.1.3 Modal Parameter Identification using Free Responses

The free response is first considered to estimate the modal parameters. The identification is performed using SSI-COV and then using SOBI. Only the first 6000 samples, corresponding to the 40 first seconds before the signal is damped

Modes 1-5	**Mode identifier**	1H	1V	1T	2T	2H
	Natural frequency [Hz]	6.55	6.56	7.69	7.78	9.39
	Damping ratio [%]	0.1	0.1	0.1	0.1	0.1
Modes 6-10	**Mode identifier**	2V	3H	3V	4H	4V
	Natural frequency [Hz]	9.39	12.20	12.21	12.45	12.46
	Damping ratio [%]	0.1	0.1	0.1	0.1	0.1
Modes 11-15	**Mode identifier**	5H	5V	6H	6V	3T
	Natural frequency [Hz]	16.93	16.94	17.04	17.04	20.93
	Damping ratio [%]	0.1	0.1	0.1	0.1	0.1
Modes 16-20	**Mode identifier**	4T	7H	7V	8H	8V
	Natural frequency [Hz]	20.95	22.65	22.65	22.67	22.68
	Damping ratio [%]	0.1	0.1	0.1	0.1	0.1

Table 5.2: Natural frequencies and damping ratios for the first 20 vibration modes of the truss satellite structure.

Modal damping	0.1 %
Sampling frequency	153.6 Hz
Number of samples	18432
Simulation time	120 sec
Number of simulated sensor	48

Table 5.3: Properties used for the simulation of the dynamic responses.

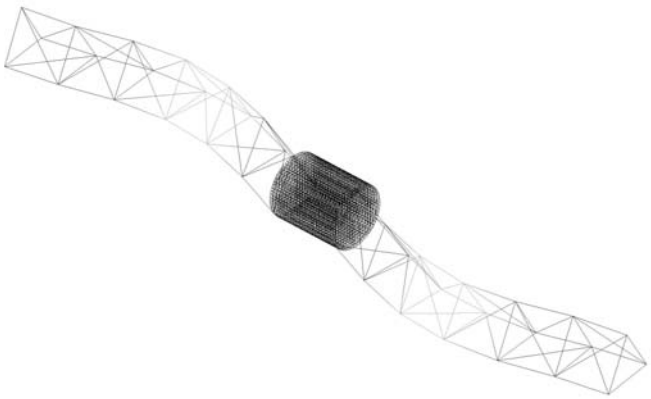

(a) Mode 6H - 17.04 Hz

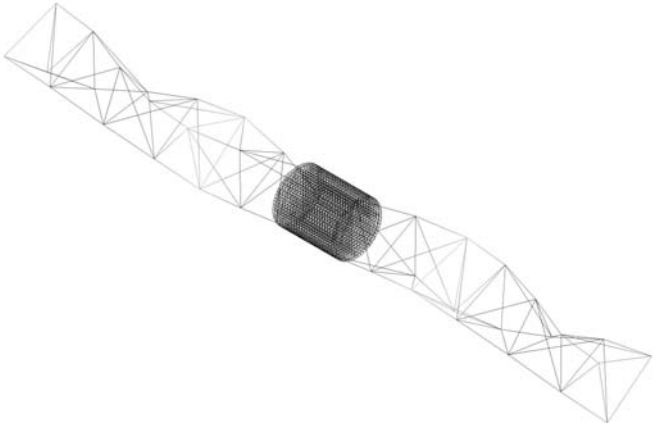

(b) Mode 3T - 20.93 Hz

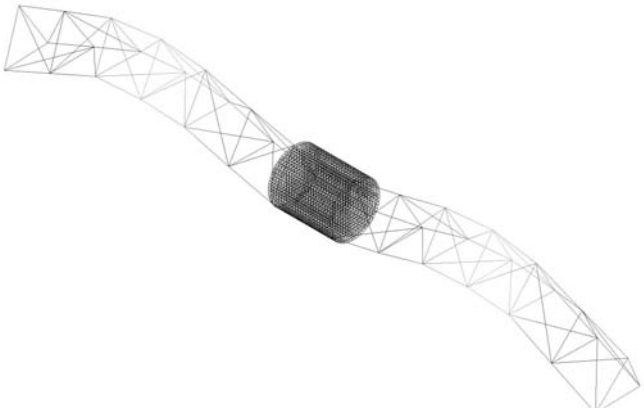

(c) Mode 7V - 22.65 Hz

Figure 5.2: **Mode shape of the truss satellite.** Mode 6H is the sixth bending mode in the horizontal plane (OXY), mode 3T is the third torsion mode around the axial direction (OX) and mode 7V is the seventh bending mode in the vertical plane (OXZ).

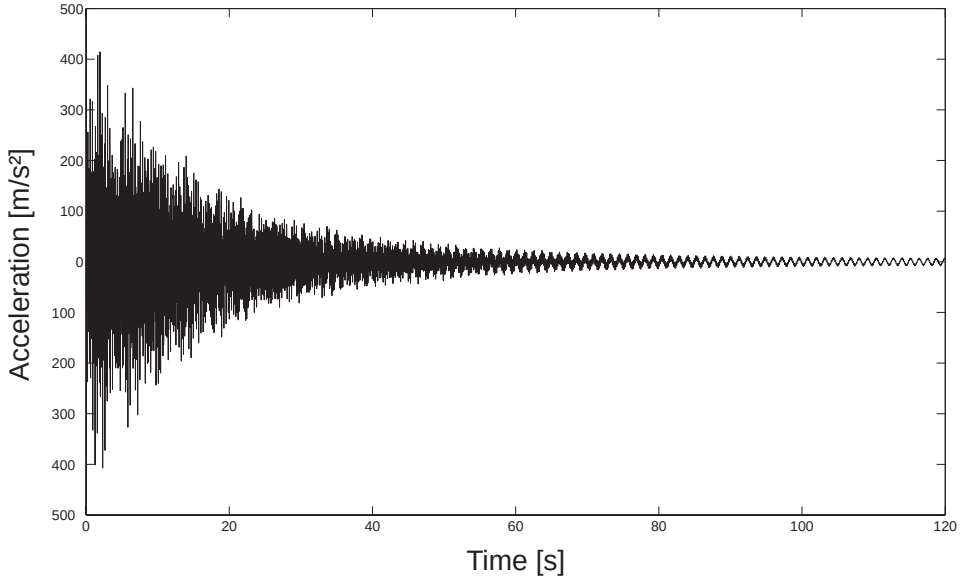

Figure 5.3: **Simulated free response of the truss satellite system.** This signal represents the evolution of the acceleration along Z-axis at the top vertex of section B.

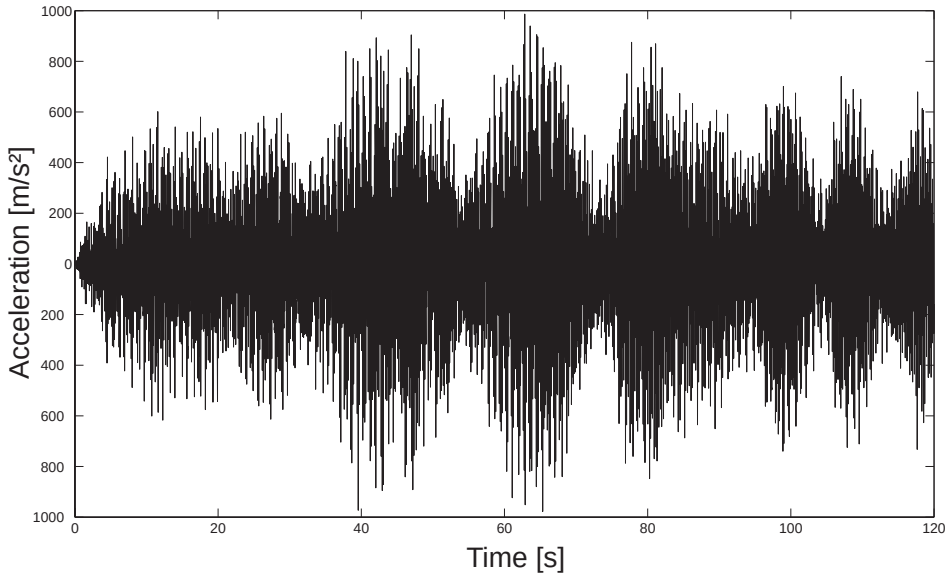

Figure 5.4: **Simulated forced response of the truss satellite system.** This signal represents the evolution of the acceleration along Z-axis at the top vertex of section B. The system is subjected to random loading along Y- and Z-axes as well as a random torque around X-axis.

out, are taken into account. The results computed using both approaches are compared using MAC indicator, defined in Sec. 4.1.3.

It is important to note that the input loading does not provide a sufficient excitation for the horizontal bending modes (from 1H to 8H) to be activated. Consequently, only the vertical bending and torsion FE modes (from 1V to 8V and from 1T to 4T) are retained for the comparison with the identified modes.

SSI-COV Identification

As detailed in Sec. 1.5, the use of SSI-COV method necessitates to choose a model order, that is directly related to the number of expected active modes. Because of the large number of natural frequencies contained in the response signal (more than 60 modes between 0 and 30 Hz), a high system order has to be considered.

The subspace identification is based on the computation of a stabilization diagram helping the user to separate the genuine from the spurious vibration modes and frequencies. This tool requires a gradual increase of the model order and a problem resolution for each of the considered orders. Presently, orders from 5 to 100 are computed.

For every single computed order (i), the identified frequencies, damping ratios and mode shapes are compared to those of the previously computed order ($i-1$) and only the stabilized frequencies are represented. A particular attention is brought to the combined stabilization of all the modal parameters (frequency, damping and mode shape). The criteria used to evaluate the stabilization of the three parameters are listed in Table 5.4.

The resulting diagram is presented in Fig. 5.5. The diagram shows the stabilization of 12 natural frequencies within the frequency range [0-23Hz]. After a visual inspection, the order 82 is chosen for modeling the system because it combines a stabilization of all the expected frequencies over several orders. However, it can be observed that the stabilization lines are not perfectly continuous. Some frequencies suddenly disappear for several orders before stabilizing again.

The MAC matrix is computed to compare the identified modes to the FE modes. Figure 5.6 graphically present the results. This figure proves the very good correlation between SSI and FE modes. Note that the 3V mode is not properly excited using the considered initial condition. This may explain the lower accuracy of the results for this mode ($MAC = 0.84$).

Figure 5.7(a) provides the identified damping ratios, previously set to 0.1 %, for all the SSI-COV modes. This parameter is clearly accurately identified by SSI-COV.

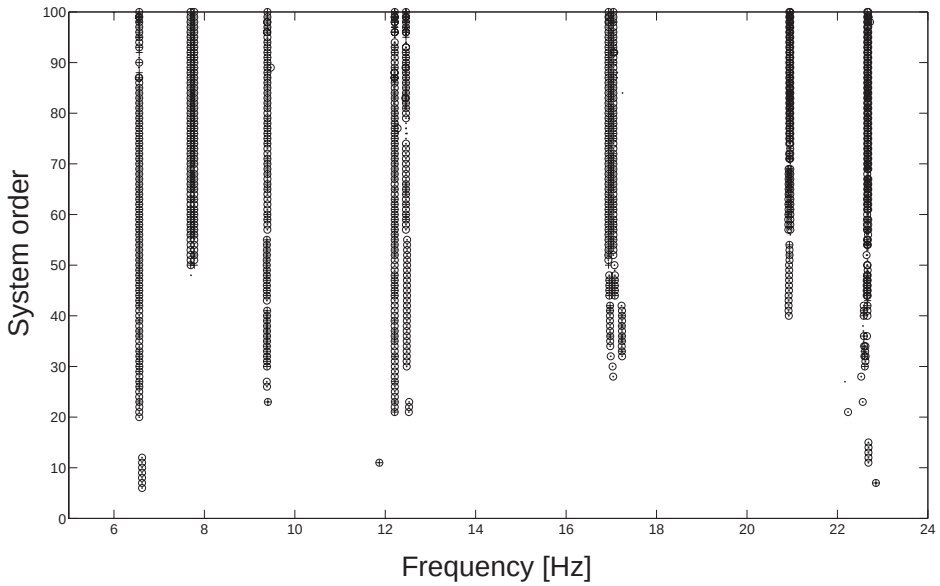

Figure 5.5: **Stabilization diagram obtained with the SSI-COV method.** The identification is computed for the system orders from 5 to 100. Only the stabilized frequencies are represented. A stabilized frequency is labeled as (·) whereas (○) is a stabilized mode and (+) is a stabilized damping ratio. (Truss satellite - Free response).

Frequency	$\frac{f_i - f_{i-1}}{f_i} < 0.05\%$
Damping ratio	$\frac{\xi_i - \xi_{i-1}}{\xi_i} < 2\%$
Mode shape	$MAC > 0.99$

Table 5.4: Criteria used to evaluate the stabilization of the modal parameters between two successive orders.

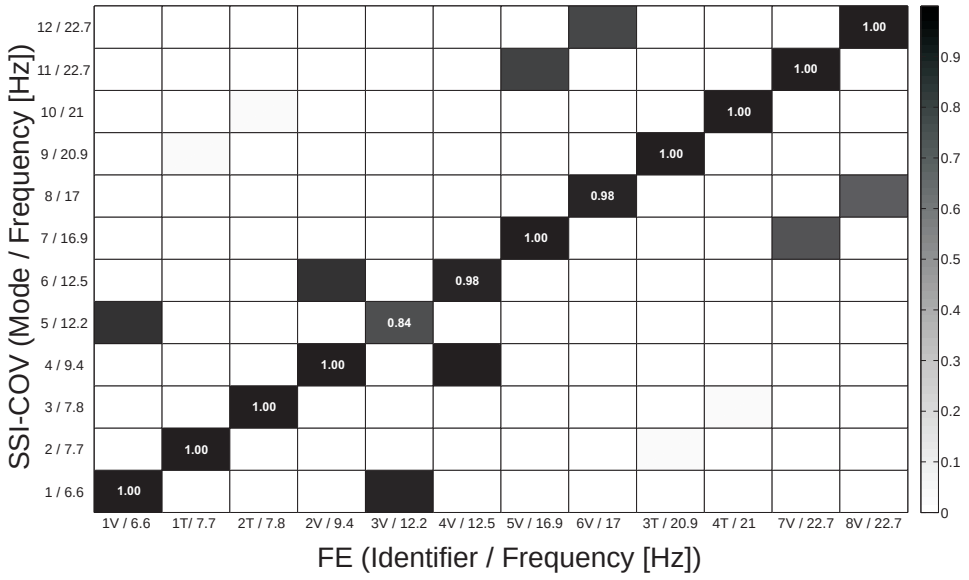

Figure 5.6: **Correlation between the FE modes and the SSI-COV modes using MAC matrix.** The white numbers indicate the numerical values of the MAC for the diagonal terms. (Truss satellite - Free response)

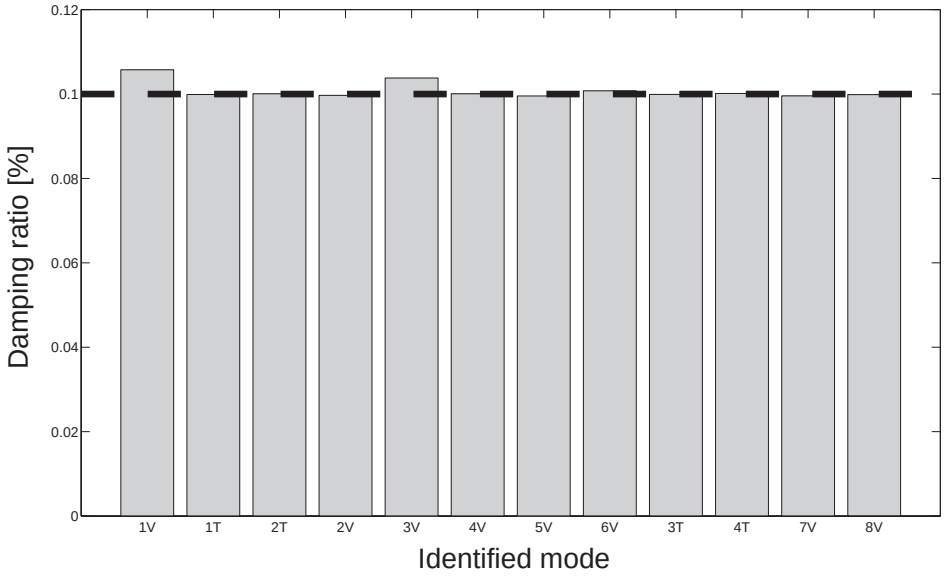

(a) Damping ratios identified using SSI-COV

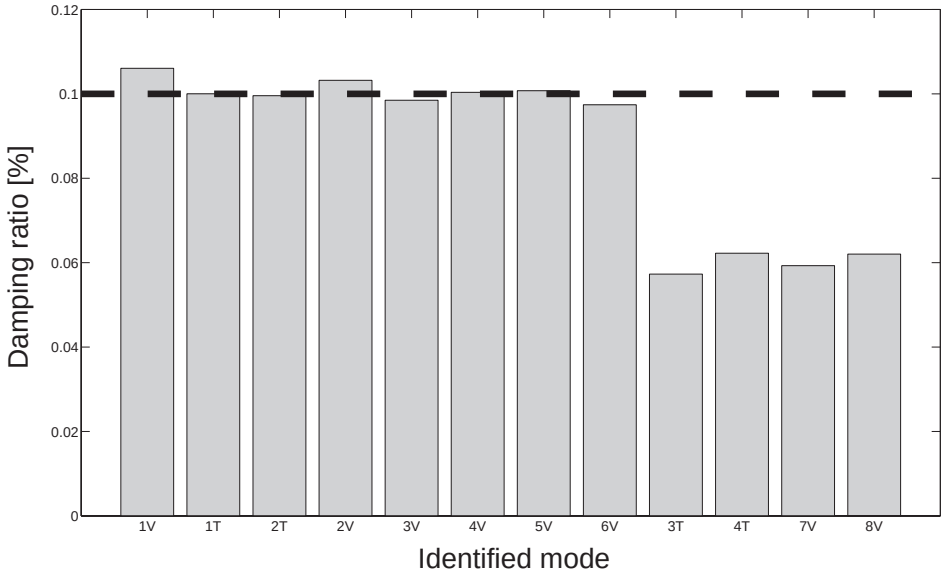

(b) Damping ratios identified using SOBI

Figure 5.7: **Values of the damping ratios for both identification methods.** The expected value is 0.1% for all modes. (Truss satellite - Free response)

SOBI-based Identification

The same first 6000 samples are now used to estimate the modal parameters using the SOBI algorithm. As proposed in Sec. 4.2, 20 delays are chosen uniformly distributed between 1/23Hz and 1/5Hz in order to built the time-lagged covariance matrices. This time range corresponds to the frequency range of interest [5-23Hz].

Because SOBI identifies as many sources (or modes) as the number of input signals, 48 independent (or as independent as possible) sources are separated by the algorithm. Then, it is necessary to separate the genuine vibration modes from the spurious ones. The procedure has been detailed in Sec. 3.4.

The proposed selection procedure relies on the fitting error which is computed for each source. Knowing the theoretical form of the sources (i.e., the modal coordinates), it is straightforward to optimize the theoretical parameters in order to match the identified signals. A fitting error e_{fit} is then easily computed using NMSE criteria, defined in Eqn. (3.16).

On the one hand, the dominant frequency of the selected sources must belong to the frequency range of interest. On the other hand, the parameter e_{fit} must remain under a certain limit. The automated mode selection is then based on the following criteria:

- Only the natural frequencies included in the considered frequency range [0-23Hz] are retained;
- The fitting error e_{fit} (in gray in the figures) has to be lower than 10%, as suggested in Chapter 3.

Another interesting parameter is the participation factor PF (in black in the figures) evaluating the importance of each source in the total response signal and so the confidence that can be placed in this source. A good-quality testing procedure should lead to a high cumulative PF. This assures that most of the information contained in the initial data has been extracted.

Before this automated post-processing, 48 modes and natural frequencies were identified but only 17 of them belong to the frequency range [0-23Hz]. The fitting errors e_{fit} combined with the participation factors PF (both defined in Sec. 3.5) are presented for these 17 identified sources in Fig. 5.8(a). The corresponding modes are graphically compared to the FE modes by means of the MAC matrix in Fig. 5.9(a).

A careful observation of Fig. 5.8(a) leads to the conclusion that 5 sources (namely s_{45}, s_{42}, s_{31}, s_{36} and s_{44}) have to be removed. These identified sources combine a high value of the fitting error e_{fit} (in gray) with a moderately low value of the participation factor PF (in black). For illustration, Figure 5.10 presents one of these sources, at the top, and one of the reliable sources, at the bottom.

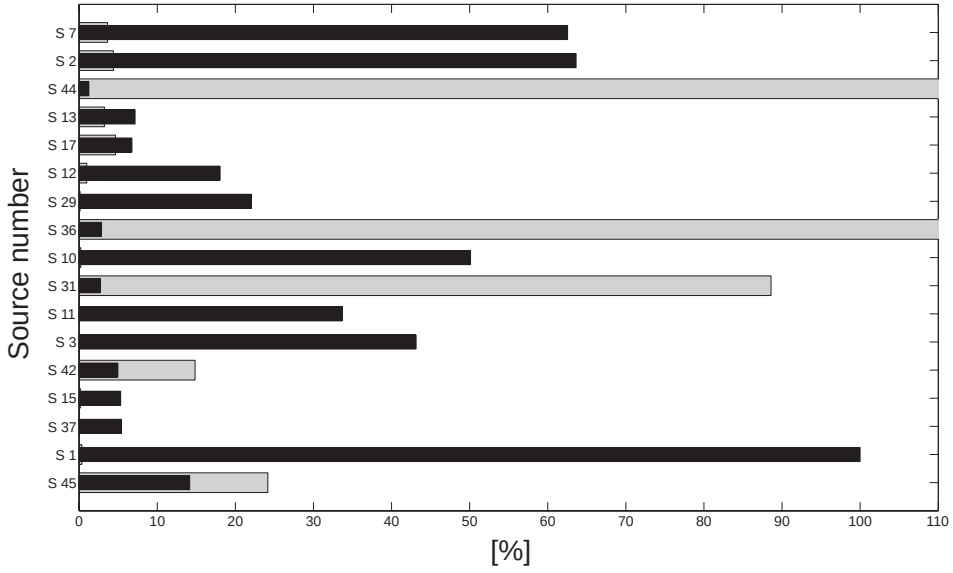

(a) Before automatic selection

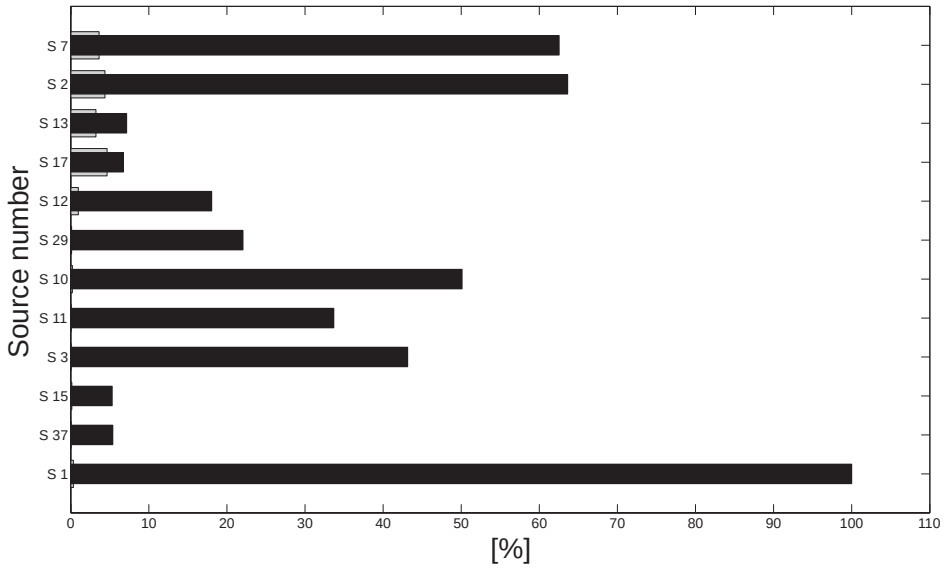

(b) After automatic selection

Figure 5.8: **Automatic selection of the genuine modes identified using the SOBI-based methodology.** All the sources identified between 0 and 23 Hz are presented before and after the automated selection. The participation factor is in black and the fitting error is in gray. (Truss satellite - Free response)

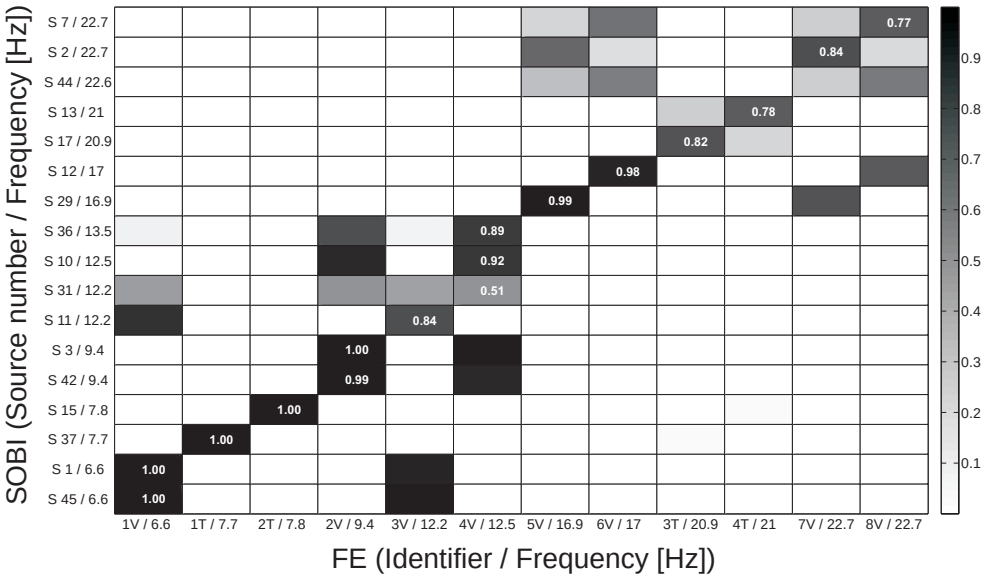

(a) Before automatic selection

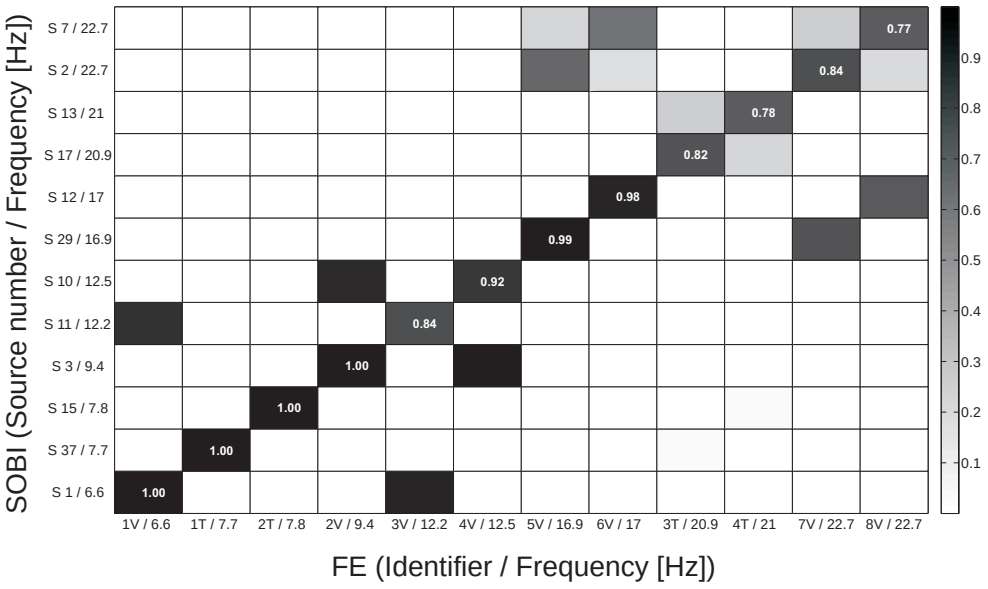

(b) After automatic selection

Figure 5.9: **Correlation between the FE modes and the SOBI modes using MAC matrix.** All the SOBI modes are considered between 0 and 23 Hz before and after the automated selection. The white numbers indicate the numerical values of the MAC for the diagonal terms. (Truss satellite - Free response)

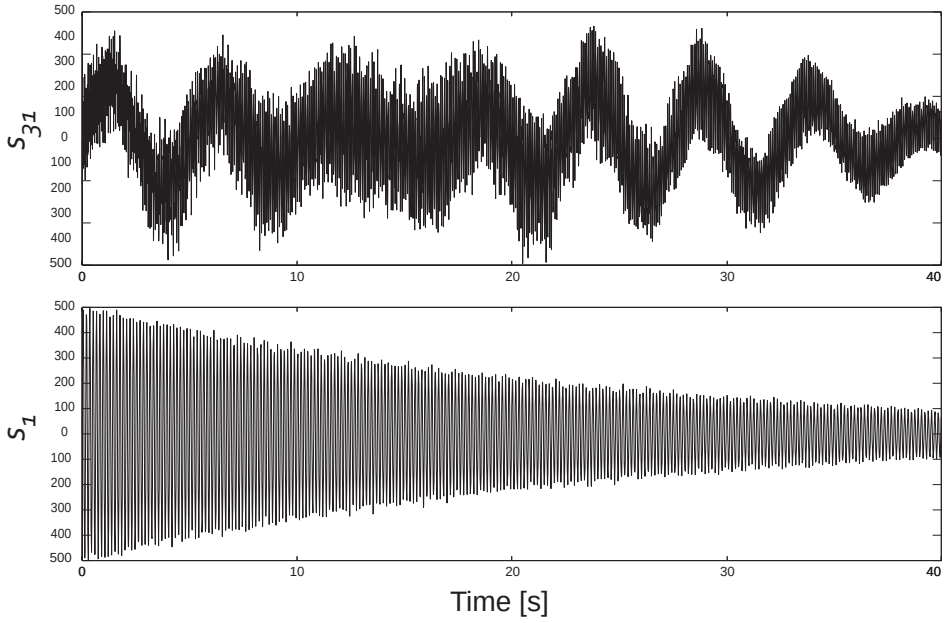

Figure 5.10: **Two representative sources resulting from SOBI.** The sources correspond to a spurious (top) and a genuine mode (bottom). The first one has to be rejected whereas the second one should be selected. (Truss satellite - Free response)

After the selection, 12 modes are retained for the comparison with the FE results. The resulting fitting errors are presented in Fig. 5.8(b) while the MAC matrix between the selected SOBI modes and FE results is presented in Fig. 5.9(b). The corresponding identified damping ratios are also graphically presented in Fig. 5.7(b).

The results of the SOBI-based identification are satisfactory even though they are not as accurate as the SSI-COV ones. The four modes denoted 3T, 4T, 7V and 8V are better estimated by the subspace methodology, as highlighted by the comparison between Figs. 5.9(b) and 5.6. It is also seen that the identified damping ratios resulting from SOBI (Fig. 5.7(b)) are underestimated. This inaccuracy is not surprising regarding the previously mentioned difficulties inherent in the test-case (i.e., close natural frequencies and/or mode shapes and low mode participation in the response).

Nevertheless, an interesting feature of the SOBI-based methodology is that a quality indicator, namely the fitting error parameter, is directly provided. It can be observed in Fig. 5.8(b) that the value of the fitting error corresponding to these four modes is around 5% whereas it is below 0.5% for the others. During experimental testings, exact solutions are unknown, and a special attention should thus be brought to this parameter in order to evaluate the reliability of the corresponding results.

5.1.4 Modal Identification using Random Forced Responses

For the forced response case, three random excitations are applied simultaneously at the location (2) during the simulation time (cf. Fig.5.1). The quality of the information contained in the response signals is thus improved and all the 20 modes (the vertical and horizontal bending modes as well as the torsion ones) are properly excited. Then, in this section, the 20 FE modes belonging to the range [5-23Hz] are considered for comparison.

The simulation generates a dynamic response for the first 180 seconds, and the sampling frequency still equals 153.6 Hz. The 18000 samples, computed after the evanishment of the transient response, are used for the identification.

SSI-COV Identification

Identically to the free response case, the SSI-COV technique is first used. Because the number of active modes is larger than in the free response case, the maximum considered system order has to be increased as well. The identifications are performed for system orders gradually increasing from 5 to 300, and the results are then postprocessed within the frequency range [5-23Hz].

The stabilization diagram is presented in Fig 5.11(a). Since some natural frequencies are very close to each other, close-up diagrams are also presented in Fig. 5.11(b). All the frequencies predicted by the FE model are detected by the SSI-COV algorithm, as indicated by the 20 stabilization vertical lines.

According to these results, a model order is selected such that all expected frequencies are stabilized. The order 178 seems to be a good candidate since it combines a stabilization over several orders for the frequencies, the damping ratios as well as for the mode shapes. However, this observation is valid for 27 modes within the frequency range [5-23] Hz. These 27 modes are compared to the FE predictions and the corresponding MAC matrix is presented in Fig. 5.12. The figure clearly shows that the subspace method fails to accurately identify all the physical modes.

Since this test-case is a numerical one, the exact solution is perfectly known and then the selection of the genuine modes can be facilitated by means of the MAC matrix between the the FE and the SSI-COV results for each system order. For this specific study, the identification is considered as successful if the MAC value is greater than 0.8. For every single computed system order, the number of the successful identifications is recorded and carried forward in Fig. 5.13.

Figure 5.13 clearly shows that the subspace method does not succeed in identifying more than 13 modes (over the 20 FE modes) at once even for high orders. Nevertheless, the successful identifications do not correspond to the same modes for all system orders, and it is possible to search for the best identification all over the orders for every single FE mode. This task, obviously totally unfeasible for practical application, is made possible thanks to the knowledge of the exact solution and leads to the MAC matrix presented in Fig. 5.14. Each considered SSI-COV mode is then computed using a different model order.

To conclude, the SSI-COV method accurately succeeded in identifying each of the structural modes, at least once over the 300 computed orders. The major difficulty for practical applications is the choice of the order that identifies the most accurately the mode, for each expected natural frequency.

SOBI-based Identification

The same 18000 samples are used for the SOBI-based identification. Similarly to the free response case, 20 time lags are chosen uniformly distributed between 1/23 Hz and 1/5 Hz for the identification. In the case of the random forced response, the identified sources do not match the theoretical expression (3.4) and then the post-processing (that remains totally automatic without any user interaction) requires the use of the NExT procedure for each of the separated source.

Because 48 sensors are used for the identification, 48 sources are separated

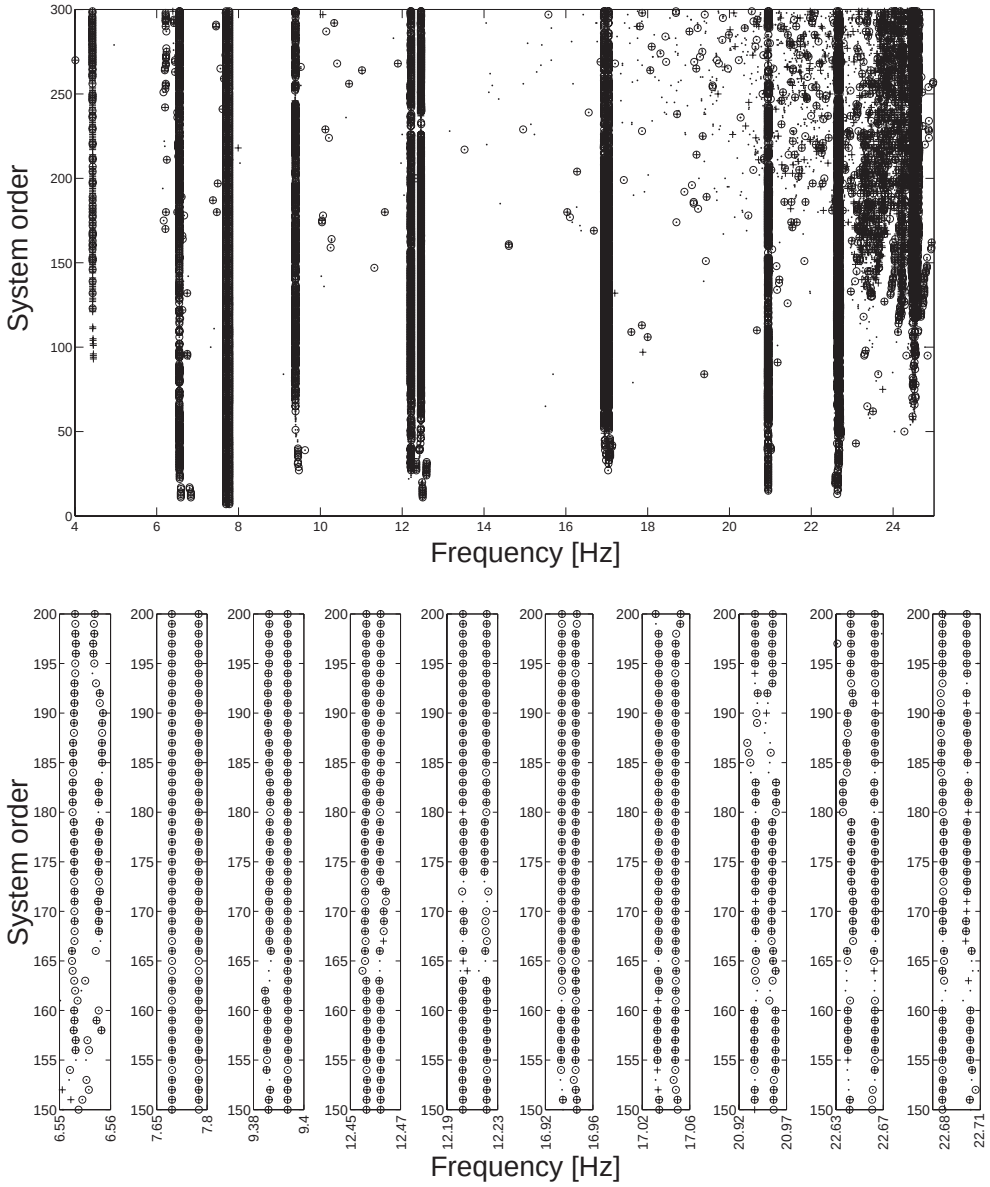

Figure 5.11: **Stabilization diagram (top) and close-ups around the natural frequencies (bottom) resulting from the SSI-COV method.** The identification is computed for the system orders from 5 to 300. Only the stabilized frequencies are represented. A stabilized frequency is labeled as (·) whereas (○) is a stabilized mode and (+) is a stabilized damping ratio. (Truss satellite - Forced response)

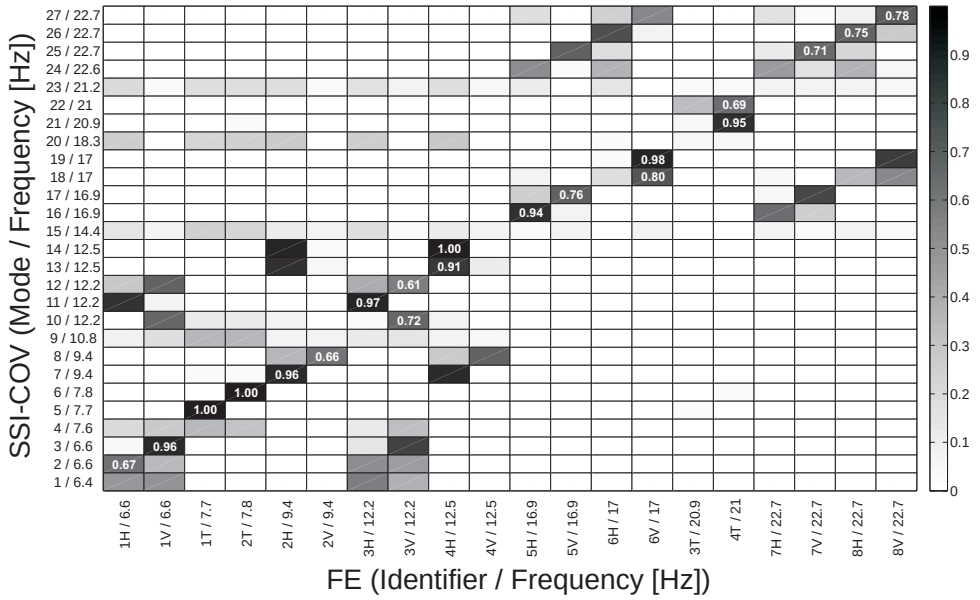

Figure 5.12: **Correlation between the FE modes and the SSI-COV stabilized modes (for the model order 178) using MAC matrix.** For any specific model order, SSI-COV fails to identify all the modes. Few of them are accurately identified and the others are absent. The white numbers indicate the numerical values of the MAC for the diagonal terms. (Truss satellite - Forced response)

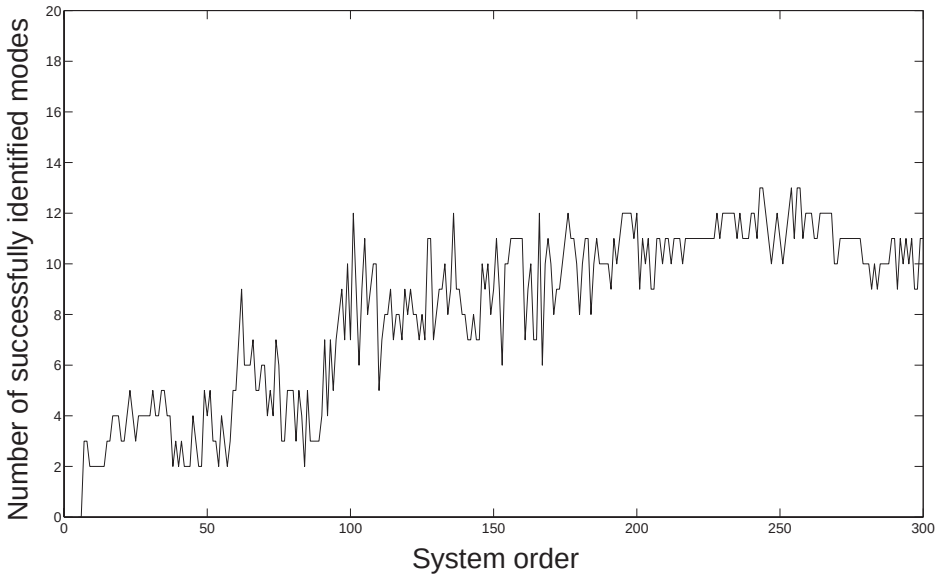

Figure 5.13: **Evolution of the number of successful identifications performed by SSI-COV, regarding the system order.** SSI-COV only succeed in identifying 13 modes over the 20 at once even for high orders. The accurately identified modes are not the same for all the considered model orders. (Truss satellite - Forced response)

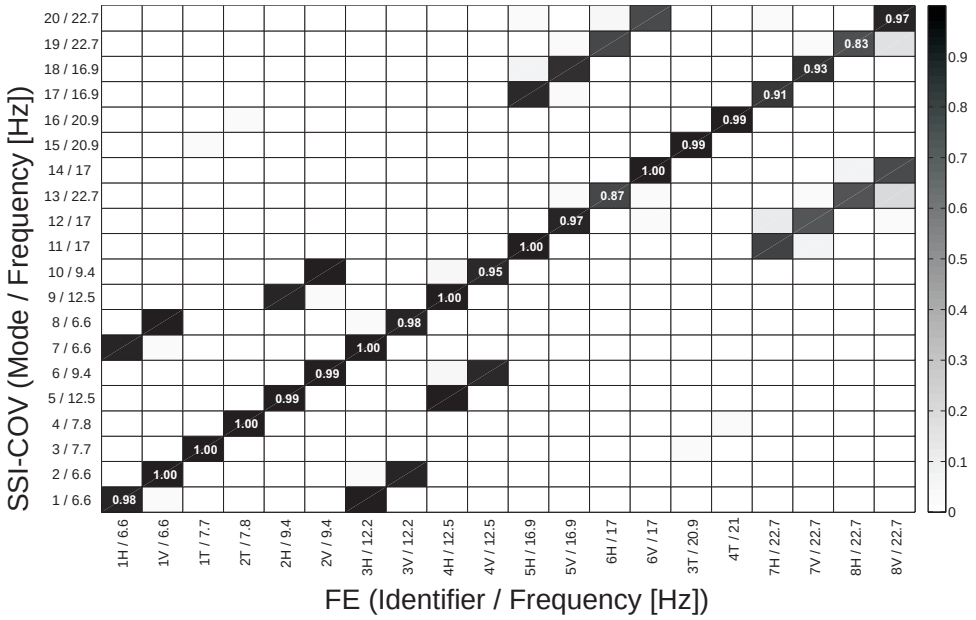

Figure 5.14: **Correlation between the FE modes and the SSI-COV modes best identified over all the computed orders.** The white numbers indicate the numerical values of the MAC for the diagonal terms. (Truss satellite - Forced response)

and the NExT post-processing is directly applied. After the mode selection which is performed using the previously mentioned criteria (i.e., a frequency belonging to [0-23Hz] and a fitting error below 10%), 20 modes are automatically selected. The fitting errors and the participation factors are presented in Fig. 5.15. It should be noted that the fitting errors are extremely low for all the selected sources (below 0.2 %).

The correlation between these genuine modes and the FE results is performed using the MAC matrix as presented in Fig. 5.16. This figure proves the excellent agreement between the SOBI and FE results. The performance of the identification is quite good and even very satisfactory if compared with the SSI-COV results presented in Fig. 5.12. Even though the test-case is chalenging, all modes are automatically extracted, and most of them are very accurate.

The damping ratios are not as well identified than in the free response case but remains acceptable for most of the modes. The values are graphically presented in Fig. 5.17(b) and can be compared to those identified using SSI-COV. Note that the SSI-COV damping ratios corresponds to the best identified SSI-COV modes from Fig. 5.14.

To conclude, it should be noted that the use of NExT causes two inconveniences. First, as previously mentioned, NExT slightly degrades the accuracy of the damping ratios. Second, although NExT simplifies the choice of the genuine sources by clarifying the fitting error indicator, the algorithm appears to clean the signals by removing most of the perturbing frequencies. The resulting signals then artificially become monochromatic, leading to the low fitting errors. Unfortunately, this error parameter provides no more information about the reliability of the initial results, contrary to the free response case. In fact, NExT acts as a sort of filter around the dominant frequency. Figure 5.18 illustrates this effect for one identified source. This is the reason why badly identified sources, such as S9 (MAC 0.48), correspond to extremely low fitting errors.

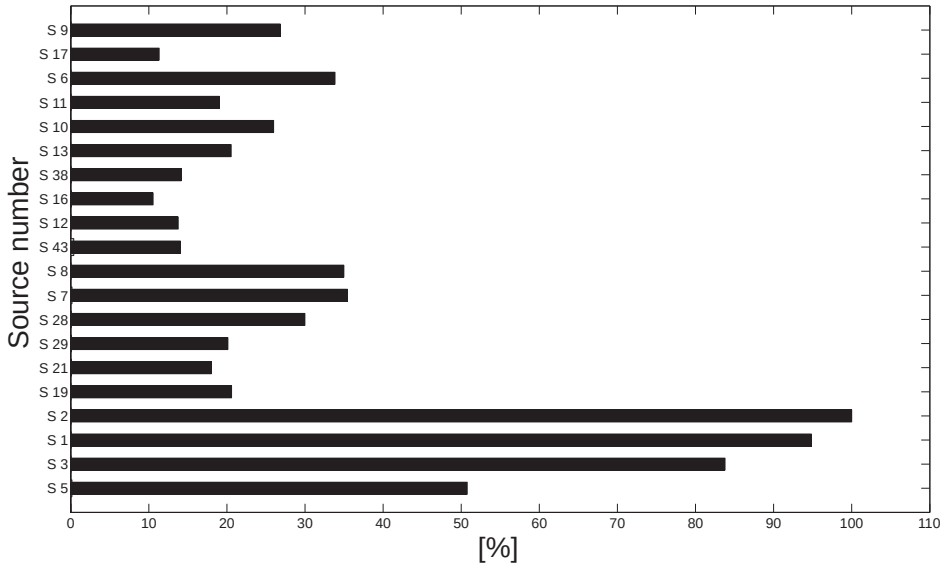

Figure 5.15: **Fitting errors and participation factors of the automatically selected sources.** Only the 20 selected sources are presented. The participation factor is in black and the fitting error is in gray, but very low (<0.5 %). (Truss satellite - Forced response)

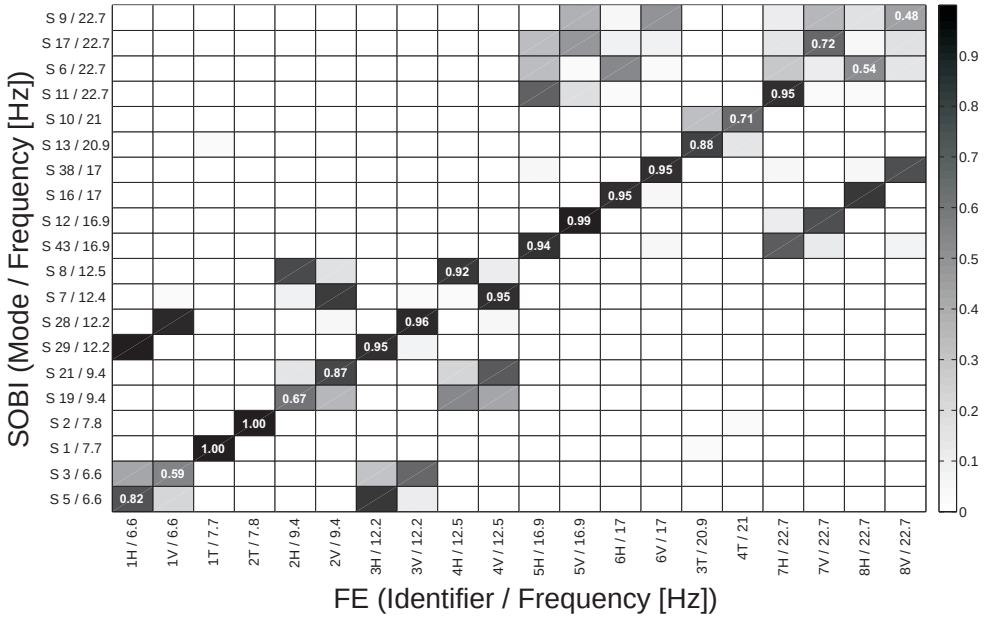

Figure 5.16: **Correlation between the FE modes and the SOBI modes using MAC matrix.** All the SOBI modes are considered between 0 and 23 Hz. The white numbers indicate the numerical values of the MAC for the diagonal terms. (Truss satellite - Forced response)

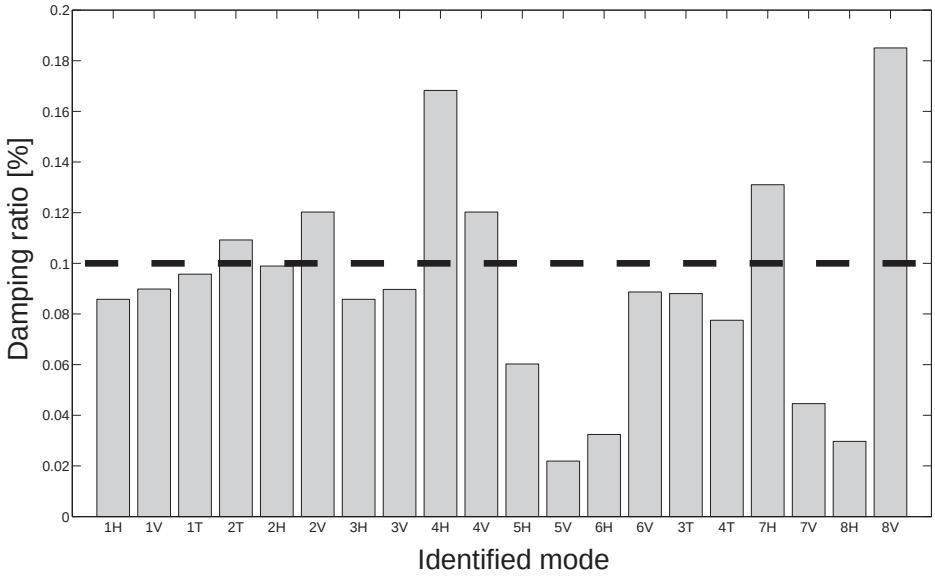

(a) Damping ratios identified using SSI-COV

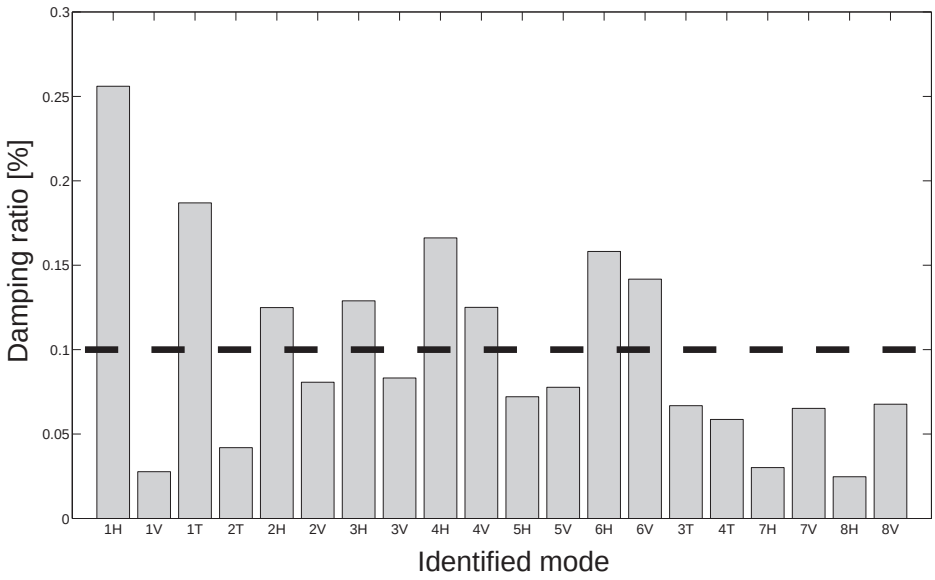

(b) Damping ratios identified using SOBI

Figure 5.17: **Values of the damping ratios for both identification methods.** The expected value is 0.1% for all modes. The damping ratios resulting from SSI-COV corresponds to the best identified modes all over the computed order. (Truss satellite - Free response)

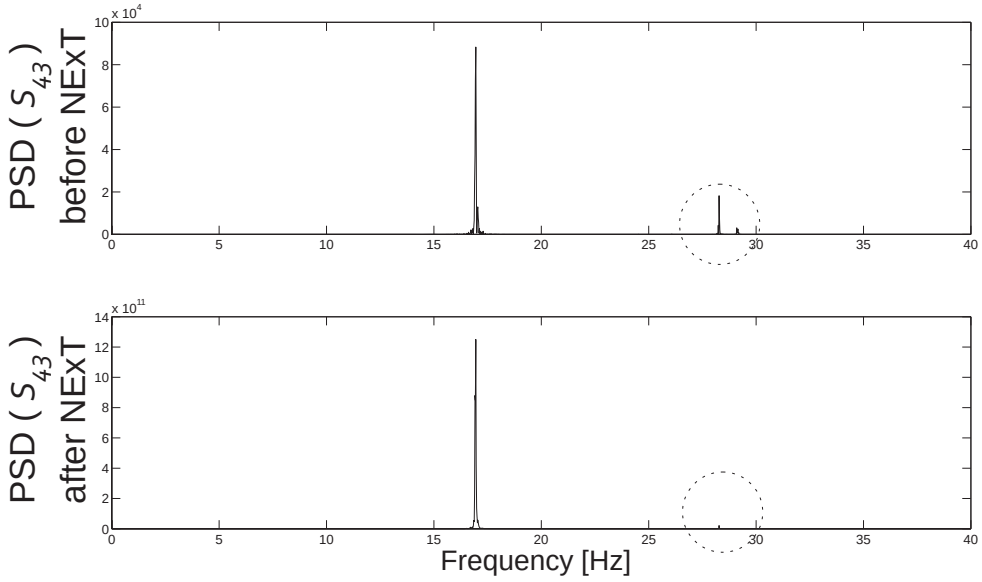

Figure 5.18: **Effect of NExT on the spectral contents of the signals.** NExT acts as a filter around the dominant frequency by reducing the effect of secondary frequencies. (Truss satellite - Forced response)

5.2 Aeroengine Stator Blade

5.2.1 Description of the experimental setup

The real-life structure considered herein is a blade extracted from the first stage of an aeroengine stator. The blade is made of titanium and is separated from other engine components such as the inner shroud. Modal testing process has been performed for the clamped-free configuration where the blade root is caught in a vice, as depicted in Fig. 5.19.

Fifteen measurement locations are uniformly distributed on the lower face of the blade. Because the blade is a light-weight structure, non-contact vibration measurements were realized using a laser vibrometer. The structural excitation is applied using a small force-transducer hammer blow such as described in Sec. 1.2.

The receptance FRFs are recorded in the range [0-5000Hz]; some of them are presented in Fig. 5.20. This figure reveals the presence of six natural frequencies around 170, 780, 1080, 2220, 2950 and 3880 Hz, respectively.

In order to apply the output-only modal analysis techniques, a set of 15 impulse response functions is obtained by applying the inverse Fourier transform to the measured FRFs. The modal parameters are then identified within the frequency range [0-5000Hz] using both SOBI and SSI-COV.

A FE model of the structure is realized using the SAMCEF software[1] and Figure 5.21 presents the FE mesh. This model also confirmed the presence of six natural frequencies in the considered frequency range as shown in Table 5.5.

5.2.2 SSI-COV Identification

The SSI-COV modal analysis technique is first applied to the impulse responses. 4000 samples are taken into account and the sampling frequency equals 10 kHz. The resulting stabilization diagram is presented in Fig. 5.22 and close-ups are proposed around the expected natural frequencies.

The diagram detects the presence of the six expected natural frequencies. The first, second and third ones (170.1, 775.3 and 1081.1 Hz) stabilize clearly from the lowest orders, if splitting beyond the order 30. The fourth and sixth frequencies (2216.7 and 3881.4 Hz) directly split in several stabilization lines corresponding to an unique physical mode. And finally, the fifth mode (around 2950 Hz) is more difficult to identify because its corresponding FRF amplitude is much lower than the others (cf. Fig. 5.20).

However, this example emphasizes one difficulty of the stabilization diagrams dealing with the choice of the genuine modes. Indeed, besides these six expected

[1] ©SAMTECH Headquarters - LIEGE science park - Rue des Chasseurs Ardennais, 8 - B4031 LIEGE (Angleur) BELGIUM (http://www.samtech.be/)

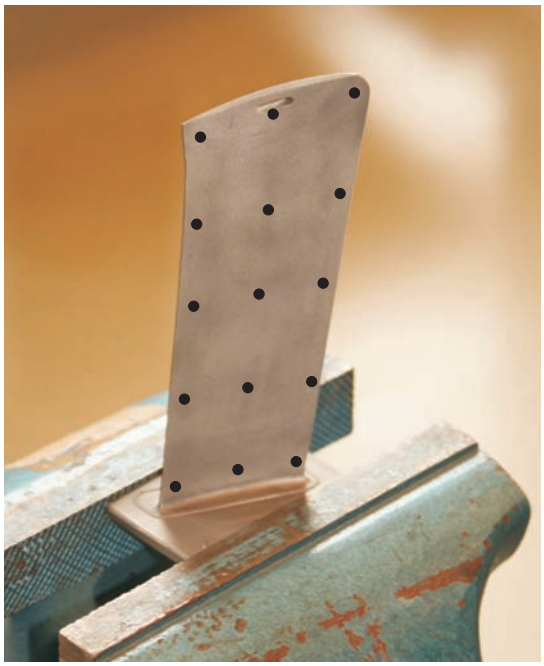

Figure 5.19: **Experimental setup consisting of the stator blade caught in a vice.** The bullets (•) refer to the measurement locations on the lower blade surface.

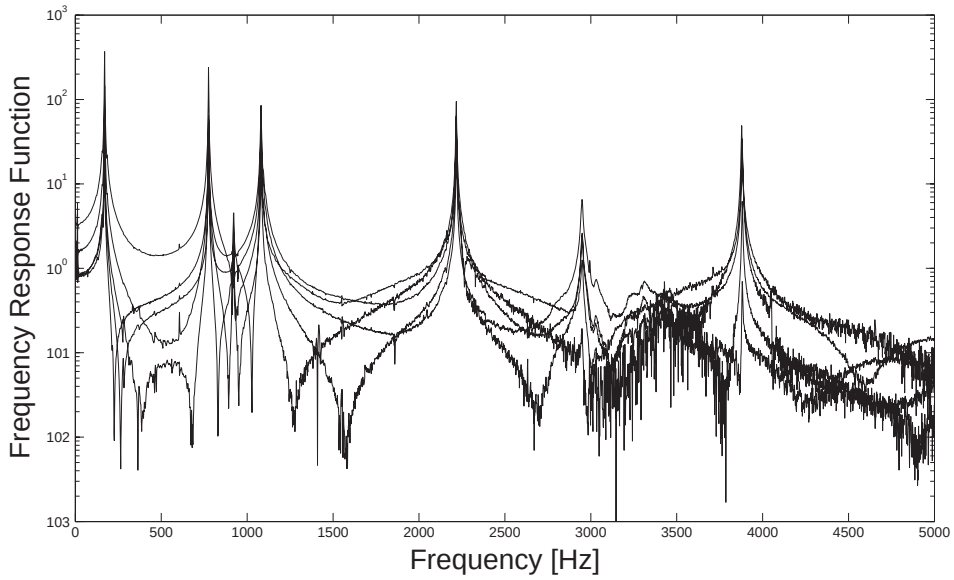

Figure 5.20: **Receptance FRFs of the stator blade.** Six peaks corresponding to the natural frequencies exist around 70, 780, 1080, 2220, 2950 and 3880 Hz.

Figure 5.21: **Finite element model of the stator blade.**

Mode	**Frequency** [Hz]	**Identifier** [-]
1-FE	171.9	1B
2-FE	774.0	1T
3-FE	1071.9	2B
4-FE	2202.1	2T
5-FE	3089.6	3BT
6-FE	3878.5	3T

Table 5.5: FE prediction of the natural frequencies for the stator blade. The identifiers B and T refer to 'Bending' and 'Torsion'.

natural frequencies, some other modes could also be considered as stabilized. These modes might be induced by the non-rigid boundary conditions, perturbing the signals or simply introduced by the computational process. The selection or rejection of these modes is a subjective decision depending on the user's expertise. For instance, it can be observed that two modes start to stabilize at high orders around 900 Hz and 2260 Hz and that a set of points also perturbs the interpretation around 3500 Hz but, thanks to the FE model and a visual inspection of the mode shapes, they are not considered as genuine.

A careful inspection of the FRFs reveals that there is a slight frequency shift between the FRFs. This frequency shift equals the frequency resolution of the measurements and probably takes its origin in the fact that the FRFs were not acquired simultaneously, but recomputed using IFFT process. The modes in closer correspondence with the expected modal form, obtained using the FE model, are therefore retained, and the others are discarded.

Note that, similarly to the satellite case study, none of the studied system order (up to 75), succeed in identifying all of the six modes at a time. A different system order is then chosen for each mode. The identified results are listed in Table 5.6.

These best-identified results are then compared to the FE predictions using the MAC matrix. The graphical representation of this MAC matrix is provided in Fig. 5.23. It can be observed that the four modes (denoted 1B, 1T, 2B and 3BT) are accurately identified. The quality of the results regarding the modes 2T and 3T, if acceptable for an experimental setup, is not satisfying. Two facts may explain this. First, the FE modal displacements are measured along the line perfectly perpendicular to the blade surface while the placement of the vibrometer cannot be so precise. Second, the experimental position of the measurement points does not perfectly correspond to the considered FE mesh nodes. Because both 2T and 3T mode shapes possess several vibration nodal lines, the nodal displacement varies a lot along the blade and a small positioning error may cause large discrepancies in the results.

5.2.3 SOBI-based Identification

The SOBI-based modal analysis method is now applied to the blade experiment. The same signal is used for the identification and 20 delays are uniformly distributed between 1/4000Hz and 1/200Hz, covering the frequency range of interest.

Because 15 measurement locations are considered, a total of 15 virtual sources are separated. The sources are fitted to match the theoretical form of the modal coordinates. Figure 5.24 depicts the fitting errors and the participation factors. The sources are sorted in ascending fitting errors.

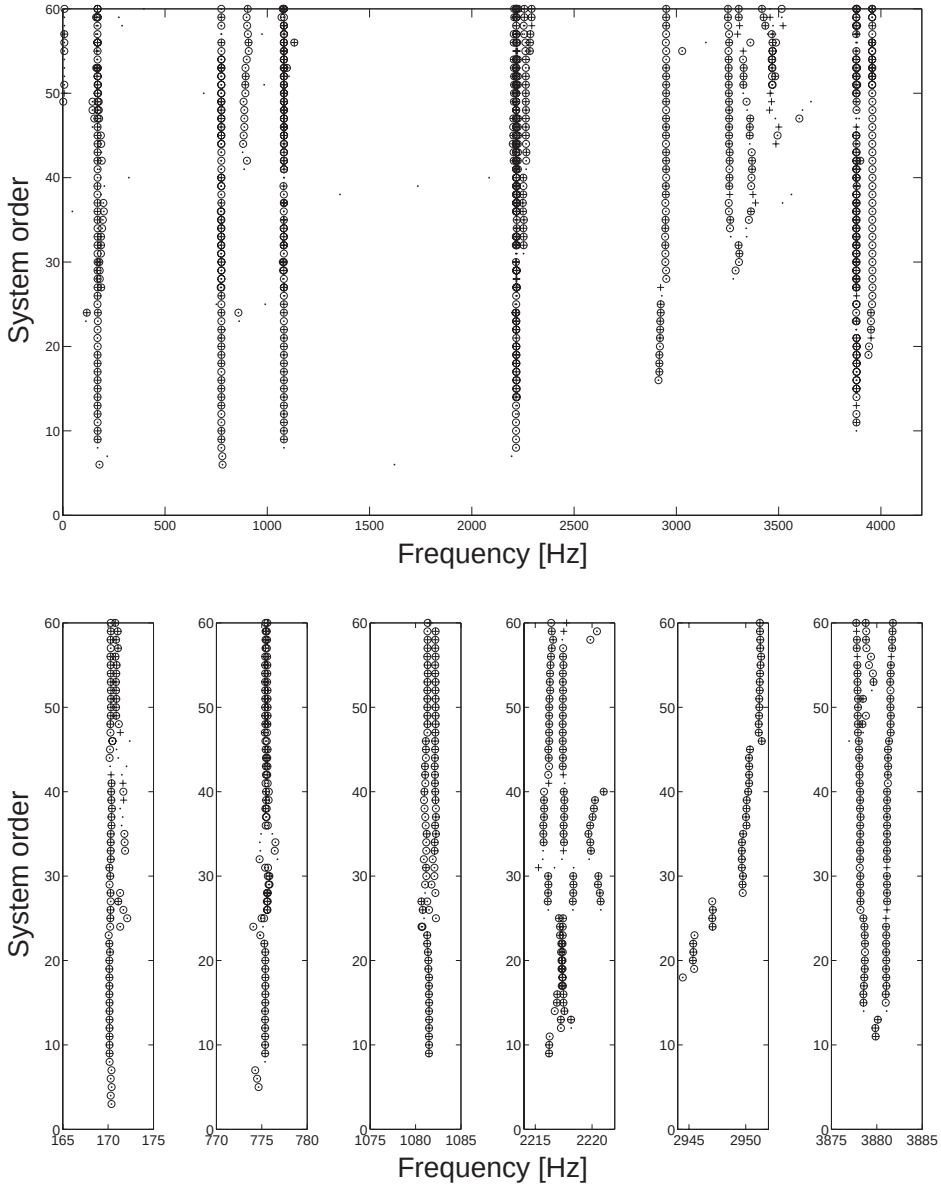

Figure 5.22: **Stabilization diagram (top) and close-ups around the natural frequencies (bottom) resulting from the SSI-COV method.** Only the stabilized frequencies are represented. A stabilized frequency is labeled as (·) whereas (○) is a stabilized mode and (+) is a stabilized damping ratio. (Stator blade)

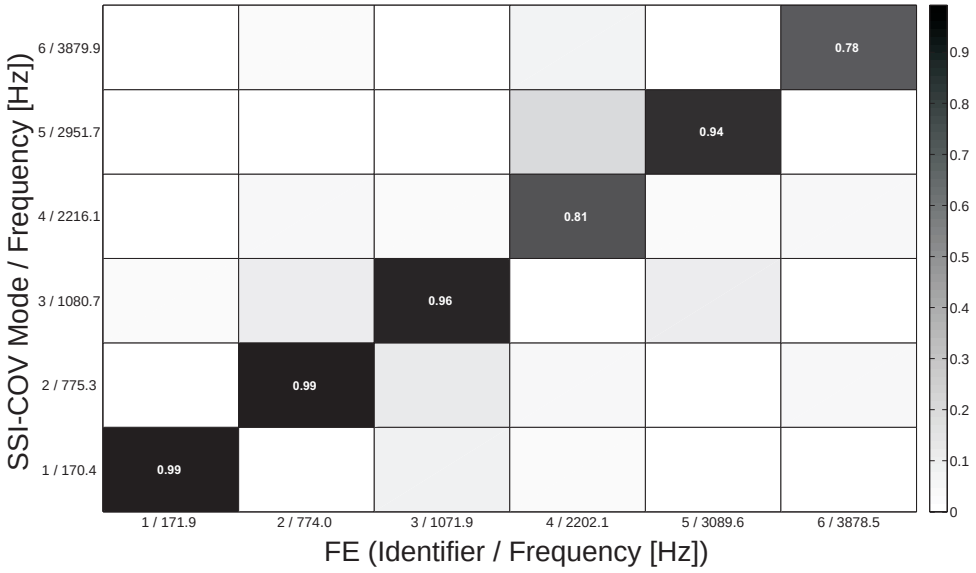

Figure 5.23: **Correlation between the FE modes and the best identified SSI-COV modes over all the computed orders.** The white numbers indicate the numerical values of the MAC for the diagonal terms.(Stator blade)

Mode	**Frequency** [Hz]	**Damping ratio** [%]	**Identifier** [-]
1-SSI	170.1	0.52	1B
2-SSI	775.3	0.12	1T
3-SSI	1081.1	0.18	2B
4-SSI	2216.7	0.10	2T
5-SSI	2950.5	0.32	3BT
6-SSI	3881.4	0.05	3T

Table 5.6: Natural frequencies and damping ratios for the stator blade identified using the SSI-COV method. The identifiers B and T refer to 'Bending' and 'Torsion'.

The number of identified sources being higher than the number of structural modes, the genuine sources have to be selected. The automated selection would obviously retain the five first sources (denotes s_1, s_2, s_3, s_4 and s_6) because they combine a small error with a high participation factor. These five sources correspond to the natural frequencies 170.2 Hz, 775.5 Hz, 1080.8 Hz, 2216.4 Hz and 3881.0 Hz.

It has been noted that the last mode (2949.8 Hz) has a lower participation, as indicated in the FRF diagram 5.20. The corresponding source, denoted s_9 in Fig. 5.24, is then logically less well fitted. It is important to underline that the automatic procedure would have neglected this source (its fitting error being higher than 10 %). Consequently, even though the fitting error indicator highly simplifies the mode selection, a particular attention must be brought to the less-participating modes.

Identically to the SSI-COV case, the several identified sources could correspond to a unique natural frequency. For instance, the source denoted s_5 has a dominant frequency equalling 2216 Hz and corresponds to a split of the genuine source s_4. Fortunately the fitting errors provide an easy way of separating the genuine modes from the others and it is not necessary to refer to the FE mode shape predictions. Nevertheless, the high value of the corresponding PF indicates that signal information has been lost during the separation process.

All the identification results are summarized in Table 5.7. A complete correspondence can be observed with the SSI-COV results previously presented in Table 5.6.

The correspondence between the SOBI-based identified modes and the FE mode shape prediction is presented in Fig. 5.25. The SOBI methodology even succeeds a slightly better correspondence (higher MAC values) with the FE prediction than the SSI-COV method, particularly for both 2T and 3T modes.

The MAC matrix between the modes identified using SSI-COV and SOBI is shown in Fig 5.26. All these results confirm that an accurate and consistent identification is carried out using SOBI.

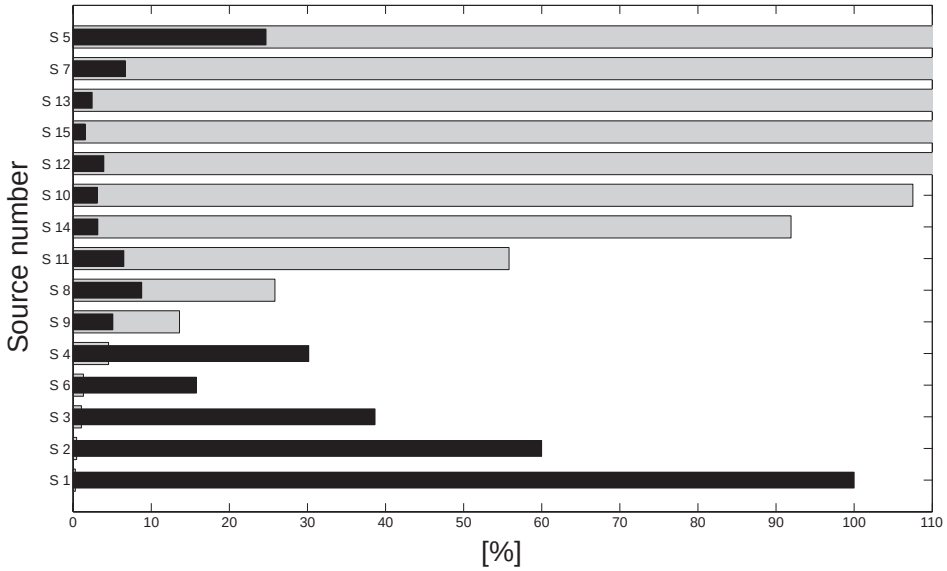

Figure 5.24: **Fitting errors and participation factors for all identified sources.** The participation factor is in black and the fitting error is in gray. (Stator blade)

Source	**Frequency** [Hz]	**Damping ratio** [%]	**Identifier** [-]
s_1	170.2	0.46	1B
s_2	175.5	0.10	1T
s_3	1080.	0.17	2B
s_6	2216.4	0.07	2T
s_4	2949.8	0.24	3BT
s_9	3881.0	0.06	3T

Table 5.7: Natural frequencies and damping ratios for the stator blade identified using the SOBI-based method. The identifiers B and T refer to 'Bending' and 'Torsion'.

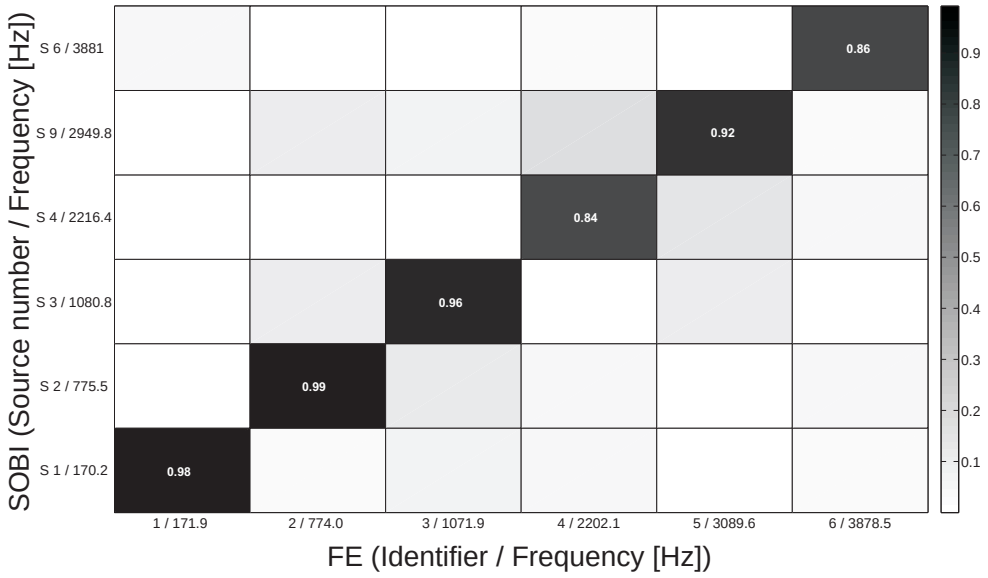

Figure 5.25: **Correlation between the FE modes and the selected SOBI-based modes.** The white numbers indicate the numerical values of the MAC for the diagonal terms. (Stator blade)

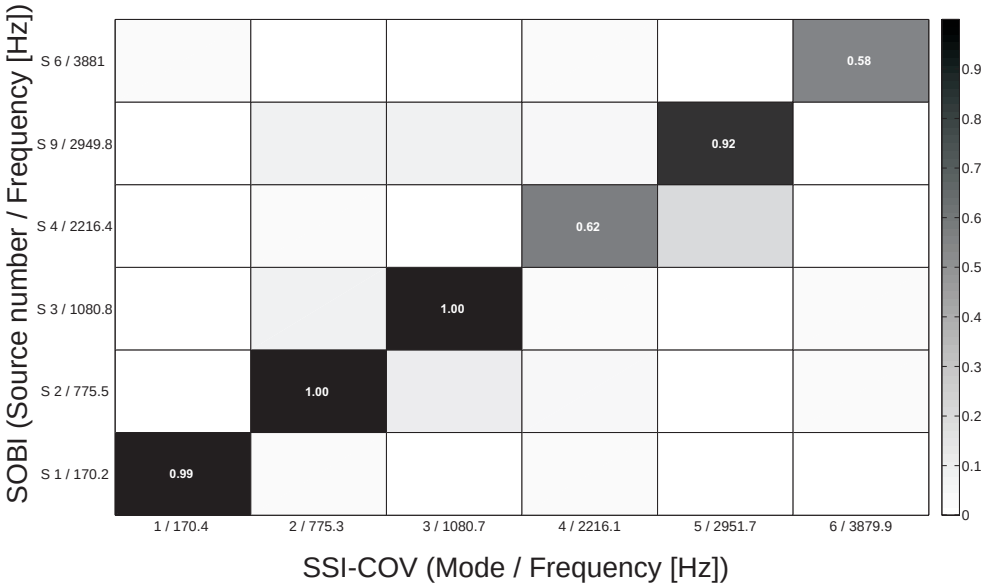

Figure 5.26: **Correlation between the SSI-COV modes and the selected SOBI-based modes.** The white numbers indicate the numerical values of the MAC for the diagonal terms. (Stator blade)

5.3 Two-story Truss

5.3.1 Description of the experimental setup

In this section, the proposed OMA technique is applied to the response of a real metallic truss. This structure is a reduced model of a two-story building which is composed of two parallelepipedal cells (38 x 24 x 40 cm) made of rectangular-cross-section bars. As illustrated in Fig. 5.27, the system is clamped at the base.

For the modal parameter identification, 16 sensors (i.e., classical 3-gramme-weight accelerometers) are distributed on the truss on both storys (two at each corner) and the response is measured in a horizontal plane along the two principal perpendicular directions. The SOBI-based identification is performed on both free and forced responses, and the modal parameters are compared to SSI-COV results.

For the free response case, the structural excitation is provided by a short hammer blow simulating a Dirac impulse. This small shock is applied horizontally at the middle of the top bar. The experimental sampling frequency equals 5120 Hz and 15000 samples are recorded, corresponding approximately to the 3 seconds following the impact.

For the random forced response, the structure is mounted on a 26kN electro-dynamic shaker, as shown in Fig. 5.27. In this case, the sampling frequency is still set to 5120 Hz and the recording time is increased because totally independent of the damping parameters. The frequency range of interest for the identification is between 0 and 400 Hz. The response signals are then preprocessed using a low-pass filter in order to prevent perturbation form the higher modes.

Contrary to the previous test-cases, the response signals are simultaneously acquired and not recomputed from the FRFs, as required in the proposed SOBI-based methodology. Consequently, it nicely reflects the interest of SOBI for practical applications.

5.3.2 Modal parameter identification based on the free response

The SOBI-based and SSI-COV methods are first applied to the free response of the truss structure. The first 6000 samples of the recorded time series are taken into account for the identification; this corresponds approximately to the first second following the excitation. For illustration, Fig. 5.28 presents one of these signals.

The SSI-COV method is first applied using 20 block rows and columns in the Hankel matrix. The resulting stabilization diagram is presented in Fig. 5.29. This figure illustrates how difficult it can be to select the stabilized modes and the

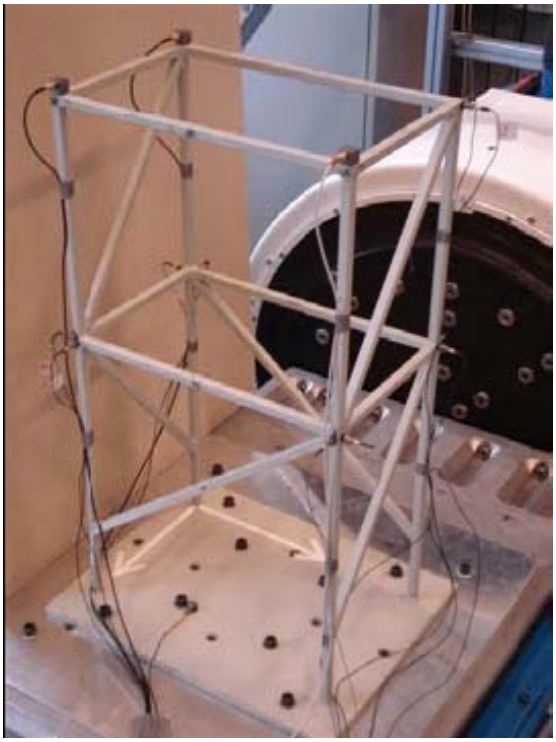

Figure 5.27: **Experimental setup consisting of a truss structure clamped at the basement.** Sixteen sensors are located at the four corners of the first and second level. Measurements are considered in the horizontal planes.

corresponding order. For instance, a mode could be considered around 200 Hz, but it is seen to be stable and disappears beyond the order 230. Finally, 11 natural frequencies are retained within the frequency range [0-400 Hz]. The results are listed in Table 5.8. An interval rather than a well-definite value is provided for the damping ratios because their values, if stabilized from one order to the following, slowly vary with the selected model order within the presented specific ranges. It can be noted that some of the modes are closely spaced in frequency.

The SOBI-based identification is performed using 20 time lags as recommended in the previous sections. The time lags are uniformly distributed between 1/400Hz and 1/10Hz in order to cover the frequency range. Because 16 measurement locations are considered, a total of 16 virtual sources are provided by the method. The identification of reliable virtual sources is facilitated by computing the error realized during the fitting of the time series of the sources with exponentially damped harmonic functions. For illustration, Figure 5.30 depicts the measured and fitted signals for two different sources. Clearly, the measured source in the top plot of Fig. 5.30 can be considered as a genuine source (the fitting error is below 1%), whereas this is obviously not the case for the source in the bottom plot (the fitting error is above 100%).

The result of the fitting process applied to all identified sources is presented in Figs. 5.31(a) and 5.31(b), before and after the automated selection, respectively. Five sources are rejected due to their high level of fitting errors. The sum of the participation of the 11 selected sources in the system response is above 97.7%, indicating that most of the information contained in the initial signals has been fruitfully extracted. Note that because the participation factors PF_i are normalized as defined in Eqn. 3.17, this value is not directly deduced from the figures.

All the results ensuing from SSI-COV and SOBI are listed and compared in Table 5.8. The correspondence between the frequencies is very good, and the SOBI-based identified damping ratio is very close to, if not within, the SSI-COV interval for all modes. The correlation between the mode shapes identified using SSI-COV and SOBI is computed using the MAC matrix and graphically presented in Fig. 5.32. An extremely good correspondence of the results obtained with both methods can be observed, confirming that an accurate and consistent identification is carried out using SOBI. However, the correlation of the fifth mode (256.3Hz) is less accurate (MAC 0.68). Note that the stabilization built for SSI-COV was also more delicate and the mode selection was certainly erroneous during the stabilization diagram processing. In order to confirm this assumption, the SOBI mode s_{12} has been compared to the corresponding SSI mode identified using the forced response and the correlation provides a MAC value of 0.97. The complete identification using the random forced response is detailed in what follows.

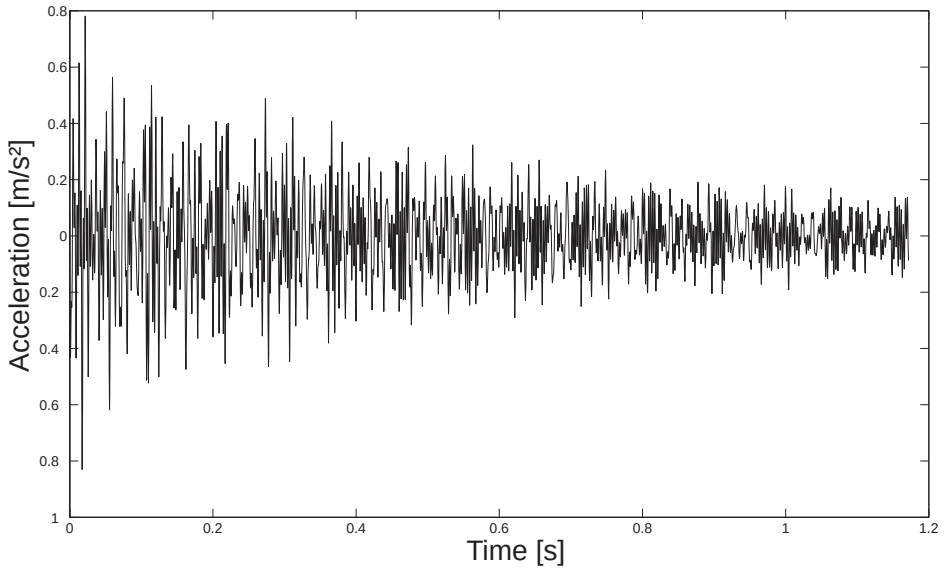

Figure 5.28: **Illustration of the free response for one sensor aligned with the excitation.** (Truss structure - Free response)

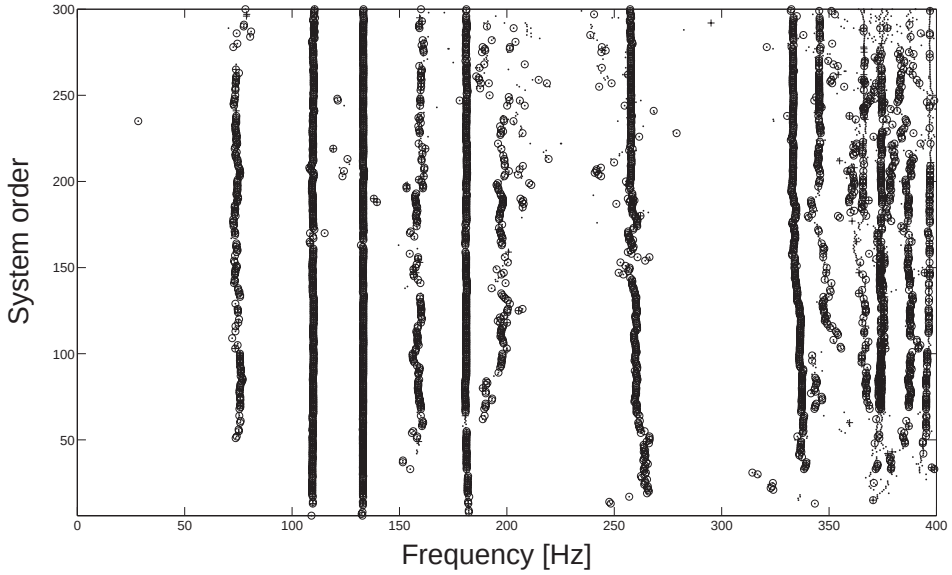

Figure 5.29: **Stabilization diagram resulting from the SSI-COV method.** (Truss structure - Free response)

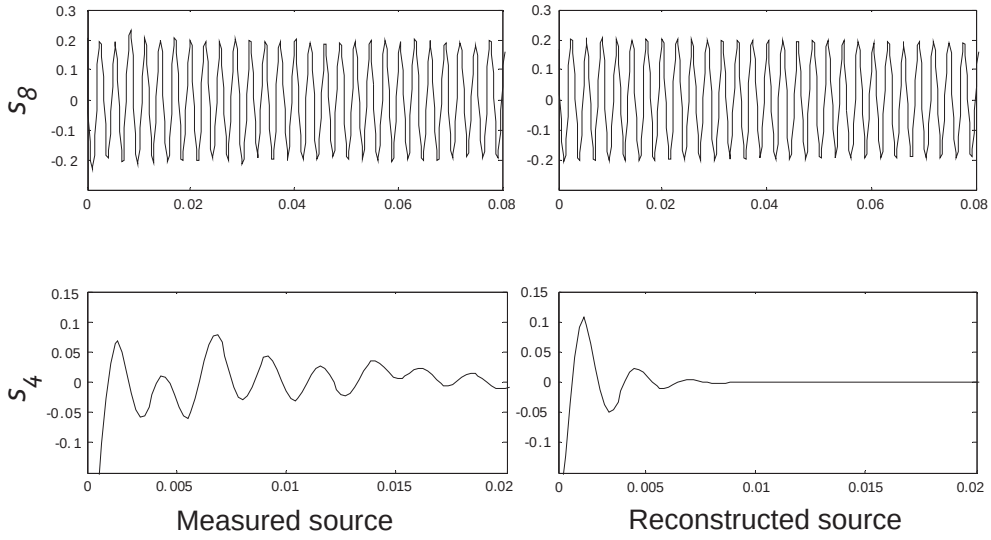

Figure 5.30: **Illustration of the fitting process for a genuine and a bad source.** The fitting error for the top plots is below 1% while it is greater than 100 %. (Truss structure - Free response)

	SSI-COV		**SOBI**	
Mode	**Frequency** [Hz]	**Damping ratio** [%]	**Frequency** [Hz]	**Damping ratio** [%]
1	75.8	[0.20-0.25]	75.9	0.21
2	111.1	[0.38-0.48]	111.4	0.36
3	130.7	[0.19-0.24]	130.8	0.21
4	181.0	[0.18-0.22]	181.1	0.18
5	256.5	[0.18-0.25]	256.3	0.18
6	334.3	[0.04-0.06]	334.2	0.05
7	345.7	[0.03-0.05]	345.8	0.05
8	365.8	[0.04-0.06]	365.8	0.05
9	374.4	[0.14-0.16]	374.3	0.15
10	380.5	[0.15-0.18]	380.5	0.16
11	396.8	[0.08-0.09]	396.9	0.09

Table 5.8: Results of the identifications performed using SSI-COV and SOBI-based methods. (Truss structure - Free response)

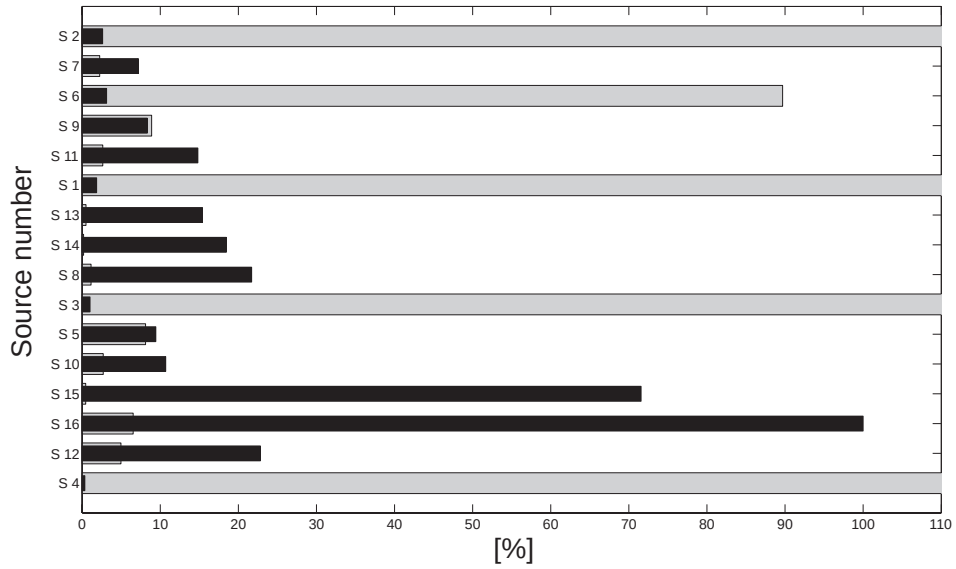

(a) Before the automated selection

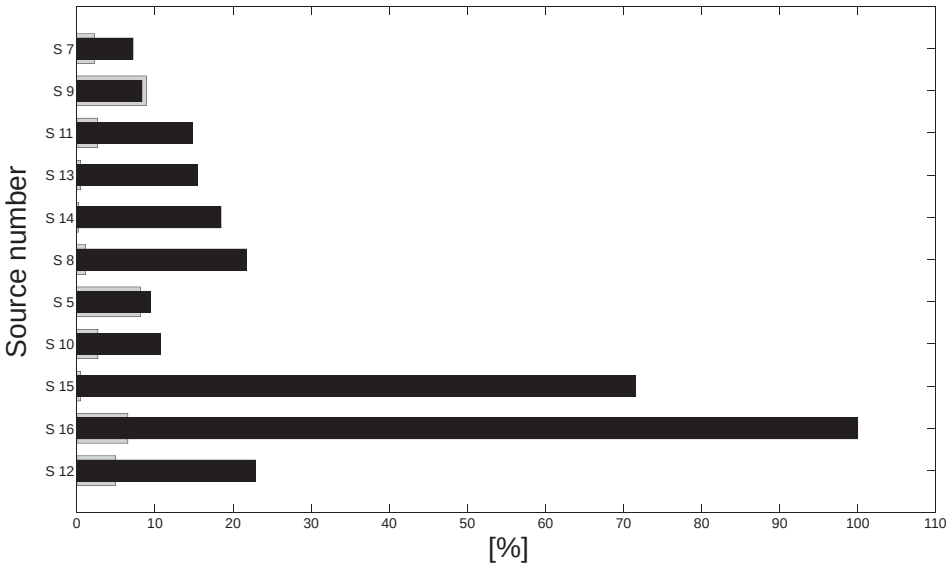

(b) After the automated selection

Figure 5.31: **Automatic selection of the genuine sources based on the fitting error.** The participation factor is in black and the fitting error is in gray. (Truss structure - Free response)

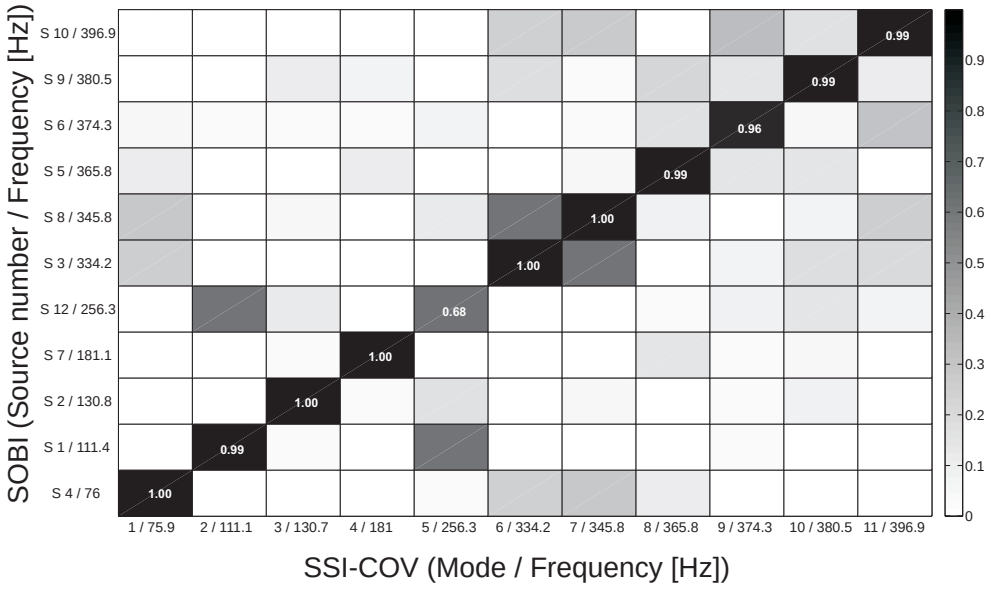

Figure 5.32: **Correlation between the SSI-COV modes and the selected SOBI-based modes for the truss structure.** The mode corresponding to the frequency 256 Hz is accurately identify using SOBI whereas SSI fails. The white numbers indicate the numerical values of the MAC for the diagonal terms. (Truss structure - Free response)

5.3.3 Modal parameter identification based on the forced response

SOBI and SSI-COV are now applied to the random forced response of the truss structure. The random force imparted to the truss structure by the electrodynamic shaker is not measured but all 16 response signals are simultaneously recorded. A number of 100000 samples of the measured time series is taken into account after the transient response, the sampling frequency being set to 5120 Hz.

As in the free response case, 20 block rows and columns are selected in the Hankel matrix for the SSI-COV method and system orders from 5 to 300 are considered for the identification. The corresponding stabilization diagram is presented in Fig. 5.33 where 14 modes appear to stabilize regarding the mode shapes and damping ratios.

Here again, the diagram 5.33 clearly shows how difficult it can be to post-process the data resulting from a SSI-COV analysis. The selection/non-selection of the modes depends on the expertise and the feeling of the operator. For example, the frequencies 190 and 205 Hz stabilize but not in terms of mode shapes and damping ratios; they are thus not retained. Conversely, the frequency 75Hz is retained while not stabilized for all system orders. Between 350 and 400 Hz, 6 frequencies are considered as genuine even if modes stabilized (from the system order 150) before disappearing for higher system orders. The numerical results of the manually selected modes are listed in Table 5.9.

For SOBI, 20 time lags were uniformly distributed between 1/400Hz and 1/10Hz. For illustration, the 16 identified sources are presented in Figs. 5.34 and 5.35. The sources correspond to the modal coordinates of the system and should be approximated by harmonic functions modulated by slowly varying envelope. In order to automatically select the genuine sources, the free-response modal coordinates are recomputed using NExT algorithm. The resulting signals are presented in the second column of Figs. 5.34 and 5.35. The third column presents the spectral contents of the signals, which should be monochromatic for genuine sources.

Apart from sources s_{13} and s_{15}, it turns out that SOBI is able to decompose the measured responses in terms of elemental components which are mostly monochromatic.

Figures 5.36(a) and 5.36(b) provides the fitting errors combined with the participation factor. Two of the 16 sources have an fitting error above 100%. They correspond to the non-monochromatic sources (i.e., sources s_{13} and s_{15}). The selection is therefore trivial and 14 modes are then retained and listed in Table 5.9 for the comparison with SSI-COV.

The correspondence between the frequencies is very good and, such as in the free response case, the SOBI-based identified damping ratio is very close to, if

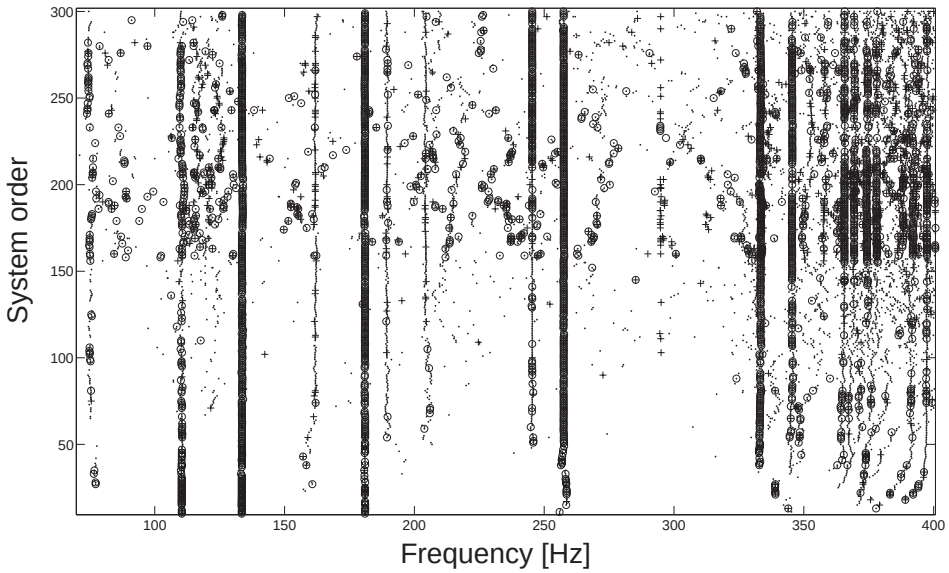

Figure 5.33: **Stabilization diagram obtained with the SSI-COV method.** Only the stabilized frequencies are represented. A stabilized frequency is labeled as (·) whereas (○) is a stabilized mode and (+) is a stabilized damping ratio. (Truss satellite - Forced response)

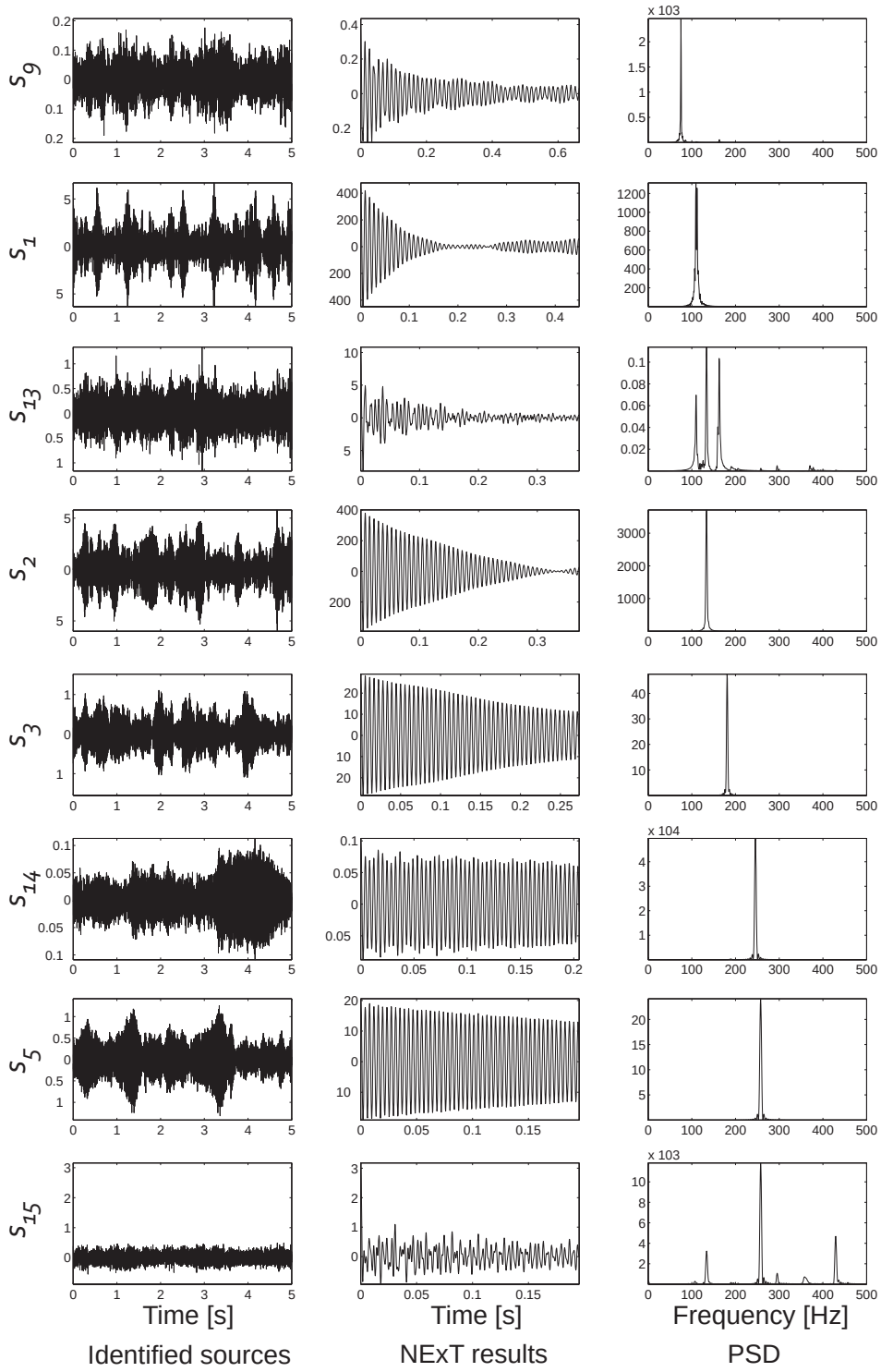

Figure 5.34: **Identified sources obtained using the SOBI algorithm (part 1).** Sixteen sources are separated and sorted by increasing major frequency. The first column presents the SOBI sources, the second presents the recomputed free response modal coordinates obtained using the NExT algorithm and the third one presents the power spectral densities for each identified signal. (Truss structure - Forced response)

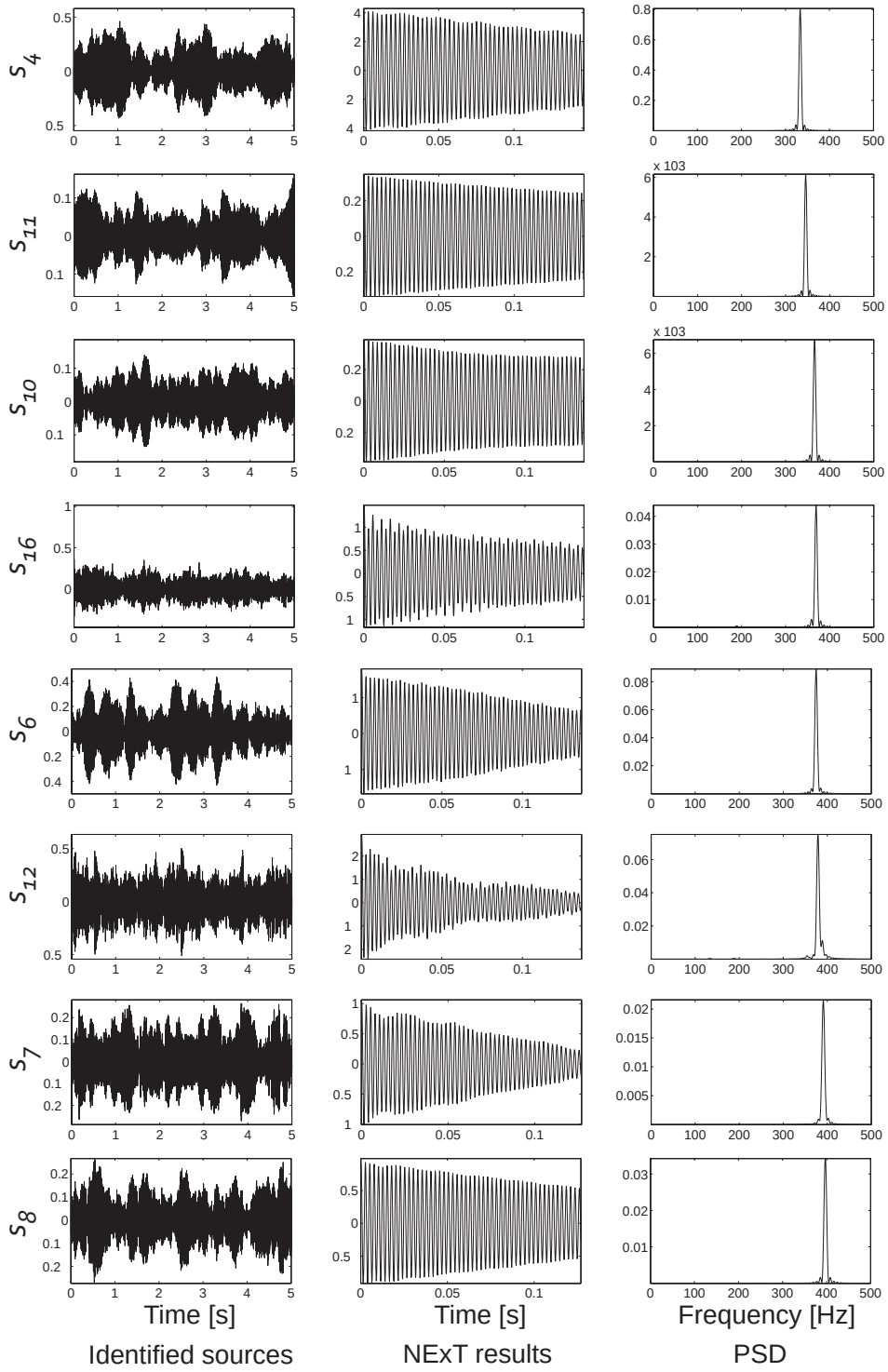

Figure 5.35: **Identified sources obtained using the SOBI algorithm (part 2).** Sixteen sources are separated and sorted by increasing major frequency. The first column presents the SOBI sources, the second presents the recomputed free response modal coordinates obtained using the NExT algorithm and the third one presents the power spectral densities for each identified signal.(Truss structure - Forced response)

not within, the SSI-COV interval for all modes.

The correlation between mode shapes is again assessed using the MAC (Fig. 5.37). There is an excellent agreement between the results obtained with both methods. Nevertheless three modes (at 75, 245 and 397 Hz) are not as accurately correlated. The cause is certainly that the corresponding structural deformation takes place in a plane orthogonal to the excitation direction. The modes have therefore a lower participation in the system response, and the identification is consequently more delicate.

Finally, the first three damping ratios identified from the random forced response are larger than those identified using the free response (cf. Tables 5.8 and 5.9). Although we have no precise explanation for this observation, we note that, for the free response experiment, the truss structure was not clamped on the electrodynamic shaker but rather on a vibration-isolating table.

5.4 Concluding Remarks

After studying the performance and robustness of BSS algorithms regarding several parameters such as noise, damping or random excitations, the applicability of SOBI for output-only modal analysis had to be demonstrated using large-scale systems. Three practical and realistic problems were considered for this purpose in this chapter. In addition, this chapter allowed the proposed methodology to be faced with a well-known modal parameter estimation method, namely the covariance-driven stochastic subspace identification (SSI-COV).

The first application (i.e., a numerical FE model of a truss satellite) combined several difficulties including numerous and closely-spaced frequencies and a large number of sensors, nevertheless SOBI performed well when compared to SSI-COV. Indeed, SSI-COV provided slightly better results than SOBI but clearly showed limitations during the post-processing (based on the stabilization diagram) for the selection of the genuine modes. None of the considered SSI-COV model order succeeded in identifying all structural modes at once. A manual selection of the appropriate order for each stabilized mode is therefore necessary for practical application, in which exact solution is not known. As for SOBI, the automated mode selection facilitated the post-processing, and all modes, if less accurate, were directly identified.

The second experiment was a real structure (a stator blade extracted from an aeroengine), representative of usual modal testings using force-transducer hammer. A precise FE model of the structure was used to correlate the results, and SOBI accurately performed the identification, even slightly better than SSI-COV. Nevertheless, one of the accurately identified mode was rejected by the automated mode selection indicating that, in some cases, the procedure is too restrictive and

	SSI-COV		SOBI	
Mode	**Frequency** [Hz]	**Damping ratio** [%]	**Frequency** [Hz]	**Damping ratio** [%]
1	75.3	[0.10-1.80]	75.0	1.14
2	110.4	[1.85-2.35]	110.5	2.33
3	133.6	[0.70-0.95]	133.6	0.86
4	180.9	[0.20-0.30]	180.8	0.31
5	245.4	[0.05-0.10]	245.4	0.06
6	257.5	[0.10-0.12]	257.5	0.12
7	333.4	[0.05-0.11]	333.5	0.16
8	345.5	[0.07-0.15]	345.5	0.11
9	365.6	[0.07-0.10]	365.6	0.11
10	369.4	[0.17-0.21]	369.1	0.23
11	374.3	[0.25-0.28]	374.6	0.27
12	378.0	[0.36-0.43]	379.1	0.54
13	392.1	[0.35-0.50]	391.0	0.39
14	397.4	[0.12-0.14]	397.1	0.17

Table 5.9: Results of the identifications performed using SSI-COV and SOBI-based methods. (Truss structure - Forced response)

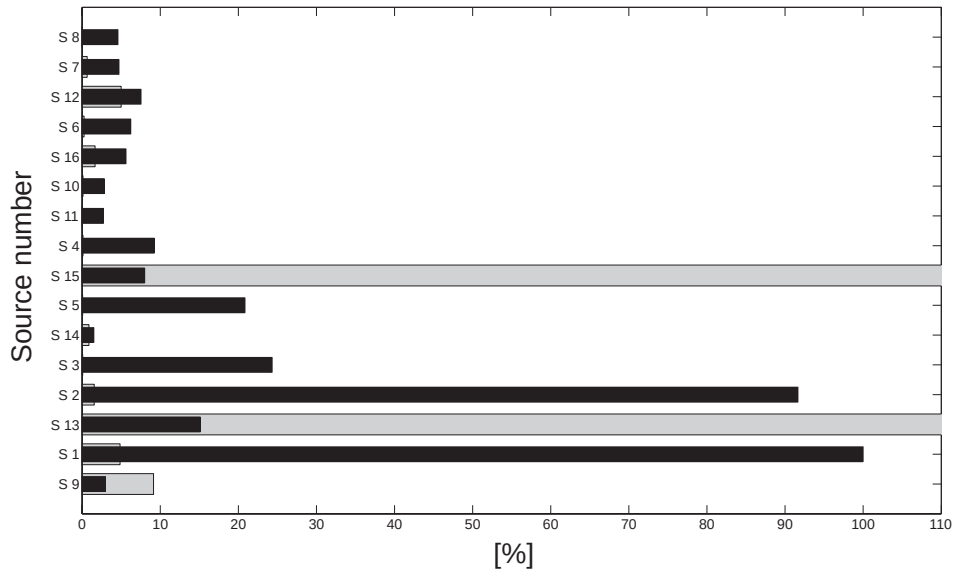

(a) Before the automated selection

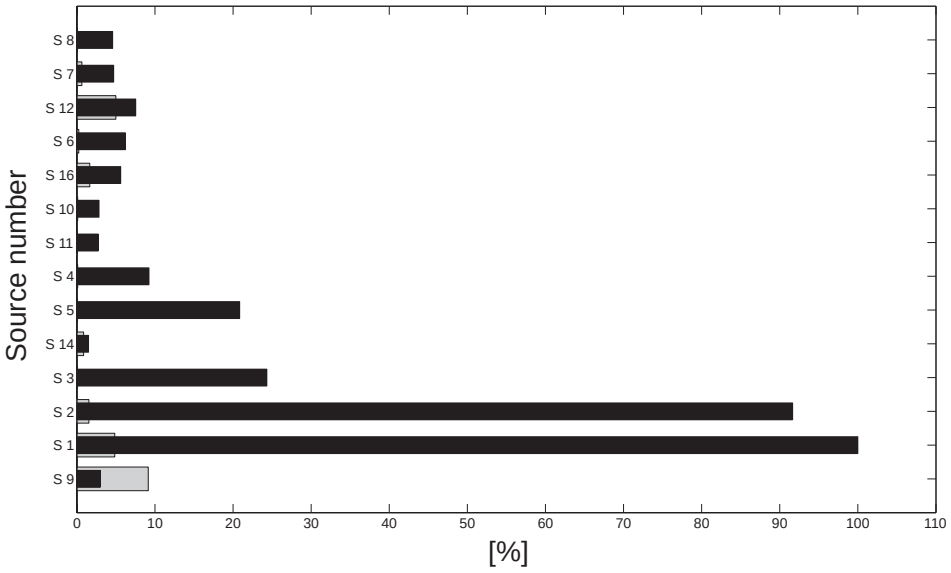

(b) After the automated selection

Figure 5.36: **Automatic selection of the genuine sources based on the fitting error.** The participation factor is in black and the fitting error is in gray. (Truss structure - Forced response)

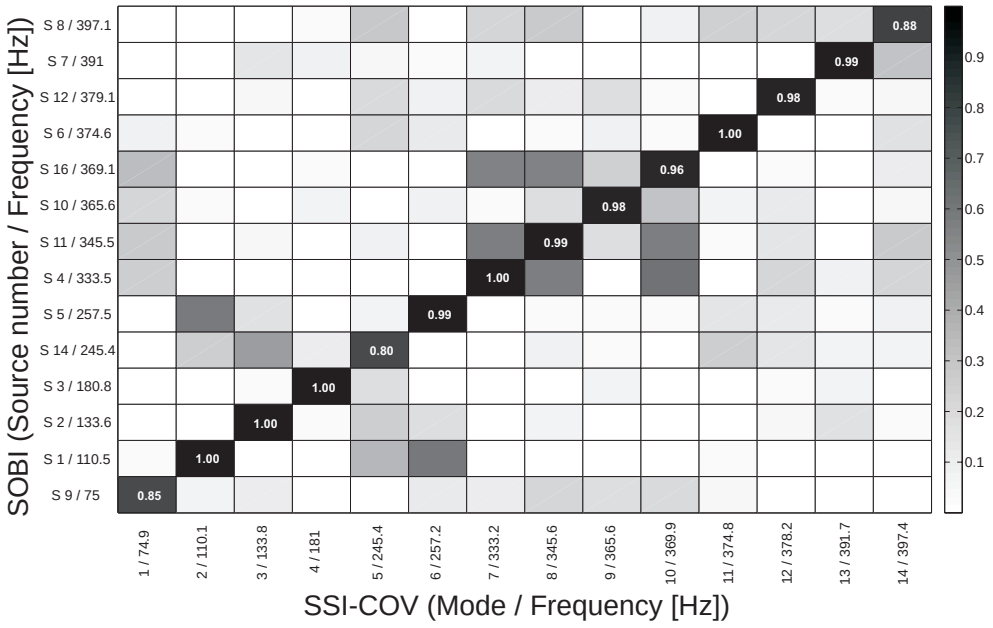

Figure 5.37: **Correlation between the SSI-COV modes and the selected SOBI-based modes for the truss structure.** The white numbers indicate the numerical values of the MAC for the diagonal terms. (Truss structure - Forced response)

that the limit value of the fitting error could be revised according to the measurement quality.

Finally, the last experiment typically represents the applications for which SOBI has been proposed. It combines numerous simultaneous response signals, unknown and unmeasurable excitation and numerous modes. The results obtained with SOBI were extremely similar to those resulting from SSI-COV. Once again, the main difference lies in the easiness of the post-processing.

According to these observations, the output-only modal analysis method based on SOBI can be considered as validated and reliable for numerical and experimental applications.

Conclusions

This thesis discussed modal identification using output-only information. The research developed modal parameter estimation approaches based on the so-called Blind Source Separation (BSS) techniques. Two separation algorithms, namely the Independent Component Analysis (ICA) and the Second-Order Blind Identification (SOBI), were considered.

During the design phase, engineers are usually faced with experimental validation, especially in the field of structural dynamics. Modal testing is traditionally used to update the numerical models and confirm their predictions.

Numerous well-established methods are available to process with the signals resulting from modal testing. However, for most of the existing methods, the order of the theoretical model is overestimated to accurately match the experimental signals. This approach provides better mode estimation but introduces fictitious modes that have to be rejected. In commercial softwares, picking out the genuine modes is traditionally performed using the so-called stabilization diagram. Nevertheless, the applications presented in this manuscript showed how delicate and time consuming it can be to obtain reliable results. Indeed, the decision between stability and instability mostly depends on the expertise and the feeling of the operator. Consequently, inconsistency between estimates of different experts may appear.

One of the main objectives that was kept in mind throughout this research was to simplify the data post-processing in order to assist the operator tasked with separating the genuine modes from the spurious ones. The proposed approach for solving this problem is based on simple criteria, such as fitting errors and modal participations, and several examples corroborated its credibility.

The proposed modal identification methodology is based on BSS techniques. First, free and random forced responses were analyzed using numerical and academic examples, and the performances of both ICA- and SOBI-based procedures

were compared regarding several parameters, leading to the rejection of ICA for the rest of the work. Second, large-scale and experimental structures were considered in order to demonstrate the utility of SOBI in practical applications. They consisted of a satellite truss, a stator blade and a metallic truss modeling a two-story building, respectively. The results showed promise and their accuracy were estimated using the well-established Covariance-driven Stochastic Subspace Identification (SSI-COV) method.

Main Contributions

The main achievements of this research work are the followings:

- The concept of virtual sources was introduced for BSS problem when applied to dynamic signals. A one-to-one relationship between the BSS modes, contained in the identified mixing matrix, and the vibration modes was then established; as for the identified sources, they correspond to the normal coordinates of the system. These theoretical findings were validated using many numerical and experimental case studies, demonstrating the applicability of the source separation algorithms for output-only modal parameter estimation. This principle and some of its ensuing applications were published in [KPG07, PKGV07, PKGM07] and also applied by other researchers in [ZC07, CAMB07, CHT09, MZ08].

- Two source separation algorithms, ICA and SOBI, were implemented and applied to the modal parameter estimation problem. They were compared to each other with respect to damping, noise and non-deterministic random excitations. Because it takes advantage of the temporal structure of the sources, SOBI proved to be more suitable for the modal identification. Three realistic applications demonstrated the applicability of SOBI for practical applications. They deal with a large number of active modes, typical impact hammer modal testing, and operational testing conditions, respectively.

- SSI-COV was used as a reference to evaluate the performances of the proposed method but advanced studies showed limitations during the post-processing using the stabilization diagram. For instance, several applications developed in this research highlighted that none of the considered SSI-COV model order succeeded in identifying all the structural modes at once. A manual and unreliable selection of the appropriate order is therefore necessary for each stabilized mode. Therefore, a systematic post-processing procedure was proposed for the BSS-based identification. The approach, based on simple parameters such as fitting errors and modal participation, was

successfully tested on various examples making way for automated modal identification.

Perspectives and Future Works

We believe that this thesis contains useful contribution to the development of automatic modal analysis methodologies. Nevertheless, there is still much work to be done to obtain a robust and generally-applicable method, effective for large-scale industrial structures.

Non-proportional damping. The proposed modal identification method assumes a purely proportional damping. Non-proportional damping is problematic because the mode shape estimates resulting from SOBI are necessarily real-valued. Unfortunately, some structural and testing conditions such as general damping, gyroscopic effects or asynchronous sampling introduce phase shifts in each response DOF, leading to complex-valued mode shapes. Restricting the mixing matrix, and so the mode shapes, to real values limits the applicability of the method. Recent publications promisingly address the question in [MZ08, MZ10].

Under-determined system. All the test-cases considered in this work assume a number of measured signals at least equal to the number of independent sources. In practical applications, the number of acquisition channels is a hardware limitation while the number of active modes is unknown. Consequently, extending the scope of the method to under-determined systems would be advised. Filtering, virtual sensors or iterative procedures are some of the trails that should be investigated.

Operational testing conditions. Validation of the proposed methodology was performed using numerical test-cases and experimental structures. However, the considered testings were meeting ideal experimental conditions and advanced study concerning real operational conditions and perturbing excitation such as harmonic signals, should be addressed.

Health monitoring. Structural health monitoring and damage detection are important fields of structural dynamics. The modal identification technique presented in the work is an output-only method. It could then be used for continuous monitoring of structures under operational conditions, for which the excitation is not measured. Because it provides the frequencies and mode shapes at once, the source separation approach could be very efficient if proved to be sensitive to local damage influence.

Automated mode selection. This thesis developed mode selection criteria based on the fitting of the identified normal coordinates. Compared to the stabilization diagram tool, this approach proved to provide results that can be easily interpreted. But normal coordinates could easily be deduced by applying the inverted mode shape matrix (estimated using other identification methods) to the measured signals. This could facilitate the mode selection for other high-performance methods such as, for instance, SSI-COV.

Nonlinear systems. Finally, this dissertation focuses on linear and time-invariant systems. Further researches are then required to address the problem of nonlinear structures.

Bibliography

[AB05] J. Antoni and S.G. Braun. Special issue on blind source separation: editorial. *Mechanical Systems and Signal Processing*, 19:1166–1180, 2005.

[AB06] R.J. Allemang and D.L. Brown. A complete review of the complex mode indicator function (CMIF) with applications. In *ISMA International Conference on Noise and Vibration Engineering*, Katholieke Universiteit Leuven, Belgium, 2006.

[AGB+99] M. Abdelghani, M. Goursat, T. Biolchini, L. Hermans, and H. Van Der Auweraer. Performance of output-only identification algorithms for modal analysis of aircraft structures. In *IMAC XVII*, volume 3727, pages 224–230, Kissimmee, FL (USA), 1999.

[AGMS04] J. Antoni, L. Garibaldi, S. Marchesiello, and M. Sidhamed. New separation techniques for output-only modal analysis. *Shock and Vibration*, 11(3-4):227–242, 2004.

[Ant05] J. Antoni. Blind separation of vibration components: Principles and demonstrations. *Mechanical Systems and Signal Processing*, 19(6):1166–1180, 2005.

[Asm97] J.C. Asmussen. *Modal analysis based on the random decrement technique: Application to civil engineering structures*. PhD thesis, University of Aalborg, 1997.

[AVVODM98] M. Abdelghani, M. Verhaegen, P. Van Overschee, and B. De Moor. Comparison study of subspace identification methods applied to flexible structures. *Mechanical Systems and Signal Processing*, 12(5):679–692, 1998.

[BAK04] H. Buchner, R. Aichner, and W. Kellermann. Blind source separation for convolutive mixtures: a unified treatment. In *Audio signal processing for next-generation multimedia communication systems*. Springer, 2004.

[BAK05] H. Buchner, R. Aichner, and W. Kellermann. A generalization of blind source separation algorithms for convolutive mixtures based on second-order statistics. *IEEE Transactions on Speech and Audio Processing*, 13(1):120–134, 2005.

[BAMCM97] A. Belouchrani, K. Abed-Meraim, J.F. Cardoso, and E. Moulines. A blind source separation technique using second order statistics. *IEEE Transactions on Signal Processing*, 45(2), 1997.

[BAZM79] D.L. Brown, R.J. Allemang, D. C. Zimmerman, and M. Mergeay. Parameter estimation techniques for modal analysis. *SAE Technical Paper Serie*, 790221, 1979.

[BCG+09] F. Braghin, F. Cheli, A. Genoese, E. Sabbioni, C. Bisaglia, and M. Cutini. Experimental modal analysis and numerical modelling of agricultural vehicles. In *IMAC XXVII*, Orlando, FL (USA), 2009.

[BCLF95] E. Balmès, C. Chapelier, P. Lubrina, and P. Fargette. An evaluation of modal testing results based on the force appropriation method. In *IMAC 13*, 1995.

[BG08] M. Böswald and Y. Govers. Taxi vibration testing - an alternative method to ground vibration testing of large aircraft. In *ISMA 2008*, pages 2413–2426, Leuven, Belgium, 2008.

[BGFG06] M. Böswald, D. Göge, U. Füllerkrug, and Y. Govers. A review of experimental modal analysis methods with respect to their applicability to test data of large aircraft structures. In *ISMA 2006*, Leuven, Belgium, 2006.

[BP93] J.S. Bendat and A.G. Piersol. *Engineering applications of correlation and spectral analysis*. John Wiley and Sons, New York, second edition, 1993.

[BS95] A.J. Bell and T.J. Sejnowski. An information-maximization approach to blind separation and blind deconvolution. *Neural Computation*, 7:1129–1159, 1995.

[BW97] Andrew D. Back and A.S. Weigend. A first application of independent component analysis to extracting structure from stock returns. *International Journal of Neural Systems*, 8, 1997.

[BZA00] R. Brincker, J. Zhang, and P. Andersen. Modal identification from ambient responses using frequency domain decomposition. In *IMAC 18*, San Antonio, TX, USA, 2000.

[CAMB07] S. Chauhan, R.J. Allemang, R. Martell, and D.L. Brown. Application of independent component analysis and blind source separation techniques to operational modal analysis. In *IMAC*, Florida, 2007.

[Car89] J.F. Cardoso. Source separation using higher order moments. In *IEEE International Conference on Acoustics Speech and Signal Processing (ICASSP)*, Glasgow, UK, 1989.

[Car97] J.F. Cardoso. Infomax and maximum likelihood for source separation. *IEEE Letters on Signal Processing*, 4:112–114, 1997.

[Car98] J.F. Cardoso. Blind source separation: statistical principles. In *IEEE*, volume 86, pages 2009–2025, 1998.

[CCCD99] A. Cunha, E. Caetano, R. Calçada, and R. Delgado. Modal identification and correlation with finite element parameters of vasco da gama bridge. In *IMAC 17*, pages 705–711, Kissimmee, FL, USA, 1999.

[CCPL05] S. Choi, A. Cichocki, H. Park, and S.Y. Lee. Blind source separation and independent component analysis: A review. *Neural Information Processing*, 6(1):57, 2005.

[CDLD05] P. Comon, L. De Lathauwer, and F. Desbouvries. Blind techniques and independent component analysis, 2005. Lecture Notes.

[CHT09] S. Chauhan, M.H. Hansen, and D. Tcherniak. Application of operational modal analysis and blind source separation / independent component analysis techniques to wind turbines. In *IMAC-XXVII*, Orlando, Florida USA, 2009.

[CM96] P. Comon and B. Mourrain. Decomposition of quantics in sums of powers of linear forms. *Signal Processing*, 53(2-3):93–107, 1996.

[CMPC08] G. Coppotelli, G. Mastroddi, G.M. Polli, and L. Cospite. Modal parameter identification and correlation of a launch-vehicle interstage using output-only experimental data. In *ISMA 2008*, pages 3103–3116, Leuven, Belgium, 2008.

[Col68] H.A. Cole. On-the-line analysis of random vibrations. *AIAA Paper*, 68(288), 1968.

[Col71] H.A. Cole. Failure detection of a space shuttle wing by random decrement. Technical report, NASA, 1971.

[Col73] H.A. Cole. Online failure detection and damping measurements of aerospace structures by random decrement signature. Technical report, NASA, 1973.

[Com94] P. Comon. Independent component analysis: a new concept? *Signal Processing*, 36:287–314, 1994.

[CS93] J.F. Cardoso and A. Souloumiac. Blind beamforming for non-gaussian signals. *IEEE Proceedings-F Radar and Signal Processing*, 140(6):362–370, 1993.

[CS96] J.F. Cardoso and A. Souloumiac. Jacobi angles for simultaneous diagonalization. *SIAM Journal of Matrix Analysis and Applications*, 17:161–164, 1996.

[CT65] J.W. Cooley and J.W. Turkey. An algorithm for the machine calculation of complex fourier series. *Mathematics of Computation*, 19:297–301, 1965.

[CZ06] D. Chelidze and W. Zhou. Smooth orthogonal decomposition-based vibration mode identification. *Journal of Sound and Vibration*, 292:461–473, 2006.

[DL95] N. Delfosse and P. Loubaton. Adaptive blind separation of independent sources - a deflation approach. *Signal Processing*, 45(1):59–83, 1995.

[DLDMV96] L. De Lathauwer, B. De Moor, and J. Vandewalle. Blind source separation by simultaneous third-order tensor diagonalization. In *EUSIPCO*, Trieste, 1996.

[DLDMVC03] L. De Lathauwer, B. De Moor, J. Vandewalle, and J.F. Cardoso. Independent component analysis of largely underdetermined mixtures. In *4th International Symposium on Independent Component Analysis and Blind Source Separation (ICA2003)*, Nara, Japan, 2003.

[EBDGS05] M. El Badaoui, J. Danière, F. Guillet, and C. Servière. Separation of combustion noise and piston-slap in diesel engine. *Mechanical Systems and Signal Processing*, 19, 2005.

[ERFGD05] M. El Rhabi, H. Fenniri, G. Gelle, and G. Delaunay. Blind separation of rotating machines signals using PMI criterion and minimal distortion principle. *Mechanical Systems and Signal Processing*, 19, 2005.

[Ewi00] D.J. Ewins. *Modal Testing : theory, practice and application*. Research Studies Press LTD, second edition edition, 2000.

[Fee02] B.F. Feeny. On the proper orthogonal modes and normal modes of continuous vibration systems. *Journal of Vibration and Acoustics*, 124:157–160, 2002.

[Fel93] A.J. Felber. *Development of a Hybrid Bridge Evaluation System*. PhD thesis, University of British Columbia, 1993.

[FK98] B.F. Feeny and R. Kappaganty. On the physical interpretation of proper orthogonal modes in vibrations. *Journal of Sound and Vibration*, 211:607–6116, 1998.

[FK99] M. Feng and K.D. Kammayer. Application of source separation algorithms for mobile communications environment. In *International Workshop on Independent Component Analysis and Blind Source Separation*, Aussois, France, 1999.

[FM95] M.I. Friswell and J.E. Mottershead. *Finite Element Model Updating in Structural Dynamics*. Solid Mechanics and its Applications. Kluwer Academic Publishers, Dordrecht, The Netherlands, 1995.

[GHVDA99] P. Guillaume, L. Hermans, and H. Van Der Auweraer. Maximum likelihood identification of modal parameters from operational data. In *IMAC 17*, Kissimmee, FL, USA, 1999.

[GQ04] M. Gu and X.R. Qin. Direct identification of flutter derivatives and aerodynamic admittances of bridge decks. *Engineering Structures*, 26(14):2161–2172, 2004.

[GR94] M. Géradin and D. Rixen. *Mechanical Vibrations, Theory and Application to Structural Dynamics*. Masson, Paris, 1994.

[GSDC09] D.F. Giraldo, W. Song, S.J. Dyke, and J.M. Caecedo. Modal identification through ambient vibration: Comparative study. *Journal of Engineering Mechanics-ASCE*, 135(8):759–770, 2009.

[GVV+03] P. Guillaume, P. Verboven, S. Vanlanduit, H. Van Der Auweraer, and B. Peeters. A poly-reference implmentation of the least-squares complex frequency-domain estimator. In *21st IMAC*, Kissimmee (FL) - USA, 2003.

[HF02] S. Han and B.F. Feeny. Enhanced proper orthogonal decomposition for the modal analysis of homogeneous structures. *Journal of Vibration and Control*, 8:19–40, 2002.

[HGVDA98] L. Hermans, P. Guillaume, and H. Van Der Auweraer. A frequency-domain maximum likelihood approach for the extraction of modal parameters from output-only data. In *ISMA 23, Noise and Vibration Engineering*, Katholieke Universiteit Leuven, 1998.

[HKO01] A. Hyvärinen, J. Karhunen, and E. Oja. *Independent Component Analysis*. John Wiley and Sons, Inc, 2001.

[HLB96] P. Holmes, J. L. Lumley, and G. Berkooz. *Turbulence, Coherent Structures, Dynamical Systems and Symmetry*. Cambridge University Press, Cambridge, UK, first edition, 1996.

[HLS02] W. Heylen, S. Lammens, and P. Sas. *Modal Analysis: Therory and Testing*. University of Leuven, Leuven, 2002.

[HO97] A. Hyvärinen and E. Oja. A fast fixed-point algorithm for independent component analysis. *Neural Computation*, 9(7):1483–1492, 1997.

[HO00] A. Hyvärinen and E. Oja. Independent component analysis: Algorithms and applications. *Neural Networks*, 13(4-5):411–430, 2000.

[HSL$^+$98] N.E. Huang, Z. Shen, S.R. Long, M.C. Wu, H.H. Shih, Q. Zheng, N.C. Yen, C.C. Tung, and H.H. Liu. The empirical mode decomposition and the Hilbert spectrum for nonlinear and non-stationary time series analysis. In *Royal Society of London, Series A - Mathematical, Physical and Engineering Sciences*, volume 454, pages 903–995, 1998.

[HVDA99] L. Hermans and H. Van Der Auweraer. Modal testing and analysis of structures under operational conditions : Industrial applications. *Mechanical Systems and Signal Processing*, 13(2):193–216, 1999.

[HVDAAG98] L. Hermans, H. Van Der Auweraer, M. Abdelghani, and P. Guillaume. Evaluation of subspace identification techniques for the analysis of flight test data. In *16th International Modal Analysis Conference*, volume 1, pages 300–306, Santa Barbara, CA, USA, 1998.

[Hyv99] A. Hyvärinen. Fast and robust fixed-point algorithms for independent component analysis. *IEEE Transactions on Neural Networks*, 10(3):626–634, 1999.

[Ibr77] S.R. Ibrahim. Random decrement technique for modal identification of structures. *Journal of Spacecraft*, 14(11):696–700, 1977.

[IM77] S.R. Ibrahim and E.C. Mikulcik. A method for the direct identification of vibration parameters from the free response. *Shock and Vibration Bulletin*, 47(4):183–198, 1977.

[IMD06] U. Iemma, L. Morino, and M. Diez. Digital holography and karhunen-loève decomposition for the modal analysis of two-dimensional vibrating structures. *Journal of Sound and Vibration*, 291:107–131, 2006.

[JCL93] G.H. James, T.G. Carne, and J.P. Lauffer. The natural excitation technique (NExT) for modal parameter extraction from operating wind turbines, 1993.

[JCL95] G.H. James, T.G. Carne, and J.P. Lauffer. The natural excitation technique (NExT) for modal parameter extration from operating structures. *International Journal of Analytical and Experimental Modal Analysis*, 10:260–277, 1995.

[JH91] C. Jutten and J. Herault. Blind separation of sources: an adaptative algorithm based on neuromimetic architecture. *Signal Processing*, 24:1–10, 1991.

[JML00] M. Joho, H. Mathis, and R.H. Lambert. Overdetermined blind source separation: using more sensors than source signals in a noisy mixture. In *Independent Component Analysis and Blind Source Separation (ICA2000)*, Helsinki, Finland, 2000.

[JMM+01] T.P. Jung, S. Makeig, M.J. McKeown, A.J. Bell, T.W. Lee, and T.J. Sejnowski. Imaging brain dynamics using independent component analysis. In *IEEE*, volume 89, pages 1107–1122, 2001.

[Jol86] I.T. Jolliffe. *Principal Component Analysis*. Springer-Verlag, New-York, 1986.

[JP85] J.N. Juang and R.S. Pappa. An eigensystem realization algorithm for modal parameter identification and model reduction. *Control and Dynamics*, 12:620–627, 1985.

[Jut00] C. Jutten. Source separation: from dusk till dawn. In *2nd Int. Workshop on Independent Component Analysis and Blind Source Separation*, Helsinki, F

[Kam91] D.C. Kammer. Sensor placement for on-orbit modal identification and correlation of large space structures. *Journal of Guidance Control and Dynamics*, 14(2):251–259, 1991.

[KG02] G. Kerschen and J.C. Golinval. Physical interpretation of the proper orthogonal modes using the singular value decompostion. *Journal of Sound and Vibration*, 249:849–865, 2002.

[KG05] G. Kerschen and J.C. Golinval. Experimental modal analysis, 2005. Lecture Notes.

[KGVB05] G. Kerschen, J.C. Golinval, A.F. Vakakis, and L.A. Bergman. The method of proper orthogonal decomposition for dynamical characterization and order reduction of mechanical systems: an overview. *Nonlinear Dynamics*, 41:147–170, 2005.

[KPG07] G. Kerschen, F. Poncelet, and J.C. Golinval. Physical interpretation of independent component analysis in structural dynamics. *Mechanical Systems and Signal Processing*, 21(4):1561–1575, 2007.

[KVL+08] G. Kerschen, A.F. Vakakis, Y.S. Lee, D.M. McFarland, and L.A. Bergman. Toward a fundamental understanding of the Hilbert-Huang transform in nonlinear structural dynamics. *Journal of Vibration and Control*, 14(1-2):77–105, 2008.

[KWVG06] G. Kerschen, K. Worden, A.F. Vakakis, and J.C. Golinval. Past, present and future of nonlinear system identification in structural dynamics. *Mechanical Systems and Signal Processing*, 20:505–592, 2006.

[LFPB98] Shumin Li, W.A. Fladung, A.W. Phillips, and D.L. Brown. Automotive applications of the enhanced mode indicator function parameter estimation method. In *IMAC 16*, Santa Barbara (CA), USA, 1998.

[LJ89] R.W. Longman and J.N. Juang. Recursive form of the eigensystem realization algorithm for system identification. *Journal of Guidance Control and Dynamics*, 12(5):647–652, 1989.

[LKL07] J. Lee, T. Kim, and S.Y. Lee. Robust independent component analysis using quadratic negentropy. In *Independent Component Analysis and Signal Separation.*, volume 4666/2007, pages 227–235. Springer Berlin, Heidelberg, 2007.

[MBCH07] B. Moaveni, A.R. Barbosa, J.P. Conte, and F. Hemez. Uncertainty analysis of modal parameters obtained from three system identification methods, 2007.

[McC95] K.G. McConnell. *Vibration Testing: Theory and Practice*. Wiley-IEEE, 1995.

[MCC08] F. Magalhaes, A. Cunha, and E. Caetano. Online automatic identification of the modal parameters of a long span arch bridge. *Mechanical Systems and Signal Processing*, 23(2):316–329, 2008.

[MS94] L. Molgedey and H.G. Schuster. Separation of a mixture of independent signals using time-delayed correlations. *Physical Review Letters*, 72(23):3634–3637, 1994.

[MS97] N. Maia and J. Silva. *Theoretical and Experimental Modal Analysis*. Engineering Dynamics Series. Research studies press ltd., 1997.

[MZ08] S.I. McNeill and D. C. Zimmerman. A framework for blind modal identification using joint approximate diagonalization. *Mechanical Systems and Signal Processing*, 22(7):1526–1548, 2008.

[MZ10] S.I. McNeill and D. C. Zimmerman. Blind modal identification applied to output-only building vibration. In *IMAC XXVIII*, Jacksonville, FL (USA), 2010.

[OD98] D. Obradovic and G. Deco. Information maximization and independent component analysis: Is there a difference? *Neural Computation*, 10(8):2085–2101, 1998.

[PAF98] A.W. Phillips, R.J. Allemang, and W.A. Fladung. The complex mode indicator function (CMIF) as a parameter estimation method. In *16th IMAC*, Santa Barbara (CA), USA, 1998.

[PBZ05] R. Peled, S.G. Braun, and M. Zackenhouse. A blind deconvolution separation of multiple sources, with application to bearing diagnostics. *Mechanical Systems and Signal Processing*, 19, 2005.

[PCdD+08] B. Peeters, H. Climent, R. de Diego, J. de Alba, J.R. Ahlquist, J.M. Carreno, W. Hendricx, A. Rega, G. Garcia, J. Deweer, and J. Debille. Modern solutions for ground vibration testing of large aircraft. In *IMAC 26*, Orlando, FL (USA), 2008.

[PDC04] G. Patanchon, J. Delabrouille, and J.F. Cardoso. Source separation on astrophysical data sets from the wmap satellite. *Computer Science*, 3195:1221–1228, 2004.

[PDR99] B. Peeters and G. De Roeck. Reference-based stochastic subspace identification for output-only modal analysis. *Mechanical Systems and Signal Processing*, 13(6):855–878, 1999.

[PDR01] B. Peeters and G. De Roeck. Stochastic system identification for operational modal analysis: A review. *Journal of Dynamic Systems, Measurement, and Control*, 123(4):659–667, 2001.

[Pee00] B. Peeters. *System identification and damage detection in civil engineering*. PhD thesis, Katholieke Universiteit Leuven, 2000.

[PG97] D.T. Pham and P. Garrat. Blind separation mixtures of independent sources through a quasi-maximum likelihood approach. *IEEE Transactions on Signal Processing*, 45(7):1712–1725, 1997.

[PGJ92] D.T. Pham, P. Garrat, and C. Jutten. Separation of a mixture of independent sources through a maximum likelihood approach. In *EUSIPCO conference*, 1992.

[PGR+94] R. Pintelon, P. Guillaume, Y. Rolain, J. Schoukens, and H. Vanhamme. Parametric identification of transfer-functions in the frequency-domain - a survey. *IEEE Transactions on Automatic Control*, 39(11):2245–2260, 1994.

[PKGM07] F. Poncelet, G. Kerschen, J.C. Golinval, and F. Marin. System identification in structural dynamics using blind source separation techniques. In M. E. Davies, C. J. James, S. A. Abdallah, and M. D Plumbley, editors, *Independent Component Analysis and Signal Separation*, volume 4666/2007 of *Lecture Notes in Computer Science*, pages 778–785. Springer Berlin, Heidelberg, 2007.

[PKGV07] F. Poncelet, G. Kerschen, J.C. Golinval, and D. Verhelst. Output-only modal analysis using blind source separation techniques. *Mechanical Systems and Signal Processing*, 21(6):2335–2358, 2007.

[PLLVDA08] B. Peeters, J. Lau, J. Lanslots, and H. Van Der Auweraer. Automatic modal analysis: Myth or reality? *Sound and Vibration*, 42(3):17–21, 2008.

[Pon09] F. Poncelet. Rapport scientifique final - Validation de modèles structuraux en présence de phénomènes dynamiques non-linéaires. Technical report, University of Liège, Belgium, 2009.

[PP97] B.A. Pearlmutter and L.C. Parra. Maximum likelihood blind source separation: A context-sensitive generalization of ICA. *Advances in Neural Information Processings Systems*, 9:613–619, 1997.

[PSL05] N.H. Pontoppidan, S. Sigurdson, and J. Larsen. Condition monitoring with mean feald independent component analysis. *Mechanical Systems and Signal Processing*, 19, 2005.

[PVDA05] B. Peeters and H. Van Der Auweraer. PolyMAX: A revolution in operational modal analysis. In *1st International Operational Modal Analysis Conference*, Copenhagen, Denmark, 2005.

[PVDAG04] B. Peeters, H. Van Der Auweraer, and P. Guillaume. The PolyMAX frequency domain method: a few standard for modal parameter estimation. *Shock and Vibration*, 11:395–409, 2004.

[RE01] S. Roberts and R. Everson. *Independent component analysis: principles and practice*. Cambridge University Press, 2001.

[RES02] M.J. Roan, J.G. Erling, and L.H. Sibul. A new, nonlinear, adaptative, blind source separation approach to gear tooth failure detection and analysis. *Mechanical Systems and Signal Processing*, 16:719–740, 2002.

[RS08] S.E. Rosenow and G. Schlottmann. Parameter identification of ship structures using classical and operational modal analysis. In *ISMA 2008*, pages 3141–3156, 2008.

[SCI06] A. Salehian, E.M. Cliff, and D.J. Inman. Continuum modeling of an innovative space-based radar antenna truss. *Journal of Aerospace Engineering*, 19(4):227–240, 2006.

[SF04] C. Servière and P. Fabry. Blind source separation of noisy harmonic signals for rotating machine diagnoseis. *Journal of Sound and Vibration*, 272:317–339, 2004.

[SP91] J. Schoukens and R. Pintelon. *Identification of linear systems: A practical Guideline to Accurate Modeling*. Pergamon Press, BPCC Wheatons Ltd. Exeter edition, 1991.

[SSAC08] B. Swaminathan, B. Sharma, R.J. Allemang, and S. Chauhan. Modal studies on a truck frame and suspension. In *ISMA 2008*, pages 2593–2608, Leuven, Belgium, 2008.

[STAB88] C.Y. Shih, Y.G. Tsuei, R.J. Allemang, and D.L. Brown. Complex mode indication function and its application to spatial domain parameter estimation. *Mechanical Systems and Signal Processing*, 2(4):367–377, 1988.

[Sto04] J.V. Stone. *Independent Component Analysis: A Tutorial Introduction*. MIT Press, 2004.

[SVIG05] A. Salazar, L. Vergara, J. Igual, and J. Gosalbez. Blind source separation for classification and detection of flaws in impact-echo testing. *Mechanical Systems and Signal Processing*, 19, 2005.

[TJ95] H.L.N. Thi and C. Jutten. Blind source separation for convolutive mixtures. *Signal Processing*, 45(2):209–229, 1995.

[TLSH91] L. Tong, R.W. Liu, V.C. Soon, and Y.F. Huang. Indeterminacy and identifiability of blind identification. *IEEE Transactions on Circuits and Systems*, 38:499–509, 1991.

[VDAOLB91] H. Van Der Auweraer, D. Otte, J. Leuridan, and W. Bakkers. Modal testing with multiple sinusoidal excitation. In *IMAC 9*, Firenze, Italy, 1991.

[Ver02] P. Verboven. *Frequency Domain System Identification for Modal Analysis*. PhD thesis, Vrije Universiteit Brussel, 2002.

[VKRR82] H. Vold, J. Kundrat, T. Rocklin, and R. Russel. A multi-input modal estimation algorithm for mini-computers. *SAE Transactions*, 91(1):815–821, 1982.

[VODM93] P. Van Overschee and B. De Moor. Subspace algorithm for the stochastic identification problem. *Automatica*, 29(3):649*–60, 1993.

[VODM96] P. Van Overschee and B. De Moor. *Subspace Identification for Linear Systems: Theory, Implementation, Applications*. Kulwer Academic Publishers, 1996.

[VODMD97] P. Van Overschee, B. De Moor, and W. Dehandschutter. A subspace algorithm for the identification of discrete time frequency domain power spectra. *Automatica*, 33(12):2147–2157, 1997.

[VSJ+00] R. Vigário, J. Särelä, V. Jousmäki, M. Hämäläinen, and E. Oja. Idependent component approach to the analysis of EEG and MEG recordings. *IEEE Transactions on Biomedical Engineering*, 47(5):589–593, 2000.

[WLL+07] J.H. Weng, C.H. Loh, J.P. Lynch, K.C. Lu, P.Y. Lin, and Y. Wang. Output-only modal identification of a cable-stayed bridgeusing wireless monitoring systems. *Engineering Structures*, 30(7):1820–1830, 2007.

[WT01] K. Worden and G.R. Tomlinson. *Nonlinearity in Structural Dynamics : Detection, Identification and Modelling*. Institute of Physics Publishing, 2001.

[YA97] H.H. Yang and S.I. Amari. Adaptative on-line learning algorithms for blind separation: Maximum entropy and minimum mutual information. *Neural Computation*, 9(7):1457–1482, 1997.

[YLPH03a] J.N. Yang, Y. Lei, S.W. Pan, and N.E. Huang. System identification of linear structures based on Hilbert-Huang spectral analysis; part 1: Normal modes. *Earthquake Engineering and Structural Dynamics*, 32:1443–1467, 2003.

[YLPH03b] J.N. Yang, Y. Lei, S.W. Pan, and N.E. Huang. System identification of linear structures based on Hilbert-Huang spectral analysis; part 2: Complex modes. *Earthquake Engineering and Structural Dynamics*, 32:1533–1554, 2003.

[ZBA05] L. Zhang, R. Brincker, and P. Andersen. An overview of operational modal analysis: major development and issues. In *1st International operational modal analysis conference - IOMAC*, Copenhagen, Denmark, 2005.

[ZC07] W. Zhou and D. Chelidze. Blind source separation based vibration mode identification. *Mechanical Systems and Signal Processing*, 21(8):3072–3087, 2007.

[ZFI04] C. Zang, M.I. Friswell, and M. Imregun. Structural damage detection using independent component analysis. *Structural Health Monitoring*, 3:69–83, 2004.